GRID-BASED TECHNIQUES FOR DENSITY FUNCTIONAL THEORY

EFFICIENT GRID-BASED TECHNIQUES FOR DENSITY FUNCTIONAL THEORY

By

JUAN IGNACIO RODRIGUEZ-HERNANDEZ
M.Sc. (Physics)

A Thesis

Submitted to the School of Graduate Studies

in Partial Fulfilment of the Requirements

for the Degree

Doctor of Philosophy

McMaster University

DOCTOR OF PHILOSOPHY (2008)
(Chemistry)

McMaster University
Hamilton, Ontario, Canada

TITLE: Efficient grid-based techniques for Density Functional Theory.

AUTHOR: Juan I. Rodríguez-Hernández

B.Sc. –Phys. and Math.
M.Sc. –Phys.
(Instituto Politécnico Nacional,
México City, México, 2001)

SUPERVISOR: Professor Paul W. Ayers

NUMBER OF PAGES: xvii, 220

ABSTRACT

Understanding the chemical and physical properties of molecules and materials at a fundamental level often requires quantum-mechanical models for these substance's electronic structure. This type of many body quantum mechanics calculation is computationally demanding, hindering its application to substances with more than a few hundreds atoms. The supreme goal of many researches in quantum chemistry—and the topic of this dissertation—is to develop more efficient computational algorithms for electronic structure calculations. In particular, this dissertation develops two new numerical integration techniques for computing molecular and atomic properties within conventional Kohn-Sham-Density Functional Theory (KS-DFT) of molecular electronic structure.

The first of these grid-based techniques is based on the transformed sparse grid construction. In this construction, a sparse grid is generated in the unit cube and then mapped to real space according to the pro-molecular density using the conditional distribution transformation. The transformed sparse grid was implemented in program deMon2k, where it is used as the numerical integrator for the exchange-correlation energy and potential in the KS-DFT procedure. We tested our grid by computing ground state energies, equilibrium geometries, and atomization energies. The accuracy on these test calculations shows that our grid is more efficient than some previous integration methods: our grids use fewer points to obtain the same accuracy. The transformed sparse grids were also tested for integrating, interpolating and differentiating in different dimensions ($n = 1, 2, 3, 6$).

The second technique is a grid-based method for computing atomic properties within QTAIM. It was also implemented in deMon2k. The performance of the method was tested by computing QTAIM atomic energies, charges, dipole moments, and quadrupole moments. For medium accuracy, our method is the fastest one we know of.

To my parents, Clemente Rodríguez and Catalina Hernández,

for all of their love, wisdom, and humbleness

May the Lord bless them

ACKNOWLEDGMENTS

First, I would like to give thanks and honor to God for helping in everything I do and giving me all I have.

I would like to thank my supervisor Prof. Paul Ayers for guiding and supporting me. Thank you for sharing your vast knowledge with me whenever I needed it. Many many thanks for being such a smart, exemplar and wonderful person.

I would like to thank James Anderson and David Thompson (I write them in alphabetical order) for all their great friendship, support, scientific-philosophical discussions, laughter, programming, games, movies, humor, beer, tequila, etc.. Thank you for all those singular moments during my Ph.D.. Special thanks also to Steven Burger. Thanks to all of you for letting me appreciate the best of the Anglo-Saxon culture in its four variants: American (Paul), British (David), Canadian (James) and a mix of all three together (Steven).

I thank Professors Alex Bain and Randy Dumont for being part of my Ph.D. committee. Thank you for your helpful comments and suggestions regarding Ph.D. work at McMaster. I gratefully acknowledge Prof. Andreas Köster for his guidance, help, and knowledge. Thank you for introducing me to deMon2k. I would also like to thank Prof. Richard Bader for trust in my capabilities and for introducing me QTAIM (there is nothing better than learning a great theory from its creator). Many thanks also to Prof. A. Cedillo, Prof. D. Sprung and Cherif Matta.

Thanks also to the Ayers' group people Annie Liu, Ivan Vinogradov, Debajit Chakraborty, Reza Khorasani, Carlos Cardenas, Rogelio Cuevas, Utpal Sarkar and Bijoy Day for all these years of working together, their support, and friendship.

Special thanks go to Gloria López and Ahmad Khodayari for all those pleasant moments. Special thanks also to my "new", smart and nice friends Natalia Ruminot and Felipe Sanhueza (por esos momentos agradables de charla y risa). To some of my first friends at Mac: Alexandra Dabkowska, Jessica Grebeldinger, Maysoon Khasani, and Marzia Bianchi, many thanks for everything you shared with me (especially for trying to understand my English and not despairing).

Thanks to the Department of Chemistry at McMaster University (and McMaster itself). In particular, I would like to thank Mrs. Carol Dada for her support. Thanks to all the Hamiltonians and the great country/people of Canada for all I have received here.

Now my Mexican family/friends/institutions:

I would like to thank my eternal, good advisor Prof. Marcela Beltrán for her support and trust in me (gracias por perdonar mi "actitud de cabezón" una y otra vez ... si siquiera pudiera saber que significa exactamente eso (aparte de sonar chistoso) podría empezar a mejorar en algo. Mil gracias Marce!) To Anita Santos, Gaby Vera and all the people in the CINVESTAV theoretical chemistry group for helping out with demon2k and their nice and funny friendship.

To my dearest friends Israel González, Rene Quiroz, Olivia Hernández, Laura Roldán, Francisco Rios, and Elizabeth Salinas, thanks for believing in me (no se les

olvide que haremos la revolución! No se nos olvide la frase del Quijote: " ... que si no acabó grandes cosas murió por acometellas.")

MANY MANY THANKS to my wonderful family: Pepe, Wil, Mario, Héctor, Guadalupe, Clemente, Carmen and Carlos for being with me (in person and spiritually) and having such wonderful children. Thanks also go to my other brothers Enrique, Martin, Mario, Susana and Olivia. Exceptional thanks to "mi general" Clemente Rodríguez and his wife Lupita Quiroz for all their immense support.

Last but not least, I acknowledge the Mexican government through the "Consejo Nacional de Ciencia y Tecnología" for awarding me my Ph.D. scholarship. This scholarship would not have been possible without the direct and indirect support/efforts of my beloved people/country of México.

TABLE OF CONTENTS

LIST OF FIGURES

LIST OF TABLES

PREFACE

The Chapters 2-5 of this thesis are reprints of articles that are published or submitted for publication. To make the thesis self-contained, essential background information and context is presented in Chapter 1. To provide context and to integrate the content of the disparate chapters, each chapter is prefaced by a section entitled "Statement of the problem" that does not appear in the submitted/published version of the paper. Chapter 6 gives our conclusions and prospects for future work. The disclosure of collaborative work is as follows.

Chapter 2 is a reprint of the article "Numerical integration of exchange-correlation energies and potentials using transformed sparse grids", accepted for publication in the *Journal of Chemical Physics*. I am the first and corresponding author on this paper. My coauthors are David C. Thompson, Paul W. Ayers, and Andreas M. Köster.

Chapter 3 is a reprint of the article "A Physically Motivated Pseudo-Gaussian Cubature Scheme with Applications to Molecular Density-Functional Theory", submitted (on 03/28/08) to the *Journal of Physics A*. I am the first and corresponding author on this paper. My coauthors are David C. Thompson, James S. M. Anderson, Jordan Thomson, and Paul W. Ayers.

Chapter 4 is a reprint of the book chapter "A novel based-grid approach to the electronic structure problem: interpolants and derivatives" in *Quantum Chemistry Research Trends*; Mikas P. Kaisas (Editor). New York: Nova Science Publisher, 2007.

The authors of this paper are James S. M. Anderson, Juan I. Rodríguez, David C. Thompson, and Paul W. Ayers.

Chapter 5 is a reprint of the article "An efficient grid-based scheme to compute QTAIM properties without explicit calculations of zero-flux surfaces", submitted (on 02/19/2008) to the *Journal of Computational Chemistry*. I am the first and corresponding author on this paper. My coauthors are Andreas M. Köster, Paul W. Ayers, Ana Santos-Valle, Alberto Vela, and Gabriel Merino.

Even though all the research articles were co-authored, the author of the thesis performed most of the work. He wrote most of the key FORTRAN subroutines, did all the implementation within deMon2k, generated all the data reported in Chapters 2 and 5 and most of data in other chapters. Chapters 2-4 were principally guided by Prof. Paul Ayers. Chapter 5 was principally guided by Prof. Andreas Köster.

"Según Demócrito, el antiguo filósofo griego, "lo dulce y lo amargo, lo caliente y lo frío, lo amarillo y lo verde, etc., no son más que opiniones; sólo los átomos y el vacío son verdaderos." Para Demócrito, opinión era un conocimiento oscuro, sin la menor garantía de realidad. . .

Preciso es que tomemos posición, como dicen los filósofos; posición defensiva, digo yo, de gatos panza arriba ante esta vieja concepción del gran filósofo de Tracia. El escepticismo, que, lejos de ser, como muchos creen, un afán de negarlo todo, es, por el contrario, el único medio de defender algunas cosas, vendrá en nuestro auxilio.
Vamos a empezar dudando de la existencia de los átomos.
Vamos, después, a aceptarla; pero con ciertas restricciones. . . ."
Juan de Mairena

A. Machado,
Juan de Mairena, sentencias, donaires, apuntes y recuerdos de un profesor apócrifo.

Chapter 1

BACKGROUND

1.1 Introduction

The vast majority of the "ordinary stable matter" in the universe consists of protons, neutrons, and electrons. At terrestrial temperatures and material densities the protons and neutrons clump together to form positively charged atomic nuclei, which bind negatively charged electrons to them. Under ordinary conditions, the discrete atomic nuclei are inert, but the cloud of electrons that surrounds the nuclei is malleable. When atoms combine to form molecules, and when atoms and/or molecules come together to form liquids and solids, the identity and properties of the atomic nuclei do not change significantly. However, the electron clouds deform dramatically: electrons from different clouds join and pair to form chemical bonds; electron clouds polarize to adapt to electronic interactions; electrons move from less electronegative to more electronegative regions; electrons in distant clouds engage in a correlated dance of avoidance giving rise to dispersion forces.[1-5] For this reason, almost all of the scientific problems and phenomena in biology, chemistry, materials science, and physics are, at the fundamental level, electronic structure problems. That is, our ability to design molecules and materials with desirable properties hinges on our ability to model and understand their electronic structure. For example, electronics —everything from cellular phones to supercomputers— relies on the electronic properties of solid-state materials (chiefly doped semiconductors). Many different areas of chemistry use insight into molecular electronic structure (chemical bonds and how they break and form) to design more

economical and/or environmentally friendly catalysts (industrial chemistry) or small molecules that inhibit or induce biological responses (medicinal chemistry). The rational design of new materials with special features (strength, ductility, spectral features, etc.) also relies on models for the electronic structure of materials like metal alloys.[1-5] The primary purpose of this thesis is to develop new auxiliary tools for the computational modeling and conceptual understanding of electronic structure of molecules and materials.

In quantum chemistry and solid state physics, solving the electronic structure problem requires the solution of the Schrödinger's equation for a system of electrons moving in the field produced by the atomic nuclei. Specifically, for a system of N electrons bound by their electronic attraction to M nuclei, the electronic Schrödinger equation can be written as

$$\hat{H}\Psi = E^{elec}\Psi . \tag{1.1.1}$$

$$\hat{H} = -\frac{1}{2}\sum_{i=1}^{N}\nabla_i^2 - \sum_{i=1}^{N}\sum_{A=1}^{M}\frac{Z_A}{\left|\vec{r}_i - \vec{R}_A\right|} + \sum_{j>i}^{N}\frac{1}{\left|\vec{r}_i - \vec{r}_j\right|}. \tag{1.1.2}$$

$\hat{H}$ is the molecular Hamiltonian for the electrons within the Born-Oppenheimer approximation.[1,6-7] $\vec{x}_i$ and $\vec{R}_A$ represent the positions of the electrons and nuclei, respectively. Z_A is the atomic number of the nucleus A. Ψ is the electronic wave-function.

In Eq. (1.1.2), and throughout the remainder of the thesis, we use atomic units, where Planck's constant, h, is equal to 2π (so $\hbar = 1$), the mass of electron is one ($m_e = 1$), and the charge of the electron is $2\sqrt{\pi\varepsilon_0}$, (so $e^2 / 4\pi\varepsilon_0 = 1$). The atomic unit of energy is the Hartree. (1Hartree=27.2eV=2.20×10^5cm^{-1}=6.58×10^{15}Hz=2.63×10^3kJ/mol) The atomic unit of length is the *Bohr*. (1Bohr =0.529Å = 5.29×10^{-11}m).[6]

After the Schrödinger equation, Eq. (1.1.1), has been solved, any measurable property of the electronic system can be evaluated by taking the expectation value of the appropriate operator (s_i represents the spin variable of electron i),

$$P = \sum_{spin} \int\int ... \int \Psi^*(\vec{r}_1, s_1, \vec{r}_2, s_2, ..., \vec{r}_N, s_N) \hat{P} \Psi(\vec{r}_1, s_1, \vec{r}_2, s_2, ..., \vec{r}_N, s_N) d\vec{r}_1 d\vec{r}_2 ... d\vec{r}_N . \qquad (1.1.4)$$

In the Born-Oppenheimer picture, the chemical properties of electronic matter are governed by the potential-energy surface on which the atomic nuclei vibrate and move. This potential-energy surface is just the sum of the electronic energy and the classical electrostatic repulsion between the nuclei,

$$U(\{\vec{R}_i\}) = \sum_{A>B}^{M} \frac{Z_A Z_B}{\left|\vec{R}_A - \vec{R}_B\right|} + E^{elec}(\{\vec{R}_i\}) . \qquad (1.1.5)$$

Notice that the electronic energy depends on the nuclear positions because the electronic Hamiltonian, Eq. (1.1.2), depends on the nuclear positions.[8]

Analytic, closed-form, solutions of the electronic Schrödinger equation (Eq. 1.1.1) are only available for one-electron systems. The difficulty of even finding accurate

approximate solutions grows rapidly as the number of electrons increases. For example, the Schrödinger equation for benzene is a partial differential equation with 126 variables! Modeling the electronic structure of atoms and molecules with more than a few (about ten) electrons requires that one approximate the wave-function or, equivalently, the Schrödinger equation.

There are two main families of approximations that are in everyday use: wave-function methods[1,6-7] and density functional theory (DFT) methods.[1,9-15] One of the simplest wave-function approaches is the Hartree-Fock method described in Section 1.1.2. The Kohn-Sham-DFT approach is described in Section 1.1.3. A more thorough overview of DFT may be found in Section 1.2.

1.1.2 Wave-function methods: The Hartree-Fock equations

In wave-function methods, an approximation to the wave-function is constructed and used as the fundamental descriptor. Properties of the electronic system are then evaluated using Eq. (1.1.4).

The restricted Hartree-Fock (HF) method is one of the simplest wave-function methods; we will use it to present the wave-function-based approach. The HF method is derived from the variational principle: The ground-state wave-function, $\Psi^{g.s.}$, is obtained by minimizing the energy subject to the normalization constraint that $\langle\Psi|\Psi\rangle = 1$. That is,

$$E^{g.s.} = \left\langle \Psi^{g.s.} \middle| \hat{H} \middle| \Psi^{g.s.} \right\rangle = \min_{\{\Psi \mid \langle \Psi | \Psi \rangle = 1\}} \left\langle \Psi \middle| \hat{H} \middle| \Psi \right\rangle. \tag{1.1.5}$$

To use the variational principle, we need to choose a (simple!) approximate form for the wave-function. In the restricted HF method for the ground state of closed-shell systems, the wave-function is approximated by a Slater determinant of one-electron wave-functions,[5-6]

$$\Psi \equiv \frac{1}{\sqrt{N!}} \begin{vmatrix} \phi_1(\vec{r}_1)\alpha(1) & \phi_1(\vec{r}_1)\beta(1) & \cdots & \phi_{N/2}(\vec{r}_1)\beta(1) \\ \phi_1(\vec{r}_2)\alpha(2) & \phi_1(\vec{r}_2)\beta(2) & \cdots & \phi_{N/2}(\vec{r}_2)\beta(2) \\ \vdots & \vdots & & \vdots \\ \phi_1(\vec{r}_N)\alpha(N) & \phi_1(\vec{r}_N)\beta(N) & \cdots & \phi_{N/2}(\vec{r}_N)\beta(N) \end{vmatrix}. \tag{1.1.6}$$

The one-electron wave-functions, $\phi_i(\vec{r})$, are normalized and orthogonal to each other. They are called orbitals; much of our current understanding is based on the "molecular orbital theory" built upon these orbitals. $\alpha(i)$ and $\beta(i)$ denote the two choices (up-spin and down-spin) for the spin of electron i. Notice that the Slater determinant wave-function in Eq. (1.1.6) is a) normalized and b) antisymmetric with respect to the exchange of the spatial- and spin-coordinates of any two electrons (Pauli antisymmetry principle), and c) zero if two electrons with the same spin are in the same space orbital (Pauli exclusion principle).

Substituting the Slater determinant, Eq. (1.1.6), into the variational principle, Eq. (1.1.5), yields the Hartree-Fock equations,[5-6]

$$\left(-\frac{1}{2}\nabla^2-\sum_{A=1}^{M}\frac{Z_A}{\left|\vec{r}-\vec{R}_A\right|}+\hat{J}(\vec{r})-\hat{K}(\vec{r})\right)\phi_i(\vec{r})=\varepsilon_i\phi_i(\vec{r});\quad j=1,...,N/2 \tag{1.1.7}$$

The Coulomb operator, $\hat{J}(\vec{r})$, and the exchange operator, $\hat{K}(\vec{r})$, are defined by the formulas,

$$\hat{J}(\vec{r})\phi_i(\vec{r})\equiv 2\sum_{j\neq i}^{N/2}\int\frac{\phi_j{}^*(\vec{r}\,')\phi_j(\vec{r}\,')d\vec{r}\,'}{\left|\vec{r}-\vec{r}\,'\right|}\phi_i(\vec{r}), \tag{1.1.8a}$$

$$\hat{K}(\vec{r})\phi_i(\vec{r})\equiv \sum_{j\neq i}^{N/2}\int\frac{\phi_j^*(\vec{r}\,')\phi_i(\vec{r}\,')d\vec{r}\,'}{\left|\vec{r}-\vec{r}\,'\right|}\phi_j(\vec{r}). \tag{1.1.8b}$$

Solving the HF equations gives the HF orbitals, $\phi_i(\vec{r})$, and orbital energies, ε_i. The orbital energies can be interpreted as approximate electron removal energies.[17]

Some salient features of the HF method are:

I. The HF equations, Eq. (1.1.7), comprise a system of one-electron equations that are coupled together by the Coulomb and exchange operators, Eq. (1.1.8). Hartree-Fock is considered to be an "independent electron" or "mean field" model because the electrons interact with each other only in the "average" way defined by $\hat{J}(\vec{r})$ and $\hat{K}(\vec{r})$.

II. The HF equations are solved using the self-consistent field method. Starting from an initial guess of the HF orbitals, $\hat{J}(\vec{r})$ and $\hat{K}(\vec{r})$ are computed. Eqs. (1.1.7) are solved, generating a new set of orbitals. If the new orbitals are sufficiently close to the starting orbitals, the equations are considered solved. Otherwise, $\hat{J}(\vec{r})$ and $\hat{K}(\vec{r})$ are constructed from the "new" orbitals, and Eqs. (1.1.7) are solved again, and again, until the "input orbitals" used to construct $\hat{J}(\vec{r})$ and $\hat{K}(\vec{r})$, and the "output orbitals" obtained from Eqs. (1.1.7) are sufficiently similar. At that point the orbitals in the HF equations are "self-consistent" and the equations are considered solved. It should be noted that this simple self-consistent field algorithm often converges very slowly or does not converge at all.[19] In practice, more efficient, but also more complicated, algorithms are used.[20-21]

Recall that the HF method is obtained by restricting the search domain in the variational principle, Eq. (1.1.5), to simple Slater determinant wave-functions. The HF energy is thus above the true ground-state energy. The difference between the exact ground-state energy, $E_{g.s.}$, and the HF energy is called the correlation energy,[6]

$$E_{corr} \equiv E_{g.s.} - E_{HF} < 0. \qquad (1.1.9)$$

The correlation energy is small on an absolute scale (~0.04 Hartree per electron pair) but large on a chemical scale (~100 kJ/mol per electron pair). For this reason, HF is not very reliable for describing chemical processes in which chemical bonds break and/or form. However, Hartree-Fock is usually reliable for predicting the equilibrium positions of atomic nuclei[22] and, with the appropriate scaling corrections, vibrational spectra.[23]

There are two main drawbacks to the HF method. The first is inherent to the approach, the second drawback is practical.

I. There are systems where the exact wave-function is very different from a Slater determinant, and so HF gives *qualitatively* incorrect results. Examples include the carbon dimer (C_2),[24-25] the chromium dimer (Cr_2),[26] and Cu_2O_2.[27-29]

II. HF calculation can only be applied to small- and medium-sized systems (fewer than 100 atoms) because the computational cost of the HF algorithm is $O(N^4)$. I.e., the computation cost grows as the fourth power of the number of electrons. In practice, however, the computational cost can be reduced to $O(N^3)$ (or even $O(N^2)$) for large molecules using clever integral evaluation algorithms. For very large molecules, it is even possible to obtain linear ($O(N)$).[30]

The first problem can be overcome by adding corrections to the HF wave-function to model the effect of electron correlation. Many of the characteristic acronyms of

molecular electronic structure theory, also called quantum chemistry, refer to methods of this type.[6,30-31] For example, HF can be corrected by a) treating electron correlation as a correction using perturbation theory (MP2, MP3, MP4, etc.), b) using a more complicated form for the wave-function in the variational principle (CISD, CISDT, CISDTQ), or c) combining between the perturbative and variational approaches (CIS(D), CCSD(T)), etc.). Unfortunately these methods are even more expensive than HF, with computational scalings that range from $O(N^5)$ to $O(N!)$. The fastest of these methods, MP2, is nowadays applicable to molecules with up to about 100 atoms.

Theoretical Method	Current computational dependence on molecular size, N	Estimate of maximum feasible molecular size in 1996	Current estimate of maximum feasible molecular size
FCI	$N!$	2 atoms	3 atoms
CCSD(T)	N^7	8-12 atoms	20 atoms
CCSD	N^6	10-15 atoms	30 atoms
MP2	N^5	25-50 atoms	75-100 atoms
HF, KS-DFT	N^2-N^3	50-200 atoms	300-500 atoms

Figure 1.1 Computational scaling of the standard electronic structure methods. The data in the three first columns was taken from Ref. (30). The data in the fourth column is our estimate.

1.1.3 DFT methods

DFT methods are based on an entirely different philosophy: in DFT one tries to approximate the electron density. The wave-function, to the extent that it enters the

theory at all, only plays an incidental role as a computational facilitator. DFT overcomes the main limitation of HF theory: it includes correlation; but has similar computational cost. In theory, DFT, which scales as $O(N^3)$, is a bit cheaper than HF. In practice, HF is often cheaper for small molecules, while DFT tends to be cheaper for large molecules and condensed matter. Because of this, DFT, or more specifically, Kohn-Sham-DFT, is the most popular computational method in modern electronic structure theory.[9-15] The next section will provide some technical details about the Kohn-Sham-DFT (KS-DFT) method. The remainder of this section will provide a broad overview of KS-DFT, with a view towards providing context and motivation for the material of this thesis.

The applicability of DFT is limited in two ways: (1) the $O(N^3)$ scaling of most computational implementations (2) the inherent error associated with the approximate density functionals used to model electron correlation and the Pauli exclusion principle (electron exchange). This thesis is focused on the first difficulty.

Because of its $O(N^3)$ scaling, standard implementations of DFT are not applicable to the large molecules of interest in such fields as medicinal chemistry and biophysics. Table 1.1 shows some computational timings of popular DFT software packages for determining the optimum geometry of different molecules. Notice that for the larger molecules, Au_{212} and hemoglobin, the DFT methods become computationally impractical. In practice, DFT calculations are impractical for molecules with more than a few hundred atoms.[11-15]

DFT is still far from being applicable to systems containing thousands of atoms. Current research on extending DFT to larger systems is focused two directions:

I. Improving the numerical algorithms used by conventional DFT computations[15,32-34]

II. Developing new "linear scaling" DFT algorithms.[1,15,35-36]

The research in this thesis falls into the first category, although it is also relevant to linear scaling DFT because the best computational approaches will combine aspects of both approaches.

Molecule	**Method**	**xc-functional**	**Basis-set**	**Software**	**Time**
H_2O	DFT-KS	B3LYP	6-31G*	Gaussian	28.5sec
H_2O	DFT-KS	B3LYP	DZVP	deMon2k	10.18sec
C_6H_6	DFT-KS	B3LYP	6-31G*	Gaussian	6min48sec
$Fe(C_5H_5)_2$	DFT-KS	LDA	DZVP	deMon2k	4min21sec
$C_{15}H_{26}N_2O_4$ (Tamiflu)	DFT-KS	B3LYP	6-31G*	Gaussian	5hrs13min
Au_{212}	DFT-KS	LDA	DZVP	SIESTA	~3months
Hemoglobin (9272atoms)	DFT-KS	LDA	DZVP	SIESTA	~7years

Table 1.1 CPU time for optimizing the geometry of some representative molecules [all calculations were performed by the author except for hemoglobin for which the time was estimated]. Only the nearest local minimum is found. For the larger molecules, finding the globally optimum geometry is much more difficult than these timings would suggest. DZVP denotes the double zeta-polarization basis set defined in reference (82).

Specifically, this thesis is devoted to the development and implementation of new numerical integration methods, with emphasis on DFT. The particular aspects of the DFT integration problem that are of relevance to this thesis include:

I) A key step in a Kohn-Sham DFT calculation is to integrate the exchange-correlation potential and energy. These functionals are impossible to integrate analytically so a numerical integration method is used.[37-45] Explicit expressions for these integrals can be found in the next section.

II) In quantum mechanics, properties are evaluated as expectation values of the corresponding operator. These integrals are often very complicated functions that cannot be integrated analytically. There are also cases where, even though the integrand is analytically integrable, the integration region is too complicated to allow facile analytical integration. An example of the latter case appears when integrating over the atomic basins in the quantum theory of atoms in molecules (QTAIM).[45-52]

III) Efficient integration grids provide the foundation for basis-set-free approaches to the electronic structure problem. The basis-set-free approach is critically dependant on the quality of the grid because all of the mathematical operations on the fundamental electronic structure descriptor (e.g., the wave-function, the density matrix, and the electron density) must be performed on that grid.[53-56]

Intelligent distribution of the grid points in the integration region provides a more accurate representation for the key mathematical operations, leading to more accurate and less expensive predictions of physicochemical phenomena.

These three areas of application demonstrate the importance of developing grids that are efficient for integrating the electron density and density-like functions. This dissertation makes a direct contribution to the first two problems and lays the groundwork for an attack on the third (and most challenging) problem.

The rest of this introductory chapter is organized as follows. In Section 1.2 we introduce DFT in more detail. In Section 1.3, the basic concepts of the quantum theory of atoms in molecules are introduced. Section 1.4 shows the mathematics of the transformed sparse integration grids. Finally, in Section 1.5 provides an overview of the remainder of the thesis.

1.2 Density Functional Theory

1.2.1 Introduction

The idea of using the electron density as the basic descriptor for electronic structure problems has its origins in 1927 with the theories of Thomas[16] and Fermi.[17] However, it was not until 1964 that Hohenberg and Kohn provided the mathematical basics for using the electron density to replace the wave-function as the basic descriptor for a system of electrons.[9] Their key results are enunciated as two theorems that are the foundation of DFT, and for which Walter Kohn won the Nobel Prize in 1998.[11] The

Hohenberg-Kohn theorems are analogous to results from wave-function theory, but with the electronic density, $\rho(\vec{r})$, playing the principal role instead of the wave function.

1st Theorem. The ground state's electron density determines all the properties of an electronic system.

2nd Theorem. The energy of the system is a functional of the electronic density, $E = E[\rho]$, and the N-electron ground state energy, $E_{g.s.}$, and ground state density, $\rho_{g.s.}(\vec{r})$, are obtained by minimizing the energy with respect to all N-electron densities,

$$E_{g.s.} = E[\rho_{g.s.}] = \underbrace{\min}_{\rho} E[\rho]. \tag{1.2.1}$$

Just like wave-function methods, one uses the variational principle, Eq. (1.2.1), to find $\rho_{g.s.}(\vec{r})$. The ground-state energy and other chemical properties then follow. Essentially, DFT changes the independent variable from ψ to ρ. This is useful because the electronic density,[12]

$$\rho(\vec{r}) \equiv \left\langle \psi(\vec{r}_1,...,\vec{r}_N) \left| \sum_{i=1}^{N} \delta(\vec{r} - \vec{r}_i) \right| \psi(\vec{r}_1,...,\vec{r}_N) \right\rangle, \tag{1.2.2}$$

only depends on three variables, while the N-electron wave function depends on $3N$ variables (plus spin). Thus the domain of the functions used to solve the electronic structure problem has been reduced from a space of $3N$ dimensions (plus spin) to a space of 3 dimensions. A problem remains, however. The first Hohenberg-Kohn theorem is one

of existence: it provides no guidance on how to determine the energy functional that is required to implement the variational principle. Hohenberg and Kohn showed, however, that the energy functional can be split into two parts,[9]

$$E[\rho] = F[\rho] + \int \rho(\vec{r}) v^{ext}(\vec{r}) d\vec{r} \; ; \tag{1.2.3}$$

The second term in this expression represents the potential energy of interaction between the electrons and the external, non-electronic, potential that binds them to the system. For an isolated molecule, this external potential is exactly the same electron-nuclear attraction potential,

$$v^{ext}(\vec{r}) = -\sum_{A=1}^{M} \frac{Z_A}{\left|\vec{r} - \vec{R}_A\right|}, \tag{1.2.4}$$

that enters into the Hartree-Fock equations. (See Eq. 1.1.7).

The first term in Eq. (1.2.3), $F[\rho]$, is usually called the Hohenberg-Kohn density functional. $F[\rho]$ represents the electronic contributions (kinetic energy and electron-electron potential energy) to the energy and, unlike $v^{ext}(\vec{r})$, $F[\rho]$ is universal. That is, the same functional applies to *every* electronic system; $F[\rho]$ is not system dependent. Thus the problem of approximating *3N*-dimentional wave-functions has been exchanged for the problem of approximating $F[\rho]$.

1.2.2 The Kohn-Sham equations

Most modern DFT calculations use the approximation to $F[\rho]$ that was proposed by Kohn and Sham in 1965.[10] Specifically,

$$F[\rho] = T_s[\rho] + J[\rho] + E_{xc}[\rho]. \tag{1.2.4}$$

$T_s[\rho]$ is the kinetic energy of a system of non-interacting electrons with electron density $\rho(\vec{r})$. $J[\rho]$ is the classical electrostatic repulsion between the electron density and itself,

$$J[\rho] = \frac{1}{2}\int\int \frac{\rho(\vec{r})\rho(\vec{r}\,')d\vec{r}d\vec{r}\,'}{|\vec{r}-\vec{r}\,'|}. \tag{1.2.5}$$

The exchange-correlation energy functional, $E_{xc}[\rho]$, contains all of the other contributions to $F[\rho]$, including

a) the reduction of the electron-electron repulsion potential energy between electrons of the same spin due to the Pauli principle (exchange energy),
b) the correction to the kinetic energy and the electron-electron potential energy because electrons are not independent, but instead move in a correlated way (correlation energy).

In Kohn-Sham-DFT, only the exchange-correlation energy component of $E_{xc}[\rho]$ has to be approximated.

The density of a system of independent electrons is given by the formula:

$$\rho(\vec{r}) = \sum_{i=1}^{N} |\psi_i(\vec{r})|^2 , \tag{1.2.6}$$

where $\psi_i(\vec{r})$ are one electron orbitals. Using the Kohn-Sham expression for $F[\rho]$ (Eq. 1.2.4), in the energy functional (Eq. 1.2.1) leads to the Kohn-Sham equations,[10]

$$\left(-\frac{1}{2}\nabla^2 + v^{ext}(\vec{r}) + J[\rho,\vec{r}] + V^{xc}[\rho;\vec{r}]\right)\psi_i(\vec{r}) = \varepsilon_i\psi_i(\vec{r}) . \tag{1.2.7}$$

The Kohn-Sham (KS) equations are similar in form to the Hartree-Fock equations, Eq. (1.1.7). The Coulomb function operator,

$$J[\rho,\vec{r}] = \int \frac{\rho(\vec{r}\,')d\vec{r}\,'}{|\vec{r} - \vec{r}\,'|} = \sum_{i=1}^{N} \int \frac{|\psi_i(\vec{r}\,')|^2 \, d\vec{r}\,'}{|\vec{r} - \vec{r}\,'|} ,$$

has exactly the same form as in Hartree-Fock. (compare Eq. (1.1.8a)). The exchange-correlation potential, which includes effects of both exchange and correlation, is the variational derivative of the exchange-correlation energy,

$$V^{xc}[\rho(\vec{r});\vec{r}] = \frac{\delta E_{xc}[\rho]}{\delta\rho} . \tag{1.2.8a}$$

Kohn and Sham expressed the exchange-correlation energy in terms of the exchange-correlation energy density, per electron, at the point $\vec{r}$, $\varepsilon_{xc}[\rho,\vec{r}]$:

$$E_{xc}[\rho] = \int \rho(\vec{r})\varepsilon_{xc}[\rho,\vec{r}]d\vec{r} . \tag{1.2.8b}$$

Then they simplified this expression by assuming that $\varepsilon_{xc}[\rho,\vec{r}]$ is a *function* of $\rho(\vec{r})$, $\varepsilon_{xc}(\rho(\vec{r}))$. This is called the local density approximation. Finally, they approximated

$\varepsilon_{xc}(\rho(\vec{r}))$ with the exchange energy density, per electron, of the uniform electron gas with density $\rho(\vec{r})$.[10]

It is important to note that the KS equations are not restricted to the local density approximation; better approximations for $E_{xc}[\rho]$ are usually used. Finding better approximations for $E_{xc}[\rho]$ is a flourishing research field.[1,57-58] Notice that if the exact $E_{xc}[\rho]$ were used in the KS equations, then KS-DFT would reproduce the ground state energy and ground state density *exactly*.

Although the KS equations (Eq. 1.2.7) look very similar to the HF equations (Eq. 1.1.7), the KS approach has several advantages. Among them,

I) The KS equations include electron correlation.

II) $V^{xc}(\vec{r})$ is a multiplicative operator function, and not a non local operator as in HF. This makes it easier to solve KS equations.

These advantages have made KS-DFT the most widely used method for modeling the electronic structure of molecules and materials.[11,13-14]

1.2.3 The Kohn-Sham-Roothaan equations

The computational methods used to solve the KS equations are similar to those used to solve the HF equations. In both cases one solves the equations by the self-

consisted field method (SCF), and in both cases the equations are usually converted from partial differential equations into a linear algebra problem by expanding the orbitals as a linear combinations of the functions in a basis set $\{\phi_\mu(\vec{r})\}$,

$$\psi_i(\vec{r}) = \sum_{\nu}^{K} C_{\nu i}\phi_\nu(\vec{r}) . \tag{1.2.9a}$$

For simplicity, we will only consider the case of closed-shell systems, so that all of the KS orbitals are either doubly occupied or unoccupied. The representation of the electron density (Eq. 1.2.2) in the basis set is thus

$$\rho(\vec{r}) = 2\sum_{a=1}^{N/2}\sum_{\mu=1}^{K}\sum_{\nu=1}^{K} C_{\mu a}C^{*}_{\nu a}\phi_\mu(\vec{r})\phi^{*}_\nu(\vec{r}) . \tag{1.2.9b}$$

The KS equations (Eq. 1.2.7) take the form

$$\sum_{\nu}^{K} C_{\nu i}\int\phi^{*}_\mu(\vec{r})\hat{H}^{KS}\phi_\nu(\vec{r})d\vec{r} = \varepsilon_i\sum_{\nu}^{K} C_{\nu i}\int\phi^{*}_\mu(\vec{r})\phi_\nu(\vec{r})d\vec{r} \;\; ; \quad i = 1,2,...,K . \tag{1.2.10}$$

Here, $\hat{H}^{KS}$ is the Kohn-Sham Hamiltonian operator,

$$\hat{H}^{KS} \equiv -\frac{1}{2}\nabla^2 + v^{ext}(\vec{r}) + \int\frac{\rho(\vec{r}\,')d\vec{r}\,'}{|\vec{r}-\vec{r}\,'|} + V^{xc}[\rho(\vec{r});\vec{r}] . \tag{1.2.11}$$

Equations (1.2.10) can be expressed in matrix form,[6]

$$H^{KS}C = CS\varepsilon . \tag{1.2.12}$$

Here H^{KS} is the matrix representation of KS operator in the basis set $\{\phi_\mu\}$,

$$H^{KS} \equiv \begin{pmatrix} \langle \phi_1 | \hat{H}^{KS} | \phi_1 \rangle & \langle \phi_1 | \hat{H}^{KS} | \phi_2 \rangle & \cdots & \langle \phi_1 | \hat{H}^{KS} | \phi_K \rangle \\ \langle \phi_2 | \hat{H}^{KS} | \phi_1 \rangle & \langle \phi_2 | \hat{H}^{KS} | \phi_2 \rangle & & \langle \phi_2 | \hat{H}^{KS} | \phi_K \rangle \\ \vdots & \vdots & & \vdots \\ \langle \phi_K | \hat{H}^{KS} | \phi_1 \rangle & \langle \phi_K | \hat{H}^{KS} | \phi_2 \rangle & \cdots & \langle \phi_K | \hat{H}^{KS} | \phi_K \rangle \end{pmatrix}; \tag{1.2.13}$$

and S is the overlap matrix,

$$S \equiv \begin{pmatrix} \langle \phi_1 | \phi_1 \rangle & \langle \phi_1 | \phi_2 \rangle & \cdots & \langle \phi_1 | \phi_K \rangle \\ \langle \phi_2 | \phi_1 \rangle & \langle \phi_2 | \phi_2 \rangle & & \langle \phi_2 | \phi_K \rangle \\ \vdots & \vdots & & \vdots \\ \langle \phi_K | \phi_1 \rangle & \langle \phi_K | \phi_2 \rangle & \cdots & \langle \phi_K | \phi_K \rangle \end{pmatrix}. \tag{1.2.14}$$

C and ε are given by

$$C = \begin{pmatrix} C_{11} & C_{12} & \cdots & C_{1K} \\ C_{21} & C_{22} & & C_{1K} \\ \vdots & \vdots & & \vdots \\ C_{K1} & C_{K2} & \cdots & C_{1K} \end{pmatrix}, \tag{1.2.15}$$

$$\varepsilon = \begin{pmatrix} \varepsilon_1 & 0 & \cdots & 0 \\ 0 & \varepsilon_2 & & 0 \\ \vdots & \vdots & & \vdots \\ 0 & 0 & \cdots & \varepsilon_k \end{pmatrix}. \tag{1.2.16}$$

It is important to notice that:

I) Eq. (1.2.12) represents a system of nonlinear algebraic equations. These are called the Kohn-Sham-Roothaan equations.[59]

II) In general, the basis functions $\{\phi_\mu(\vec{r})\}$ are not orthogonal. So S is not always the identity matrix.

III) Eq. (1.2.12) represents a generalized eigenvalue problem. The matrices C and ε represent the eigenvectors and eigenvalues, respectively.

IV) The matrix elements of $\hat{H}_{\mu\nu}^{KS}$ can be split into the one-electron term, $\hat{H}_{\mu\nu}^{KS-core}$, the Coulomb term, $\hat{H}_{\mu\nu}^{KS-J}$, and the exchange-correlation term, $\hat{H}_{\mu\nu}^{KS-xc}$,

$$H_{\mu\nu}^{KS} = H_{\mu\nu}^{KS-core} + H_{\mu\nu}^{KS-J} + H_{\mu\nu}^{KS-xc}, \tag{1.2.17a}$$

$$H_{\mu\nu}^{KS-core} \equiv \int \phi_\mu^*(\vec{r})(-\frac{1}{2}\nabla^2 - \sum_A \frac{Z_A}{|\vec{r}-\vec{R}_A|})\phi_\nu(\vec{r})d\vec{r}, \tag{1.2.17b}$$

$$H_{\mu\nu}^{KS-J} \equiv \int\int \frac{\phi_\mu^*(\vec{r})\phi_\nu(\vec{r})\rho(\vec{r}\,')}{|\vec{r}-\vec{r}\,'|} d\vec{r}\,d\vec{r}\,' = 2\sum_{a=1}^{N/2}\sum_{\lambda}^{K}\sum_{\sigma}^{K} C_{\lambda a}C_{\sigma a}^* \int\int \frac{\phi_\mu^*(\vec{r})\phi_\nu(\vec{r})\phi_\lambda(\vec{r}\,')\phi_\sigma^*(\vec{r}\,')}{|\vec{r}-\vec{r}\,'|} d\vec{r}\,d\vec{r}\,',$$

... (1.2.17c)

$$H_{\mu\nu}^{KS-xc} = \int V^{xc}[\rho;\vec{r}]\phi_\mu^*(\vec{r})\phi_\nu(\vec{r})d\vec{r}\ . \tag{1.2.17d}$$

The KS-Roothaan equations are solved by transforming Eq. (1.2.12) into a standard eigenvalue, problem solving the transformed equations, and transforming the solutions back to the original form. The first step is accomplished by finding the matrix, D, that diagonalizes the overlap matrix S,

$$D^{-1}SD = 1. \tag{1.2.18}$$

Define the matrix C' as

$$C' = D^{-1}C. \tag{1.2.19}$$

The matrix representation of the KS equations, Eq. (1.2.7), can now be rewritten in the form of a standard eigenvalue problem,

$$H'^{KS}C' = C'\varepsilon. \tag{1.2.20}$$

Here $H'^{KS} \equiv D^{-1}HD$.

Because H'^{KS} depends on the electron density, it depends on the coefficients C'. So, as in HF, Eq. (1.2.20) is solved by a self-consistent field (SCF) approach:[6]

I) Specify the molecule geometry. (I.e, specify the nuclear charges Z_A and coordinates $\vec{R}_A$.) Choose a basis set, $\{\phi_\mu(\vec{r})\}$.

II) Calculate all the integrals that do not depend on the coefficients C:

$S_{\mu\nu}$, $H_{\mu\nu}^{KS-core}$, and $\iint \frac{\phi_\mu^*(\vec{r})\phi_\nu(\vec{r})\phi_\lambda(\vec{r}')\phi_\sigma^*(\vec{r}')}{|\vec{r}-\vec{r}'|} d\vec{r}\,d\vec{r}'$.

III) Diagonalize S to obtain the matrix D. (See Eq. (1.2.18).)

IV) Guess the electron density $\rho(\vec{r})$. (One common choice is to assume that the molecular density is close to the sum of atomic densities.[60])

V) Calculate the $H_{\mu\nu}^{KS-J}$ and $H_{\mu\nu}^{KS-xc}$ (Eq. 1.2.17c and 1.2.17d) using the current approximation to the electron density. Calculate $H_{\mu\nu}^{KS}$ (Eq. 1.2.17a) using the integrals computed in (II) and $H_{\mu\nu}^{KS-xc}$.

VI) Calculate the transformed Kohn-Sham matrix $H'^{KS} \equiv D^{-1}HD$

VII) Solve Eq. (1.2.20) by diagonalizing $H'^{KS}_{\mu\nu}$ to obtain C' and ε.

VIII) Calculate $C = DC'$.

IX) Construct the electron density, $\rho(\vec{r})$, from C using Eq. (1.2.9b).

X) Determine whether the procedure has converged. I.e., determine whether the new density of step (IX) is similar enough to the density that was used to construct $H_{\mu\nu}^{KS}$. If the procedure has not converged, return to step (V) using the new electron density.

XI) If the procedure has converged, then use the solution (C, ε, $H_{\mu\nu}^{KS}$, etc.) to calculate molecular and atomic properties.

Notice that the integrals in step (II) are only computed once at the beginning of the SCF procedure. But, in step (V), one uses the integrals computed in step (II) and adds

the Coulomb term (Eq. 1.2.17c) and the exchange-correlation term (Eq. 1.2.17d). The latter integral is difficult to compute and has to be calculated in every cycle in the SCF procedure. Hence step (V) is one of the most time consuming steps within the SCF procedure.

Among the molecular properties that can be computed with DFT, the one that is most important for chemical properties is the electronic energy, since this is the key ingredient in the potential energy surface, Eq. (1.1.3). Using Eqs. (1.2.3)-(1.2.4) we can write an expression for the KS energy in terms of the KS molecular orbitals,

$$E^{KS}[\psi_i] = -\sum_{i=1}^{N/2} \psi_i^*(\vec{r})\nabla^2\psi_i(\vec{r}) + 2\int \sum_{i=1}^{N/2} \psi_i^*(\vec{r})\psi(\vec{r})[v^{ext}(\vec{r}) + \frac{1}{2}\int \frac{\rho(\vec{r}')d\vec{r}'}{|\vec{r}-\vec{r}'|} + \varepsilon_{xc}(\vec{r})]d\vec{r} ,$$

$$E^{KS} \equiv -\sum_{i=1}^{N/2} \psi_i^*(\vec{r})\nabla^2\psi_i(\vec{r}) + \int \rho(\vec{r})v^{ext}(\vec{r})d\vec{r} + \frac{1}{2}\int\int \frac{\rho(\vec{r})\rho(\vec{r}')}{|\vec{r}-\vec{r}'|} d\vec{r}d\vec{r}' + \int \rho(\vec{r})\varepsilon_{xc}(\vec{r})d\vec{r} . \tag{1.2.21}$$

It is also possible to derive the expression of the energy in terms of the KS orbital energies:

$$E^{KS} = \sum_{i=1}^{N} \varepsilon_i - \frac{1}{2}\int\int \frac{\rho(\vec{r})\rho(\vec{r}')d\vec{r}d\vec{r}'}{|\vec{r}-\vec{r}'|} + E_{xc}[\rho(\vec{r})] - \int \rho(\vec{r})V^{xc}(\vec{r})d\vec{r} . \tag{1.2.22}$$

To derive Eq. (1.2.22) from Eq. (1.1.6), we used the fact that the KS orbitals, $\{\psi_i(\vec{r})\}$, form an orthonormal set, even though the basis set $\{\phi_\mu(\vec{r})\}$ might not be orthonormal.

As previously noted, the integrals associated with the exchange-correlation potential and energy,

$$H_{\mu\nu}^{KS-xc} = \int V^{xc}[\rho;\vec{r}]\phi_\mu^*(\vec{r})\phi_\nu(\vec{r})d\vec{r}\,,$$

$$E_{xc} = \int \varepsilon^{xc}[\rho;\vec{r}]\rho(\vec{r})d\vec{r} = \sum_i^N \sum_\mu^K \sum_\nu^K C_{\mu i} C_{\nu i}^* \int \varepsilon^{xc}(\rho)\phi_\mu(\vec{r})\phi_\nu^*(\vec{r})d\vec{r}\,,$$

can not be performed analytically. Efficient integration grids are needed to perform these integrations.[37-45] To give the reader an idea of the complexity of these integrals, the expression of these integrals in a simple local density approximation (LDA) is now given.

Dirac's exchange energy functional gives the exact exchange energy for the uniform electron gas:[61]

$$E_x^{Dirac} = \int \rho(\vec{r})\varepsilon_x^{Dirac}(\rho(\vec{r}))d\vec{r}\,, \qquad (1.2.23a)$$

$$\varepsilon_x^{Dirac}(\rho) = -\frac{3}{4}\left(\frac{3}{\pi}\right)^{1/3}\rho(\vec{r})^{1/3}, \qquad (1.2.23b)$$

$$V_x^{Dirac}(\vec{r}) = -\left(\frac{3}{\pi}\right)^{1/3}\rho(\vec{r})^{1/3}. \qquad (1.2.23c)$$

The correlation energy of the uniform electron gas can not be computed exactly, but it is accurately modeled by the correlation energy functional of Vosko-Wilkes-Nusair (VWN),[62]

$$E_c^{VWN} = \int \rho(\vec{r}) \varepsilon_c^{VWN}(\rho(\vec{r}))d\vec{r}\,, \tag{1.2.24a}$$

$$\begin{aligned}\varepsilon_c^{VWN}(\rho; r_s) = &-\frac{C}{2}[(1+x^3)\rho(1+\frac{1}{x})+\frac{x}{2}-x^2-\frac{1}{3}] \\ &-\frac{r_s}{3}\frac{d}{dr_s}\{\frac{Ae^2}{2}[\ln[\frac{y^2}{Y(y)}]+\frac{2b}{Q}\tan^{-1}(\frac{Q}{2y+b}) \\ &-\frac{by_0}{Y(y_0)}[\ln[\frac{(y-y_0)^2}{Y(y)}]+\frac{2(b+2y_0)}{Q}\tan^{-1}(\frac{Q}{2y+b})]\}\end{aligned}\,, \tag{1.2.24b}$$

$$V_c^{VWN}(\vec{r}) = \varepsilon_c^{VWN}(\rho) - \frac{1}{3}\frac{e^2}{2}\frac{c(y-y_0)-by_0y}{2(y-y_0)(y^2+by+c)}\,. \tag{1.2.24c}$$

Here:

$$x = r_s/21; \quad r_s = \left(\frac{3}{4\pi\rho}\right)^{1/3}$$

$$y = \sqrt{r_s},$$

$$Y(y) = y^2 + by + c,$$

$$Q = (4c - b^2)^{1/2},$$

$$y_0 = -0.104,$$

$$b = 3.72744,$$

$$c = 12.935,$$

$$A = 0.062.$$

In Chapter II, we develop and test a new method for integrating expressions like these.

1.3 The Quantum Theory of Atoms in Molecules

1.3.1 Introduction

As discussed in the last section, the Hohenberg-Kohn theorems established that the electron density can be used as the basic descriptor of electronic systems. This provides the foundation for DFT. DFT is primarily a quantitative theory of electronic structure. As such, DFT does not provide definitions for important *qualitative* chemical concepts like the chemical bond or the properties of atoms in molecules like atomic charges and energies.

The quantum theory of atoms in molecules (QTAIM) provides a way to fill the "concept gap" of DFT. QTAIM provides a formal definition for the concept of an atom within a molecule and a method for defining atomic properties based on quantum mechanical principles.[46,63-67] In addition, QTAIM provides precise mathematical definitions for important chemical concepts like the chemical bond, molecular structure, and atomic charges. QTAIM is a powerful and beautiful theory because of all these concepts are derived from the empirically observable molecular electron density.[46] Thus, QTAIM can be considered as a complementary theory to DFT.

1.3.2 The basics concepts

In QTAIM, chemical concepts like bonds and properties of atoms in molecules are defined using the topology, or shape, of the electron density. [46, 63-67]

The electron density, as any scalar field, generates a vector field through its gradient, $\nabla\rho(\vec{r})$. The density's critical points (i.e., points at which the gradient vanishes)

$$\nabla\rho(\vec{r}_c)=0, \tag{1.3.1}$$

have special physicochemical significance. For example, nuclei are associated with local maxima of the electron density. Sometimes there are also maxima that are not associated with the nuclei. These maxima are called non-nuclear attractors and only occur in special molecules at special geometries. Sodium and Lithium clusters are examples of molecules that exhibit non-nuclear attractors. Other critical points are also significant. For example, bond critical points are saddle points located in the "mountain pass" between two maxima in the electron density. Properties of the electron density (and/or other quantities) at a bond critical point can be used to characterize the nature of that chemical bond.

In QTAIM, atoms in molecules are defined by partitioning real space into non-overlapping regions called *atomic basins*. The boundary, S_{Ω_i}, of an atomic basin, Ω_i, is a surface that satisfies the zero-flux condition,

$$\nabla\rho(\vec{r}_s)\bullet\hat{n}_{\vec{r}_s}=0, \tag{1.3.2}$$

where $\hat{n}_{\vec{r}_s}$ is the unit vector normal to the surface at the point $\vec{r}_s$. From the definition of the atomic basin and the divergence theorem,[68] it follows that the integral of the Laplacian of the electron density over any atomic basin is zero,

$$\int_{\Omega_i}\nabla^2\rho(\vec{r})d\vec{r}=0. \tag{1.3.3}$$

Figure 1.2 shows some results from a QTAIM partitioning of the BF_3 molecule. The left-hand side of Figure 1.2a shows level curves of the electron density in the plane containing the atomic nuclei. The right-hand side of Figure 1.2a plots the vector field from the gradient of the density. In accord with Eq. (1.3.2), on the surface of the atomic basins, $\nabla\rho(\vec{r})$ is either parallel to the surface or $\nabla\rho(\vec{r}) = 0$ (at a critical point). Note that all of the gradient paths in a given atomic basin terminate at a maximum in the electron density that is associated with an atomic nucleus (or sometimes a non-nuclear attractor).

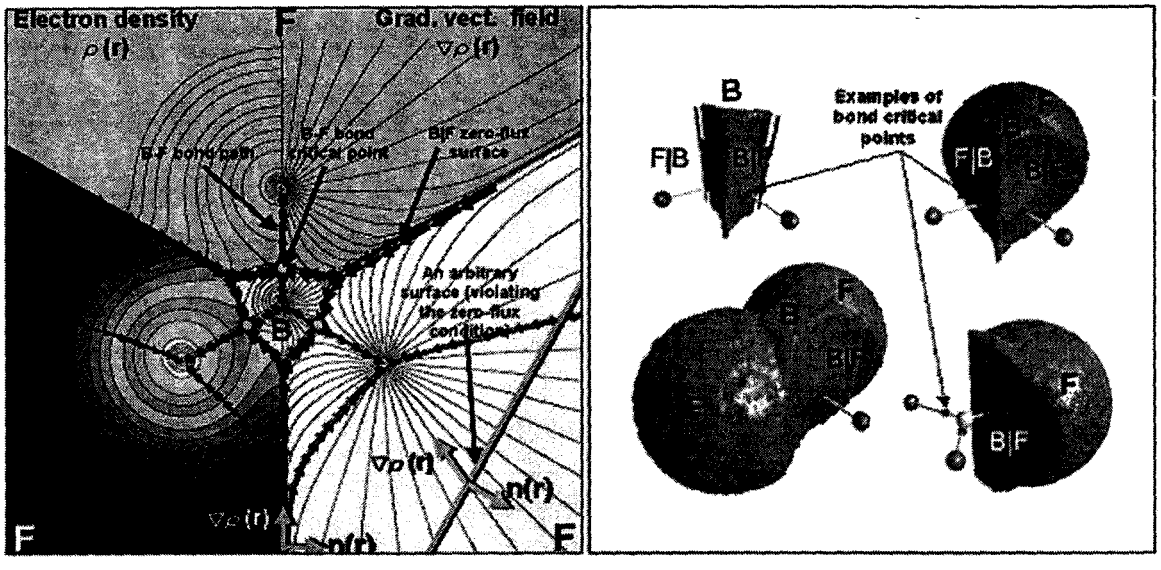

(a) **(b)**

Figure 1.2 QTAIM analysis of BF_3. **(a)** The main topological features of the electron density. **(b)** Three-dimensional pictures of the atomic basins. [Figure reproduced from Reference (66) with the permission from authors and publisher.]

All of the other critical points lie on the boundary between two atoms (bond critical points) or more than two atoms (so called "ring" and "cage" critical points). Figure 2b is a representation of the atomic volumes. Notice that each atomic volume contains exactly one atomic nucleus and that the bond critical points occur on the boundary surfaces between two atoms.

1.3.3 Atomic and molecular properties

In QTAIM, the value of a property, P, for an atom in a molecule is defined by the expectation value of an effective single-particle property density, $p(\vec{r})$, over the atom's basin, Ω_i,[46,63-67]

$$P(\Omega) = \int_{\Omega_i} p(\vec{r}) d\vec{r} \ . \tag{1.3.4}$$

Because the atomic basins fill space,

$$\mathbb{R}^3 = \bigcup_i \Omega_i \ , \tag{1.3.5}$$

the value of a molecular property, $P^{molecule}$, is equal to the sum of the corresponding atomic properties,

$$P^{Molecule} = \int_{R^3} p(\vec{r}) d\vec{r} = \sum_i \int_{\Omega_i} p(\vec{r}) d\vec{r} = \sum_i P(\Omega_i) . \tag{1.3.6}$$

As examples of atomic properties and property densities, we consider two different definitions for the atomic kinetic energy,[46]

$$K(\Omega) = \int_{\Omega} k(\vec{r})d\vec{r} = \int_{\Omega} \{-\frac{N}{2} \int \ldots \int \Psi^*(\vec{r},\vec{r}_2,\ldots,\vec{r}_N)\nabla^2\Psi(\vec{r},\vec{r}_2,\ldots,\vec{r}_N)d\vec{r}_2\ldots d\vec{r}_N\}d\vec{r}\,, \qquad (1.3.7)$$

$$G(\Omega) = \int_{\Omega} g(\vec{r})d\vec{r} = \int_{\Omega} \{\frac{N}{2} \int \ldots \int \nabla\Psi^*(\vec{r},\vec{r}_2,\ldots,\vec{r}_N) \bullet \nabla\Psi(\vec{r},\vec{r}_2,\ldots,\vec{r}_N)d\vec{r}_2\ldots d\vec{r}_N\}d\vec{r}\,. \qquad (1.3.8)$$

Ψ is the N-electron wave-function. It follows from Green's first identity and the zero flux condition, Eq. (1.3.3), that these two expressions for the kinetic energy of an atom in a molecule give the same result:

$$L(\Omega) = K(\Omega) - G(\Omega) = \int_{\Omega} [k(\vec{r}) - g(\vec{r})]d\vec{r} = -\frac{1}{4}\int_{\Omega} \nabla^2\rho(\vec{r})d\vec{r} = 0\,. \qquad (1.3.9)$$

The electronic energy of an atom in a molecule (AIM) can then be defined using the local virial theorem,

$$E_{\Omega} \equiv -K(\Omega) = -G(\Omega)\,. \qquad (1.3.10)$$

The total electronic energy is then computed as the sum of the atomic energies,

$$E = \sum_{\Omega_i}^{M} E_{\Omega_i}\,. \qquad (1.3.11)$$

The other important properties that will be considered in this thesis are the electrostatic moments of the AIM,[46]

$$\int_{\Omega_i} x^j y^k z^l \rho(\vec{r})d\vec{r}\,. \qquad (1.3.12)$$

The $j = k = l = 0$ moment represents the number of electrons in the AIM.

Notice that evaluating atomic properties typically requires numerical integration over regions with complicated shapes.[46-52] Although many numerical methods for computing atomic properties have been proposed, none of these methods is practical for large molecules. Even for small molecules, the time required to compute atomic properties is often one or two orders of magnitude greater than the time required to compute the electron density with Kohn-Sham DFT.[46-52] For example, it takes 30 minutes to perform a QTAIM atomic property analysis on the water molecule,[49] but only 30 seconds to compute the density with KS-DFT.

The most time-consuming and the most numerically ill-conditioned portion of traditional QTAIM algorithms is the explicit construction of the zero-flux surfaces. In Chapter 4, a grid-based method for computing atomic properties that does not require explicitly computing the zero-flux surfaces is presented. The resulting method appears to be one to two orders of magnitude faster than previous approaches.[47-52]

1.4 Integration Grids

1.4.1 Introduction

In the previous sections, we have learned that efficient numerical integration techniques are essential in both KS-DFT (Section 1.2) and QTAIM (Section 1.3). Numerical integration techniques for molecular problems are the unifying theme of this thesis. The purpose of this section is to provide the essential background for the

numerical integration methods considered here. Sections 1.4.2 provides a very brief overview of one-dimensional integration, with emphasis on the vocabulary of numerical integration methods. Section 1.4.3 and 1.4.4 introduce three-dimensional formulae for the unit cube. Section 1.4.5 discusses how one can transform integration formulae from the unit cube to other regions. Section 1.4.6 presents an entirely different approach based on the direct construction of atomic numerical integration formulas. Further mathematical details are deferred to later chapters, where they are presented in their chemical context.

1.4.2 One-dimensional numerical integration grids

Approximate numerical integration methods in one dimension are called quadrature formulae or simply one-dimensional integration grids.[69-71] Quadrature formulae have the same form as the Riemann sum approximation to the integral

$$\int_a^b f(x)p(x)dx = \sum_i^m w_i f(x_i) . \qquad (1.4.1)$$

The points, $x_i \in \mathbb{R}$, where the function is evaluated are sometimes referred to as nodes or abscissas. The grid points x_i are usually, but not always, located in the integration interval $[a,b]$. The grid points are usually not equally spaced. The numbers $w_i \in \mathbb{R}$ are called the integration weights. The w_i are usually, but not always, positive real numbers. The integration weights are usually not all equal. The nonnegative and integrable function $p(x)$ is called the weight function for the integration formula.[69-71]

The weights and nodes in a quadrature formula are usually chosen so that the integral, Eq. (1.4.1), is exact when $f(x)$ is a polynomial of degree D or less,

$$f(x)=\sum_{n=0}^{D} a_n x^n \,. \tag{1.4.2}$$

Sometimes, however, one considers trigonometric quadratures formulae, which are exact when $f(x)$ can be expanded as a Fourier series truncated at order D,

$$f(x)=a_0+\sum_{n=1}^{D} a_n \cos(\frac{2\pi n}{b-a})+b_n \sin(\frac{2\pi n}{b-a}) \,. \tag{1.4.3}$$

If the weights and nodes are chosen so that the degree of the quadrature formula is maximized, then they constitute a Gaussian quadrature formula. Gaussian quadrature formulae are important because the expansion of well-behaved functions in terms of polynomials (Eq. 1.4.2) or Fourier series (Eq. 1.4.3) is rapidly convergent. However, sometimes is useful to consider quadrature formulae that do not achieve the maximum possible degree of accuracy. For example, it is often convenient to choose the nodes so that they are nested (e.g., so that the points in the *m*-point quadrature formula are reused by the *2m*-point formula), even though nested quadrature formulae have lower degree than Gaussian quadrature formulae.[70-71]

In this dissertation, the most important quadrature formulae are the rectangle-rule formula[69-70] and the Clenshaw-Curtis formula.[72-73] Both formulae are nested, and both formulae are commonly defined for integrals over $[-1,1]$ with weight function, $p(x)=1$. Clenshaw-Curtis is a "polynomial-based" quadrature formula, while the rectangle-rule is

a "trigonometric" quadrature formula. If $f(-1)=f(1)=0$, the rectangle-rule is identical to the composite trapezoidal rule,[69] in which the trapezoidal rule is applied to each subinterval $[x_i, x_{i+1}]$,[69]

$$\int_{x_i}^{x_{i+1}} f(x)dx = \frac{(f(x_i)+f(x_{i+1}))(x_{i+1}-x_i)}{2}. \qquad (1.4.4)$$

Because we are primarily interested in integrating functions that, like the wave-function, vanish at the endpoints of integration, the contribution to expression (1.4.1) from nodes at the endpoints of the interval is zero. So these nodes are omitted.

The points and weights in the *m*-point rectangle-rule quadrature are given by,

$$x_i = -1+ih; \qquad i=1,...,m \qquad (1.4.5a)$$

$$w_i = h; \qquad i=1,...,m \qquad (1.4.5b)$$

$$h=\frac{2}{m+1}. \qquad (1.4.5c)$$

The points and weights in the *m*-point Clenshaw-Curtis quadrature are given by,[72-73]

$$x_i = -\cos(\frac{\pi(i-1)}{m-1}); \qquad i=2,...,m-1 \qquad (1.4.6a)$$

$$w_i = \frac{2}{m-1}[1-\frac{\cos(\pi(i-1))}{m(m-2)}-2\sum_{k=1}^{(m-3)/2}\frac{1}{4k^2-1}\cos(\frac{2\pi k(i-1)}{m-1})]; \qquad i=2,...,m-1. \qquad (1.4.6b)$$

The rectangle-rule and Clenshaw-Curtis quadrature formulae are nested if the number of points is chosen according to the rule $m_l = 2^l - 1$, where $l = 1,2,....$ We will often use the number as an index defining the "effort" associated with a given quadrature formulae. The nodes and weights for the m_l -point formula are then denoted as

$$\{x^l\} = x_1^l, x_2^l, ..., x_{m_l}^l \tag{1.4.7a}$$

$$\{w^l\} = w_1^l, w_2^l, ..., w_{m_l}^l . \tag{1.4.7b}$$

1.4.3 Three-dimensional numerical integration grid: the simple product grid

Higher dimensional quadrature formulae, which are often called cubature formulae, can be constructed from the tensor product of a quadrature formula associated with each dimension. For example, one can use the one-dimensional quadrature formulae defined in the previous section (Eq. (1.4.5)-(1.4.6)) to construct numerical integration rules for $[-1,1]^3$:

$$\int_{[-1,1]^3} f(\vec{x})d\vec{r} = \int_{-1}^{1}\int_{-1}^{1}\int_{-1}^{1} f(\vec{x})d\vec{x} = \sum_{i=1}^{m_{l_x}}\sum_{j=1}^{m_{l_y}}\sum_{k=1}^{m_{l_z}} w_i^{l_x} w_j^{l_y} w_k^{l_z} f(x_i^{l_x}, x_j^{l_y}, x_k^{l_z}) \equiv \sum_{p=1}^{M_L} w_p^L f(\vec{x}_p^L). \tag{1.4.8}$$

This family of numerical integration formulae is called the full-tensor product or, alternatively, the simple product grid.[70] The number of nodes in the simple product grid is the product of the number of nodes in each one-dimensional grid.

$$M_L = m_{l_x} m_{l_y} m_{l_z} . \tag{1.4.9}$$

Simple product grids can obviously be constructed for any number of dimensions. However, the number of grid points grows very rapidly (exponentially fast!) with increasing dimension. For example, one might commonly need a grid with ~70 points to evaluate a one-dimensional integral sufficiently accurately. Obtaining results of comparable accuracy for a three-dimensional integral using a simple product grid would require $70^3 = 343,000$ points! Fortunately, there are "sparse" tensor product formulae[70,74-75] that are more efficient than the simple product formula, Eq. (1.4.8). Such formulae are the topic of the next section.

1.4.4 Three-dimensional numerical integration grid: the sparse grid

Sparse tensor product formulae for the numerical integration of well-behaved multivariate functions contain only a small subset of the points in a simple product formula but achieve similar accuracy. The Smolyak cubature formula is the only sparse tensor product formula that we consider in detail in this thesis.[74-75] Like one-dimensional quadrature formulae, the Smolyak cubature formula is designed to ensure that all multivariate polynomials (or, alternatively, all multivariate Fourier series) up to certain degree are correctly integrated.

In n dimensions, the Smolyak cubature formula for integration over the hypercube $[-1,1]^n$ can be written in the form

$$\int_{[-1,1]^n} f(\vec{x})d\vec{x} \cong \sum_{L\le|\vec{k}|_1\le L+n-1} (-1)^{L+n-|\vec{k}|_1-1}\binom{n-1}{|\vec{k}|_1-L}\sum_{i_1}^{m_{l_1}}\cdots\sum_{i_n}^{m_{l_n}} w_{i_1}^{l_1}\ldots w_{i_n}^{l_n} f(x_{i_1}^{l_1},\ldots,x_{i_n}^{l_n}), \qquad (1.4.10)$$

which has the standard form of a cubature formula in $[-1,1]^n$,

$$\int_{[-1,1]^n} f(\vec{x})d\vec{x} = \sum_{i}^{M_L} w_i^L f(\vec{x}_i^L). \qquad (1.4.11)$$

In Eq. (1.4.10), l_i denotes the order of the one-dimensional quadrature formula for the i^{th} dimension and $L=1,2,...$ denotes the order of the Smolyak formula. $\vec{k}\in\mathbb{N}^n$ and $|\ |_1$ denotes the norm,

$$|\vec{k}|_1 \equiv k_1+\ldots+k_n, \qquad (1.4.12)$$

$\binom{m}{p}=\frac{m!}{p!(m-p)!}$ is the conventional combinatorial symbol. The number of points in the Smolyak cubature formula is $O(m_l l^{n-1})$,[71-72] which is much smaller than the number of points in the comparable simple product formula, $(m_l)^d$ (see Eq. 1.4.9). For example, a three-dimensional simple product of rectangular-rule grids (Eq. 1.4.8) with $L=7$ contains $(2^7-1)^3=2,048,383$ points, but the $L=7$ Smolyak cubature contains only 6,223 points. Further information about Smolyak cubature can be found in Chapters 2 and 3, where the method is applied to DFT calculations.

The Smolyak formula, Eq. (1.4.10), can be used to construct a *n*-dimensional cubature formula from any type of one-dimensional quadrature formula. However, the number of points in the Smolyak cubature is much smaller if nested grids are used.

1.4.5 A universal transformation for cubature grids

The domain of interest in most of physical and chemical problems is not the hypercube $[-1,1]^n$. For example, in fluid dynamics, engineering design,[76] and QTAIM,[46] the domain of integration usually has a very complicated shape. In molecular electronic structure theory, the domain of integration is usually unbound, $\mathbb{R}^n$. So we need a way to transform grids defined on $[-1,1]^n$ to other integration domains.

We use the conditioned distribution method[74] to perform the transformation. The conditional distribution method is a mapping between points in the hypercube, $\vec{\xi} \in [-1,1]^n$, and points in real space, $\vec{x} \in \mathbb{R}^n$. The specific form of the mapping depends on a non-negative integrable function, $P(\vec{r})$, through the expressions:

$$\xi_1(x_1) = -1 + 2\frac{\int_{-\infty}^{x_1}\int_{-\infty}^{\infty}\cdots\int_{-\infty}^{\infty} P(t_1,t_2,\ldots,t_n)dt_1dt_2\ldots dt_n}{\int_{-\infty}^{\infty}\int_{-\infty}^{\infty}\cdots\int_{-\infty}^{\infty} P(t_1,t_2,\ldots,t_n)dt_1dt_2\ldots dt_n},$$

$$\xi_2(x_1,x_2) = -1 + 2\frac{\int_{-\infty}^{x_2}\int_{-\infty}^{\infty} P(x_1,t_2,...,t_n)dt_2...dt_n}{\int_{-\infty}^{\infty}\int_{-\infty}^{\infty} P(x_1,t_2,...,t_n)dt_2...dt_n}, \tag{1.4.13}$$

$$\vdots$$

$$\xi_n(x_1,x_2,...,x_n) = -1 + 2\frac{\int_{-\infty}^{x_n} P(x_1,x_2,...,t_n)dt_n}{\int_{-\infty} P(x_1,x_2,...,t_n)dt_n}.$$

For the sake of simplicity and correctness, we will henceforth consider only the three-dimensional case of this transformation with $x_1 = x$, $x_2 = y$, $x_3 = z$. In three dimensions, the Jacobian matrix of the transformation is

$$J = \begin{pmatrix} \frac{\partial \xi_1}{\partial x} & 0 & 0 \\ \frac{\partial \xi_2}{\partial x} & \frac{\partial \xi_2}{\partial y} & 0 \\ \frac{\partial \xi_3}{\partial x} & \frac{\partial \xi_3}{\partial y} & \frac{\partial \xi_3}{\partial z} \end{pmatrix}. \tag{1.4.14}$$

The determinant of the Jacobian matrix follows from the form of the transformation, Eq. (1.4.13), and the fundamental theorem of calculus,[68]

$$|J|_{\vec{r}} = \left| \frac{\partial \xi_1}{\partial x} \frac{\partial \xi_2}{\partial y} \frac{\partial \xi_3}{\partial z} \right|_{\vec{r}} = K_p P(\vec{r}), \tag{1.4.15}$$

Here $K_p = \frac{1}{8}\left[\int_{-\infty}^{\infty} \int_{-\infty}^{\infty} \int_{-\infty}^{\infty} P(t_1,t_2,t_3) dt_1 dt_2 dt_3 \right]^{-1}$. The expressions in Eq. (1.4.13) can be used to explicitly map points in real space to the cube. Our purpose, however, is to map the integration points in $[-1,1]^3$ to integration points in real space. This requires the inverse mapping $\vec{r}(\vec{\xi}) = \vec{\xi}^{-1}(\vec{r})$. Suppose that one is given a point $(\xi_1^{(p)}, \xi_2^{(p)}, \xi_3^{(p)})$ in the unit cube. The inverse mapping is constructed, one coordinate at a time, from Eq. (1.4.13). Specifically, one first solves for x using the first equation, $\xi_1^{(p)} = \xi_1(x^{(p)})$, in Eq. (1.4.13). Then using this value of $x^{(p)}$, one solves for y using the second equation, $\xi_2^{(p)} = \xi_2(x^{(p)}, y^{(p)})$, in Eq. (1.4.13). These values of $x^{(p)}$ and $y^{(p)}$ are then used to solve the third equation $\xi_3^{(p)} = \xi_3(x^{(p)}, y^{(p)}, z^{(p)})$. Each step is this procedure requires solving a *univariate* nonlinear equation; we used the bisection method.[75] As long as $P(\vec{r})$ is positive, it follows from Eq. (1.4.15) that the mapping is one-to-one and invertible. So the nonlinear equations have a unique solution.

Using the transformation in Eq. (1.4.13) and the Jacobian determinant, Eq. (1.4.15), we can rewrite integrals in real space as integrals in $[-1,1]^3$ using the change of variables theorem,[68]

$$\int_{\mathbb{R}^3} f(\vec{x})d\vec{x} = \int_{[-1,1]^3} f(\vec{\xi}^{-1}(\vec{x}))|J|^{-1} d\xi_1 d\xi_2 d\xi_3 . \qquad (1.4.16a)$$

We can then perform integrations in $\mathbb{R}^3$ with respect to the weight function, $P(\vec{r})$, using the expression,

$$\int_{\mathbb{R}^3} f(\vec{x})d\vec{x} = \sum_{i=1}^{M_L} w_i^L \left|J\right|_{\vec{\xi}(\vec{x}_i^L)}^{-1} f(\vec{\xi}^{-1}(\vec{x}_i^L)) . \qquad (1.4.16b)$$

Here w_i^L, $\vec{\xi}_i^L$ and M_L denote the weights, points, and total number of points in the cubature grid on $[-1,1]^3$.

Equation (1.4.16b) is the key to applying the Smolyak-based cubature formula on $\mathbb{R}^3$. Integrals over domains with complicated shapes can be performed by choosing $P(\vec{r})$ so that it is zero outside the domain of integration. Because the boundary points are omitted in Eqs. (1.4.5) and (1.4.6), it is essential that $P(\vec{r})$ be chosen so that $f(\vec{r})/P(\vec{r})$ decays to zero asymptotically.

In chapters 2 and 3, we will use Eq. (1.4.16) and the Smolyak formula to integrate expressions that arise in DFT. What is the correct choice for the weight function $P(\vec{r})$ for applications to DFT? Pérez-Jordá, Becke and San-Fabián[40] noted that, how well a grid

performs for evaluating exchange-correlation energies, (cf. Eq. 1.2.8b) is correlated with how well it performs for integrating the electron density,

$$N = \int \rho(\vec{r}) d\vec{r} \,. \tag{1.4.17}$$

If we choose the weight function, $P(\vec{r})$, to resemble the electron density, then the function in the right side of Eq. (1.4.16b) will be nearly constant and the cubature formula will be very accurate. Choosing $P(\vec{r})$ to simply be the electron density is problematic because:

a) we do not know the electron density until the DFT calculation is completed,

b) even if we know the electron density, it is unlikely to be provided in a form conducive to rapid evaluation of the coordinate transformation, Eq. (1.4.13).

To address the first issue, we approximate the molecular density as the sum of atomic densities, $\rho_A(\vec{r})$, each centered at the location of corresponding atomic nucleus, $\vec{R}_A$. The resulting approximation is called the promolecular density,[79]

$$P(\vec{r}) = \rho_{pro}(\vec{r}) = \sum_A \rho_A(\vec{r} - \vec{R}_A) \,. \tag{1.4.18a}$$

We then approximate the atomic densities as the sum of Gaussian-type functions,

$$\rho_A(\vec{r}) = \sum_i C_{Ai} e^{-\alpha_{Ai} r^2} . \qquad (1.4.18b)$$

The coefficients and exponents in this equation are taken from the work of Constans and Carbó.[80] The Constans-Carbó fits are quite accurate, so the biggest approximation is Eq. (1.4.18a).

Figure 1.3 shows the results of the promolecular transformation Eq. (1.4.18a). In the simple product grid using the rectangle-rule (first row of Figure 1.3), the points are uniformly distributed in $[-1,1]^3$. In $\mathbb{R}^3$, the form of the transformation indicates that the probability distribution function for the grid points is proportional to the promolecular density. The second and third rows in Figure 1.3 show the results for the Smolyak cubature using the rectangle-rule and the Clenshaw-Curtis quadrature formulae, respectively. These formulae contain roughly the same number of points as the simple product rule in the first row, but their order of accuracy, L, is *much* higher. Notice that, once again, the transformation concentrates points where the promolecular density is large (near the nuclei and in the bonding regions between them).

1.4.6 Atomic-center grids

To evaluate the accuracy of the transformed Smolyak grids discussed in previous sections, we implemented these grids in the Kohn-Sham-DFT program deMon2k[81] and compared the results to those obtained using the default integration method in that

program. We also used the default grids in deMon2k to evaluate atomic properties in QTAIM.

The purpose of this section is to present the ideas behind the integration method in deMon2k, which are based on Axel Becke's atomic center decomposition.[45] Becke-type atomic-center grids are easily the most popular integration method in DFT, and are also used in many other electronic structure programs.[37-45] There are many minor variations of Becke's approach; here we will discuss one of the simplest versions.

Atomic-centered grids are based on partitioning integrals into atomic contributions, which can then be integrated using standard techniques. First, one constructs a partition of unity into atomic contributions,

$$\sum_{A=1}^{M} \omega_A(\vec{r}) = 1. \tag{1.4.19}$$

$$\omega_A(\vec{r}) \geq 0. \tag{1.4.20}$$

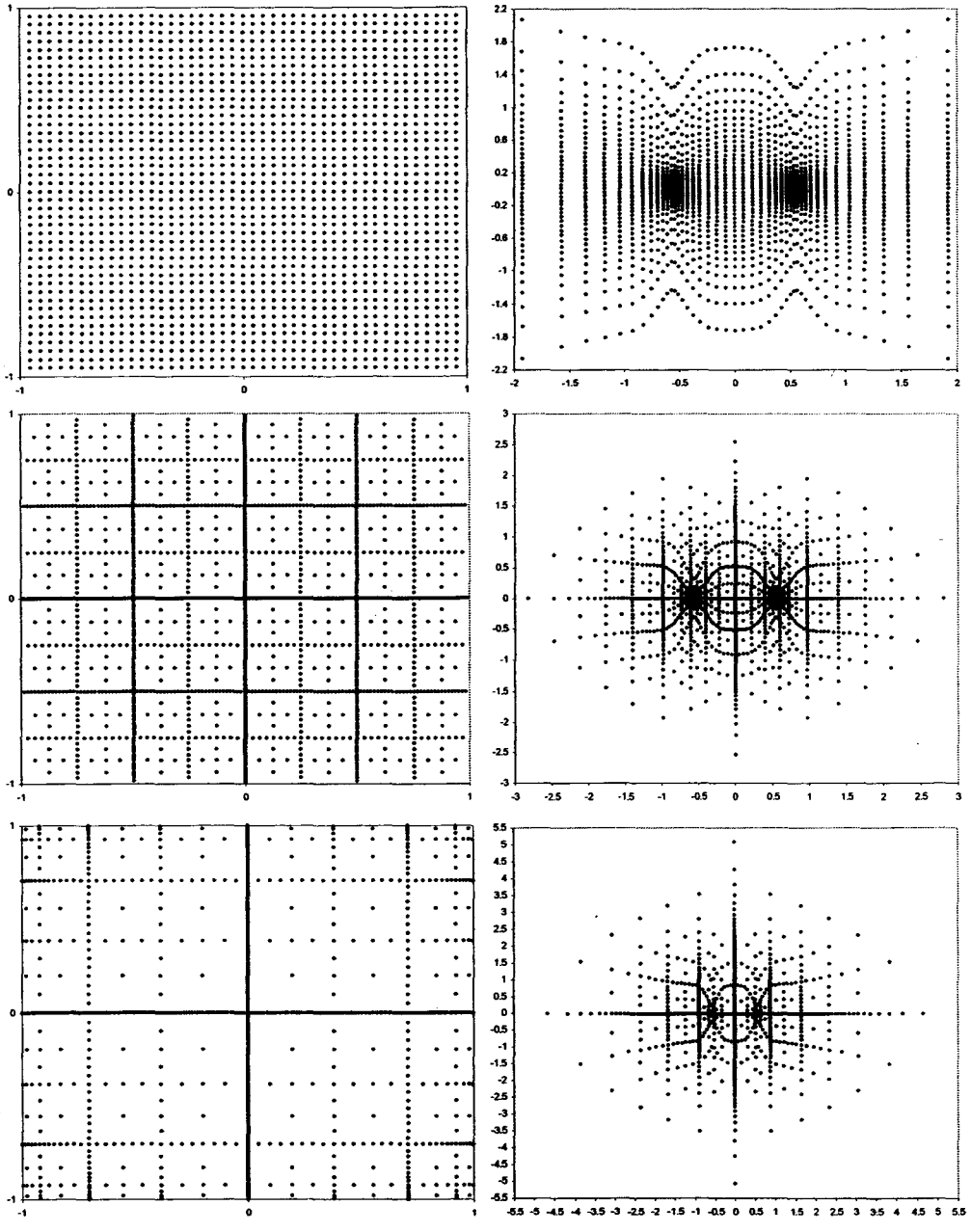

Figure 1.3. Grids in the unit cube (left column) and real space (right column) for N_2 at its equilibrium geometry. Only points in the x-y plane are shown. The first row shows simple product grids using the rectangle-rule. The Smolyak grids obtained using the rectangle-rule and the Clenshaw-Curtis formulae are in the second and third rows, respectively. Units are Angstroms.

Each atomic weight function, $\omega_A(\vec{r})$, is equal to one close to the atomic nucleus A and equal to zero near other atomic nuclei and far away from nucleus A. Becke accomplished this using fuzzy Voronoi Polyhedra.[45] The Voronoi Polyhedron corresponding to atom A consist of all points in space that are closer to nucleus A than any other nucleus. (In solid state physics, the Voronoi polyhedron is called the Wigner-Seitz cell.) It is difficult to perform an integral over an irregular shaped atomic Voronoi polyhedron, so the boundaries of the polyhedron are blurred by choosing $\omega_A(\vec{r})$ so that it changes smoothly from a value of one in the interior of the polyhedron to a value of zero outside of it. The atomic volumes defined by $\omega_A(\vec{r})$ are called fuzzy Voronoi Polyhedra. More information about how to construct the atomic weight functions may be found in references (40) and (43).

Using the atomic partition of unity in Eq. (1.4.19), any function can be divided into atomic contributions,

$$f(\vec{r}) = \sum_{A=1}^{M} f_A(\vec{r}), \tag{1.4.21}$$

$$f_A(\vec{r}) \equiv \omega_A(\vec{r}) f(\vec{r}). \tag{1.4.22}$$

The integral of $f(\vec{r})$ can then be obtained by adding together the integrals of the atomic contributions,

$$I = \int f(\vec{r}) d\vec{r} = \int \sum_{A=1}^{M} f_A(\vec{r}) d\vec{r} = \sum_{A=1}^{M} \int f_A(\vec{r}) dr \equiv \sum_{A=1}^{M} I_A. \tag{1.4.23}$$

The atomic integrations can be performed using a spherical quadrature formula. In spherical coordinates, the atomic integrals are written as

$$I_A = \int_0^{\infty} r^2 [\int_0^{2\pi} \int_0^{\pi} f_A(r,\theta,\phi) r^2 \sin\theta d\theta d\phi] dr \,. \qquad (1.4.24)$$

This type of integral is evaluated using a tensor product between a radial integration formula (for the outer integral) and angular cubature formula (for the integration over solid angle). The angular cubature exactly integrates all spherical harmonics up to a specific order, l. deMon2k uses Lebedev cubature formulae of various orders (up to $l = 59$) for the angular integration.[42] The radial quadrature is usually constructed by taking a standard quadrature formula on $[-1,1]$ and transforming it to $(0,\infty)$. deMon2k uses a Gauss-Chebyshev and the logarithmic transformation,[42]

$$r_i = \frac{1}{\ln(2)} \ln(\frac{2}{1-x_i}), \qquad (1.4.25)$$

for this purpose. Performance benchmarks for the integration method in deMon2k can be found in references (41) and (42).

1.5 Overview

The rest of this thesis is organized as follows.

In Chapter 2, we present the results from testing the Smolyak transformed grids introduced in Section 1.4. In order to test these grids we implemented them as the

numerical integrator for the exchange-correlation energy and potential (see Eqs. (1.2.17), (1.2.23), and (1.2.24)) in a modified version of deMon2k.[81] Then we evaluated the grids' ability to reproduce ground-state energies, equilibrium geometries, and atomization energies for a set of representative molecules. This chapter is an article accepted for publication in the *Journal of Chemical Physics*.

In Chapter 3, we extend the transformed Smolyak procedure to different dimensions and present results for $n=1, n=2, n=3,$ and $n=6$. For the three-dimensional case, the grids are applied to compute atomic interactions within the Gordon-Kim model. The six-dimensional integrals are based on the exchange energy model of Lee and Parr.[12] This chapter in an article submitted (on 03/28/08) to the *Journal of Physics A*.

Chapter 4 shows the generalization of the Smolyak construction for interpolating and differentiating multivariate functions. We discuss these schemes' potential application in both basis-set-based and basis-set-free calculations within the electronic structure theory problem. We published these results as a book chapter in *Quantum Chemistry Research Trends*; Mikas P. Kaisas (Editor) (Nova Science Publisher: New York, 2007).

Chapter 5 describes a novel grid-based method for computing atomic properties within QTAIM. We also implemented this method in deMon2k. We tested the

performance of our method by computing QTAIM energies, charges, dipole moments, and quadrupole moments for a set of representative molecules. This chapter is an article submitted (on 02/19/2008) to the *Journal of Computational Chemistry*.

Finally, in Chapter 6, we state our conclusions and discuss prospects for future work.

1.6 References for chapter 1

1. R. M. Martin, *Electronic Structure. Basic Theory and Practical Methods*. Cambridge: Cambridge University Press, 2004.

2. J. C. Slater, *Quantum Theory of Molecules and Solids.* New York: McGraw-Gill, 1979.

3. J. Kohanoff, *Electronic Structure Calculations for Solids and Molecules: Theory and Computational Methods*. Cambridge: Cambridge University Press, 2006.

4. McWeeny, R. *Methods of Molecular Quantum Mechanics*. London: Academic Press, 1992.

5. Ashcroft, N. W., and Mermin N. D. *Solid State Physics.* New York: Montreal: Holt, Rinehart and Winston, 1976.

6. A. Szabo, and N. S. Ostlund *Modern Quantum Chemistry. Introduction to Advanced Electronic Structure Theory*. New York: Dover Publications Inc., 1989.

7. T. Veszprémi, and M. Fehér *Quantum Chemistry*. USA: Kuwler Academic/Plenum Publishing (1999).

8. D. J. Wales. *Energy Landscapes.* Cambridge: Cambridge University Press, (2003).

9. P. Hohenberg, and W. Kohn. Phys. Rev. 136, B864 (1964).

10. W. Kohn, and L. Sham. Phys. Rev. 140, A1133 (1965).

11. W. Kohn. Rev. Mod Phys. 51, 1253 (1999).

12. W. Yang and R. G. Parr. *Density Functional Theory of Atoms and Molecules*. New York: Oxford University Press, Inc. (1989).

13. R. O. Jones and O. Gunnarson, Rev. Mod. Phys. 61, 689 (1989).

14. Dreizler, R. M. and Gross, E. K. U. *Density functional theory: an approach to the quantum many-body problem*. New York: Springer-Verlag (1990).

15. Goedecker, S. Rev. Mod. Phys. 71, 1085 (1999).

16. Thomas, L. H. Proc. Camb. Philol. Soc. 23, 542 (1927).

17. Fermi, E. Z. Phys. 48, 73 (1928).

18. Koopmans, T. Physica 1, 104-113, (1934).

19. Cances, E., and Le Bris, C. Math Model and Num Ana 34, 749 (2000).

20. Pulay, P. J. Comput. Chem. 3, 556 (1982).

21. Cances, E., and Le Bris, C. *Int. J. Quantum Chem.* 79, 82 (2000).

22. Levy, M., and Perdew J. P. *J. Chem. Phys.* 84, 4519 (1986).

23. Scott, A. P., and Radom, L. *J. Chem. Phys.* 100, 16502 (1996).

24. Peterson, K. A. *J. Chem. Phys.* 102, 262 (1995)

25. Tong, W., Morrison, R. C., and Day, O. W. *Int. J. Quantum Chem.* 60, 411 (1996).

26. Roos, B. O., Anderson K., Fulscher, M. P., Malmquist, P. A., Serrano-Andres, L., Pierloot, K., Merchan, M. *Adv. Chem. Phys.* 93, 219 (1996).

27. Cramer, C. J., Wloch, M., Piecuch, C., Puzzarini, C., Galdiardi, L. J. Phys. Chem. A 110, 1991 (2006).

28. Cramer, C. J., B. A. Smith, Tolman, W. B., J. Am. Chem. Soc. 118, 11283 (1996).

29. Marti, K. H., Ondik, I. M., Moritz, G., Reiher, M. *J. Chem. Phys.* 128, 014104 (2008).

30. Head-Gordon, M. J. Phys. Chem. 100, 13213 (1996).

31. Raghavachari, K., Anderson, J. B. J. Chem. Phys. 100, 12960 (1996).

32. Defranceschi, M., and Delhalle (Editors), *Numerical Determination of the Electronic Structure of Atoms, Diatomic and Plolyatomic Molecules.* Norwell (MA): Kluwer Academic Publishers, 1989.

33. Artacho, E., Sánchez-Portal, D., Ordejón, P., García, and Soler J. M., Phys. Status Solidi B 215, 809 (1999).

34. Ordejón P., Artacho, E., and Soler J. M., Phys. Rev. B 53,10441 (1996).

35. Yang, W. T., Phys. Rev. Lett. 66, 1438 (1991).

36. Li, X. P., Nunes, W., Vanderbilt, D. Phys. Rev. B 47, 10891 (1993).

37. M. R. Pederson and K. A. Jackson, Phys. Rev. B 41, 7453 (1990).

38. G. te Velde and E.J. Baerends, J. Comput. Phys. 99, 84 (1992).

39. P. M. W. Gill, B. G. Johnson, and J. A. Pople, Chem. Phys. Lett. 209, 506 (1993).

40. J. M. Pérez-Jordá, A. D. Becke, and E. San-Fabián, J. Chem. Phys. 100, 6520 (1994).

41. M. Krack and A. M. Köster, J. Chem. Phys. 108, 3226 (1998).42. A. M. Köster, R. Flores-Moreno, and J. Ulises-Reveles, J.Chem. Phys. 121, 681 (2004).

43. S. Chien and P. M. W. Gill, J. Comput. Chem. 27, 730 (2006).

44. S. T. Brown, L. Fusti-Molnar, and J. Kong, Chem. Phys. Lett. 418, 490 (2006). J. Kong, S. T. Brown, and L. Fusti-Molnar, J. Chem. Phys. 124, 094109-1 (2006).

45. A. D. Becke, J. Chem. Phys. 88, 2547 (1988).

46. R. F. W. Bader, *Atoms in Molecules: A Quantum Theory*, Clarendon Press, Oxford (1990).

47. J. Cioslowsky and B. B. Stefanov, Mol. Phys. 84, 707 (1995).

48. B. B. Stefanov and J. Cioslowsky, J. Comput. Chem. 16, 1394 (1995).

49. P. L. A. Popelier, Mol. Phys. 87, 1169 (1996).

50. P. L. A. Popelier, Comp. Phys. Commun. 108, 180 (1998).

51. G. Henkelman, A. Arnalsson, and H. Jónsson Comput., Mater Sci. 36, 354 (2006).

52. E. Sanville, S. D. Kenny, R. Smith, and G. Henkelman, J. Comput. Chem. 28, 899 (2007).

53. A. D. Becke, Ph. D. dissertation, McMaster University, 1981; J. Chem. Phys. 76, 6037 (1982); 78, 4787 (1983).

54. A. D. Becke, Numol, Intern. J. Quantum Chem. Symp. 23, 1280 (1989).

55. L. Laaksonen, D. Sundholm, and P. Pyykkö, Int. J. Quantum Chem. 27, 601 (1985).

56. J. R. Chelikowsky, N. Troullier, and Y. Saad, Phys. Rev. Lett. 72, 1240 (1994).

57. J. P. Perdew, and S. Kurth, in Density Functionals: Theory and Applications, edited by D. Joubert. Berlin: Springer (1998)

58. Perdew, J. P., Ruzsinszky, A., Csonka, G. I., Vydrov, O. A., Scuseria, G. E., Staroverov, V. N., Tao, J. Phys. Rev. A 76, 040501(R), (2007).

59. C. C. J. Roothaan, Rev. Mod. Phys. 23, 69 (1951).

60. J. Harris, Phys. Rev. B 31, 1770 (1985).

61. P. A. M. Dirac, Proc. Cambridge Philos. Soc. 26, 376 (1930).

62. S. H. Vosko, L. Wilk, and M. Nusair, Can. J. Phys. 58, 1200 (1980).

63. C. F. Matta and R.J.Boyd (editors), *The Quantum Theory of Atoms in Molecules. From Solid State to DNA and Drug Design.* Wiley-VCH, Weinheim (2007).

64. P. L. A. Popelier, *Atoms in Molecules. An Introduction* .Prentice Hall, Edinburg (2000).

65. R. F. W. Bader, Monatshefte für Chemie 136, 819 (2005).

66. C. F. Matta and R.J.Boyd in *The Quantum Theory of Atoms in Molecules. From Solid State to DNA and Drug Design.* C. F. Matta and R.J.Boyd (Editors), Wiley-VCH, Weinheim (2007).

67. R. F. W. Bader in *The Quantum Theory of Atoms in Molecules. From Solid State to DNA and Drug Design.* C. F. Matta and R.J.Boyd (Editors), Wiley-VCH, Weinheim (2007).

68. S. Lang, *Calculus of Several Variables.* Springer-Verlag, New York (1987).

69. R. L. Burden and J. D. Faires, *Numerical Analysis*, Belmont (2005).

70. P. J. Davis and P. Rabinowitz, *Methods of numerical integration.* Academic Press. Florida (1984).

71. Gautschi, W. *Orthogonal Polynomials: Computation and Approximation.* New York: Oxford UP, 2004.

72. W. Fraser and M. W. Wilson, SIAM Review **8**, 322 (1966).

73. C. W. Clenshaw and A. R. Curtis, Numerische Mathematik **2**, 197 (1960).

74. E. Novak and M. Griebel, Numerical Algorithms 18, 209 (1998).

75. E. Novak and K. Ritter, Numer. Math. 75, 79 (1996).

76. P. Knupp and S. Steinberg, *Fundamentals of Grid Generation.* Florida: CRC Press, 1993.

77. L. Devroye, (Springer-Verlag, New York, 1986)

78. W. H. Press, B. P. Flannery, S. A. Teukolsky and T. Vetterling, *Numerical Recipes in Fortran*, Cambridge University Press (1992).

79. F. L. Hirshfeld Theor. Chim. Acta 44, 129 (1977).

80. P. Constans and R. Carbó, J. Chem. Inf. Sci. 35, 1046 (1995); See http://www.molspaces.com.

81. *deMon2k,* A. M. Köster, P. Calaminici, M. E. Casida, R. Flores-Moreno, G. Geudtner, A. Goursot, T. Heine, A. Ipatov, F. Janetzco, J. M. del Campo, S. Patchkovskii, J. U. Reveles, D. R. Salahub, and A. Vela, deMon developers 2006. See http://www.demon-software.com

82. N. Godbout, D. R. Salahub, J. Andzelm, and E. Wimmer, Can. J. Chem. 70, 560 (1992).

"...Nor have I ever observed that, through the method of disputations practiced in the schools, any truth has been discovered that had until then been unknown. For, so long as each person in the dispute aims at winning, he is more concerned with making much out of probability than with weighing the arguments on each side; and those who have long been good advocates are not, on that account, afterward better judges."

R. Descartes, "Discourse on Method" (1637).

Chapter 2

NUMERICAL INTEGRATION OF EXCHANGE-CORRELATION ENERGIES AND POTENTIALS USING TRANSFORMED SPARSE GRIDS*

* The content of this chapter was accepted (24/03/08) as an article in the *Journal of Chemical Physics*. (Authors: Juan I. Rodríguez, David C. Thompson, Paul W. Ayers, and Andreas M. Köster.)

2.1 Statement of the problem

To test the utility of the integration scheme introduced in Section 1.3, we implemented the transformed Smolyak grids in a development version of the deMon2k density-functional theory program, where it is used to evaluate integrals of the exchange-correlation energy density and the exchange-correlation potential. In this chapter we present our "proof of principle" results: ground state energies, atomization energies and molecular geometries are accurately computed. Our results show that the transformed Smolyak grids are suitable as the numerical integrator in basis-set-set programs like deMon2k. The biggest advantages of the grid are its flexibility (it is easy to change the number and distribution of grid points) and its "whole molecule" nature. The latter feature is potentially helpful for basis-set-free computational algorithms.

2.2 Introduction

Computational evaluation of expectation values in quantum mechanics requires numerical integration techniques. This motivates studies like the present paper, which focuses on new approaches to numerical integration. In particular, we are interested in density-functional theory (DFT) methods for molecular electronic structure.[1,2]

In conventional wavefunction-based electronic structure methods, one can avoid numerical integration by expanding the wavefunction in terms of intelligently chosen basis functions (e.g., Gaussians).[3-5] This is not true in DFT, however, because some of the

functionals that need to be evaluated are very nonlinear. In particular, the integrals associated with the exchange-correlation energy,

$$E_{xc}[\rho] = \int \varepsilon_{xc}[\rho;\mathbf{r}]d\mathbf{r} \tag{2.2.1}$$

and the exchange-correlation potential,

$$\langle \rho v_{xc} \rangle = \int \rho(\mathbf{r}) v_{xc}[\rho;\mathbf{r}]d\mathbf{r} = \int \rho(\mathbf{r}) \frac{\delta E_{xc}[\rho]}{\delta \rho(\mathbf{r})} d\mathbf{r} \tag{2.2.2}$$

usually cannot be evaluated analytically.

One is tempted, perhaps, to evaluate the integrals that arise using standard off-the-shelf subroutines. This is satisfactory for very small systems. However, DFT is primarily applied to molecules that are too large for wavefunction-based electronic structure methods. Evaluating Eqs. (2.2.1) and (2.2.2) for systems containing tens, hundreds, or even thousands of atoms requires efficient numerical integration techniques that are custom-built for DFT problems.

Many of the most efficient DFT integration grids are based on the techniques pioneered by Axel Becke.[6] He started by decomposing real space into (slightly-overlapping) atomic regions—typically fuzzy Voronoi polyhedra. Then, the atomic contributions to the molecular integral are individually approximated using numerical integration grids. The atomic grids are a tensor-product between a radial quadrature formula (Gauss-Chebyshev, Gauss-Legendre, Euler-McLaurin, multi-exponential,[7] etc.) and an angular quadrature formula (usually one of the Lebedev formulae[8-12]).

Most molecular DFT programs use some variant of the Becke integration scheme. Among the most important variants are those that "prune" away some of the grid points, so that the number of angular points varies between radial shells.[7,13-22] Pruning generates optimized sparse-tensor product grids, which give much better accuracy for a given computational cost. However, like basis-set-driven integration methods (and unlike the original Becke method), it is not easy to systematically adjust the accuracy of these grids. This can be overcome by adaptively choosing the number of angular points to achieve a user-specified accuracy.[15,23,24] Extremely high accuracy can be obtained by suitably tuning the number of radial and angular points, although the infinite accuracy limit cannot be obtained because the conventional Lebedev angular grids are not known to arbitrarily high orders. In practice this is not a problem, and the 59^{th}-order formula implemented in most programs is sufficient for all purposes.[10,11] Even if it were not, a 131^{st} order formula is known and could be used, if needed.[12] Usually, much lower orders suffice.

Although grids based on atomic-center decomposition have excellent computational accuracy/computational cost for integration, they are sometimes inconvenient. Some fast numerical methods are most efficient for grids of regular points, because finite-difference formulae and fast-Fourier transformation are simplest on those grids. This has motivated attempts to adapt atom-decomposed grids to numerical

methods, either directly[25-30] or by interpolating the irregular point pattern from the atomic grids onto an underlying regular grid.[31,32]

Alternatively, one can use whole-molecule grids. Most whole-molecule grids are built from uniform grids[33-36] or hierarchically refined uniform grids.[37-55] However, because the physically important portion of the molecular electron density typically ranges over six orders of magnitude (even more, for molecules containing heavy atoms), hierarchical refinement is rarely efficient unless pseudopotentials are used to excise the core electrons. Wavelet-based approaches are similar to the other hierarchical refinement techniques; practical calculations using wavelets typically employ pseudopotentials also.[56-58]

The other approach to whole-molecule grids uses a transformation of coordinates to deform a regular grid so that the grid points are concentrated in regions where the electron density is high and depleted in regions where the electron density is low. This paper makes a contribution in this area, which was pioneered by Gygi and Pérez-Jordá.[59-64] In fact, our approach can be viewed as a generalization of what Pérez-Jordá proposed in the following senses: (a) our transformation of coordinates is more general and (b) our underlying grid has fewer points than an ordinary regular grid. One advantage of our more general transformation is that it facilitates non-pseudopotential calculations.

2.3 Description of the method

2.3.1 Overview

There are many approaches for constructing very efficient integration grids on the unit cube, $[0,1]^3$. (See, for example, references [65-67].) However, many of these approaches are not easily extended to high-accuracy grids, and most of them give grids that are not nested. These difficulties are not present in Smolyak's method for constructing cubature grids, which is the focus of this paper.[68] The Smolyak approach can be used to produce nested grids, which can be systematically refined to arbitrarily high order. Smolyak grids can be constructed from the simple product grids employed by Gygi and Pérez-Jordá by pruning away most of the grid points and reweighting the few that remain. Although the Smolyak grids have many fewer points than the corresponding simple product grids, for sufficiently smooth integrands, the order of accuracy is the same.[69-73] The Smolyak method is introduced in the next section, II.B.

Given an efficient grid on the unit cube, we need to transform the grid to real space. We do this using the conditional distribution method commonly employed in the Monte Carlo literature;[74] this is the same mathematical idea Pérez-Jordá used in his work.[63,75] This allows us to transform an integration rule on the unit cube $[0,1]^3$ to an integration rule in real space with respect to an arbitrary positive-definite weight

function, $(-\infty,\infty)^3_{w(\mathbf{r})}$. The details of our transformation procedure will be reviewed in II.C.

Having constructed grids that extend over the appropriate domain, we subsequently tested them as the numerical integrator in a modified version of *deMon2k*, a basis-set-based DFT package.[76] We evaluated the grids' ability to reproduce ground-state energies, molecular geometries and exchange-correlation energies. Results of these tests are presented in section III.

For our calculations in *deMon2k*, we used the DZVP Gaussian basis set[77] and the local-spin density approximation with the exchange functional of Dirac and the correlation functional of Vosko, Wilk, and Nusair.[78-80] Unless stated otherwise, we used the default settings for the electronic energy calculations. The grid generation, energy optimization, and geometry optimization were all performed without exploiting molecular symmetry. We did not use density-fitting to simplify integral evaluations.[81,82] Geometry optimizations were performed using a quasi-Newton algorithm and were considered to be converged when the root-mean-square force on the atoms was less than 0.0003 a.u..[83]

2.3.2 Grids on the unit cube

A. Theory of Multi-Dimensional Integration

We can approximate a function, $f(\mathbf{r}) = f(x,y,z)$, whose domain is the unit cube $[0,1]^3$, by expanding the function in terms of orthogonal polynomials,

$$f(x,y,z)=\sum_{k=0}^{\infty}\sum_{l=0}^{\infty}\sum_{m=0}^{\infty}a_{klm}P_k(x)P_l(y)P_m(z), \tag{2.3.1}$$

or using a (half-range) Fourier series,

$$f(x,y,z)=\sum_{k=0}^{\infty}\sum_{l=0}^{\infty}\sum_{m=0}^{\infty}c_{klm}\cos(k\pi x)\cos(l\pi y)\cos(m\pi z). \tag{2.3.2}$$

The asymptotic convergence of the coefficients in these expansions is determined by the smoothness of the function being expanded.[84,85] For functions that are r-times differentiable,

$$\left|\frac{\partial^{n_x}\partial^{n_y}\partial^{n_z}f(x,y,z)}{\partial x^{n_x}\partial y^{n_y}\partial z^{n_z}}\right|<\infty \qquad n_x+n_y+n_z\le r, \tag{2.3.3}$$

the asymptotic decay of the expansion coefficients is

$$|a_{klm}|:\ |c_{klm}|:\ \max(k,l,m)^{-r}. \tag{2.3.4}$$

The decay rate is much faster if the r^{th}-order mixed derivatives are also bounded:

$$\left|\frac{\partial^{n_x}\partial^{n_y}\partial^{n_z}f(x,y,z)}{\partial x^{n_x}\partial y^{n_y}\partial z^{n_z}}\right|<\infty \qquad \max(n_x,n_y,n_z)\le r \tag{2.3.5}$$

$$|a_{klm}|:\ |c_{klm}|:\ (k+l+m)^{-r}. \tag{2.3.6}$$

For functions whose differentiability supersedes even this, the coefficients in the expansion converge even faster.[84-86]

The integrands associated with molecular quantum mechanics and density-functional theory have bounded mixed derivatives.[87] So the best integration formulae for

our applications will integrate correctly all polynomials through a certain degree, $D = k+l+m$. I.e., the integration weights, $\{w_i\}_{i=1}^{M_D}$ and points, $\{(x_i,y_i,z_i)\}_{i=1}^{M_D}$, should be chosen so that

$$\int_0^1\int_0^1\int_0^1 P_k(x)P_l(y)P_m(z)\,dxdydz = \sum_{i=1}^{M_D} w_i P_k(x_i)P_l(y_i)P_m(z_i), \qquad (2.3.7)$$

$$\text{for all } |k+l+m| \le D.$$

Such a formula is said to be polynomially exact through degree D. In analogy to the one-dimensional case, an integration formula that is exact for polynomials of degree D or less and contains the fewest possible points is called a *Gaussian cubature formula.* [88,89] The number of points in 3-dimensional Gaussian cubature formulae is less than $\binom{D+3}{3} = \frac{(D+3)!}{3!D!}$ but greater than or equal to $\binom{\lfloor D/2 \rfloor+3}{3}$.[89]

Unfortunately, it is very difficult to construct Gaussian cubature formulae.[88,89] Currently, the only people in the electronic structure theory community who appear to be working on this problem are Hall and Rees.[90-96] Our goal is less ambitious: we are willing to consider a formula with more points than the Gaussian cubature formula if it is reasonably efficient and can be simply constructed up to any desired degree of polynomial exactness. The construction originally proposed by Smolyak,[68] and later developed by many others,[69-73,97,98] achieves this goal: the number of points in the

Smolyak integration formula is not too dissimilar to the optimal integration formula (when it is known) and represents a pragmatic alternative.

B. One-Dimensional Integration

The Smolyak procedure exploits the fact that it is easy to construct efficient quadrature rules on the unit interval, [0,1]. In this paper, we are primarily interested in the Clenshaw-Curtis formula[99,100]

$$
\begin{aligned}
x_j^{(l)} &= \frac{1}{2}\left(1+\cos\left(\frac{j\pi}{n_l}\right)\right) \\
w_j^{(l)} &= \frac{1}{2}\left(\sum_{k=0}^{n_l/2} c_j^{[k]} - \frac{1}{2}\left(c_j^{[0]} + c_j^{\left[n_l/2\right]}\right)\right) \\
c_j^{[k]} &= \frac{-4}{n_l\left(4k^2-1\right)}\cos\left(\frac{2kj\pi}{n_l}\right) \\
n_l &= 2^{l-1};\ m_l = n_l + 1 \\
l &= 1,2,\mathsf{K} \\
j &= 0,1,\mathsf{K}\ n_l
\end{aligned}
\qquad (2.3.8)
$$

and the rectangle rule,

$$
\begin{aligned}
x_j^{(l)} &= \frac{j}{n_l} \\
w_j^{(l)} &= \frac{1}{n_l} \\
n_l &= m_l = 2^l \\
l &= 1,2,\mathsf{K} \\
j &= 0,\mathsf{K}\ ,n_l - 1
\end{aligned}
\qquad (2.3.9)
$$

In Eqs. (2.3.8) and (2.3.9), m_l denotes the number of points in the one-dimensional quadrature formula.

For reasons that will be clear later, multi-dimensional grids generated by the Smolyak method are most efficient when the points in the lower order formula are reused by the higher-order formula; such quadrature formulae are said to be nested. The choice of $n = 2^l$ ensures that this is true for both the Clenshaw-Curtis and rectangle formulae. Following the work of Novak and Ritter, we have defined the 1-point ($l = 1$) Clenshaw-Curtis formula as $x_1^{(l)} = \frac{1}{2}$, $w_1^{(l)} = 1$.[72] We did not attempt to define a 1-point rectangle rule, which is why the rectangle rule has more points than the Clenshaw-Curtis rule for any given value of l.

For periodic functions (i.e., $f(0) = f(1)$), the rectangle rule is identical to the composite trapezoidal rule. Researchers in DFT often refer to the composite trapezoidal rule as the Euler-MacLaurin rule, even though the derivative-containing terms in the Euler-MacLaurin formula are almost never used.[18] The rectangle rule can be considered a trigonometric Gaussian quadrature for the Fourier expansion of a one-dimensional function. The Clenshaw-Curtis rule is *not* a Gaussian quadrature method, but the error in the Clenshaw-Curtis formula mimics that of Gaussian quadrature until the number of points is quite large.[101,102] For this reason, the Clenshaw-Curtis formulae are probably better for our application than other nested quadrature rules (like the Gauss-Patterson

schemes[103]), which have similar accuracy but more points. Based on these arguments, we believe that the Clenshaw-Curtis and rectangle rules are near-optimal choices for one-dimensional integration. If these formulae were true Gaussian quadrature formulae, instead of just near-Gaussian quadrature formulae, the order of the formulae would be $D_l = 2m_l - 1$, where m_l is the number of grid points.

C. Tensor Product Integration Formulae

A three-dimensional integration formula is commonly constructed from the tensor product of one-dimensional formulae. Denoting the one-dimensional formulae as

$$U^{(l)}[f] = \sum_{i=1}^{m_l} w_i^{(l)} f\left(x_i^{(l)}\right) \approx \int_0^1 f(x)\,dx, \tag{2.3.10}$$

the three-dimensional tensor product formula is

$$\begin{aligned} U^{(l_x)} \otimes U^{(l_y)} \otimes U^{(l_z)}[f] &= \sum_{i=1}^{m_{l_x}} \sum_{j=1}^{m_{l_y}} \sum_{k=1}^{m_{l_z}} w_i^{(l_x)} w_j^{(l_y)} w_k^{(l_z)} f\left(x_i^{(l_x)}, y_j^{(l_y)}, z_k^{(l_z)}\right) \\ &\approx \int_0^1 \int_0^1 \int_0^1 f(x,y,z)\,dxdydz \end{aligned} \tag{2.3.11}$$

The tensor product formula with $l = l_x = l_y = l_z$ is optimal when mixed derivatives of f are not bounded, as in Eqs. (2.3.3) and (2.3.4). Notice the similarity between (a) the number of polynomials that must be correctly integrated to achieve a given order of accuracy ($\sim D_l^3$) and (b) the number of points in the tensor product formula (m_l^3). Notice also that the number of grid points grows exponentially with increasing dimensionality.

Figure 2.1a shows the tensor-product rectangle rule for $L = 6$. This grid contains 250,047 points.

D. Sparse Tensor Products

When bounded mixed derivatives also exist (cf. Eqs. (2.3.5) and (2.3.6)), the function is smoother and so the space of polynomials that needs to be integrated correctly is much smaller ($\sim\binom{D_l+3}{3}$). The Smolyak procedure integrates correctly all of the polynomials in this space using a sparse tensor product. The basic idea behind the sparse tensor product is that if one considers a larger number of points in the x direction (large l_x; high degree polynomial in x), then the number of points required in the y and z directions will be much smaller (small l_y and l_z; low-degree polynomials in y and z). The specific formula Smolyak introduced to achieve this can be written[68,69]

$$U^{(L)}[f] = \sum_{\{L-2\le|\mathbf{l}|_1\le L\}} (-1)^{L-|\mathbf{l}|_1}\binom{2}{L-|\mathbf{l}|_1} U^{(l_x)}\otimes U^{(l_y)}\otimes U^{(l_z)}[f] \qquad (2.3.12)$$
$$|\mathbf{l}|_1 = l_x + l_y + l_z$$

The number of points in Smolyak quadrature rules is similar, in the asymptotic limit of high accuracy, to the number of points in many-dimensional Gaussian quadrature formulae.

Figures 2.1b and 2.1c show the $L = 6$ Smolyak grid built using the rectangle rule (1,023 points) and the Clenshaw-Curtis rule (271 points), respectively. Even though these grids have *many* fewer points than the full tensor-product grid in Figure 2.1a, all three grids have the same order of accuracy.

Recall that many of the pruned atom-centered grids commonly used in DFT calculations can be written as the sparse-tensor product between a radial grid and the Lebedev angular grids.[7,13-24] In those cases, the order of the angular grids associated with different radial shells is chosen based on *empirical* or *numerical* criteria, in a way designed to give optimal accuracy with the minimal number of points. Our sparse tensors are derived from formal *mathematical* considerations, and are not tuned to the specific system of interest. This is both a strength of our approach (our approach is more universal) and a weakness (our grids are not explicitly optimized).

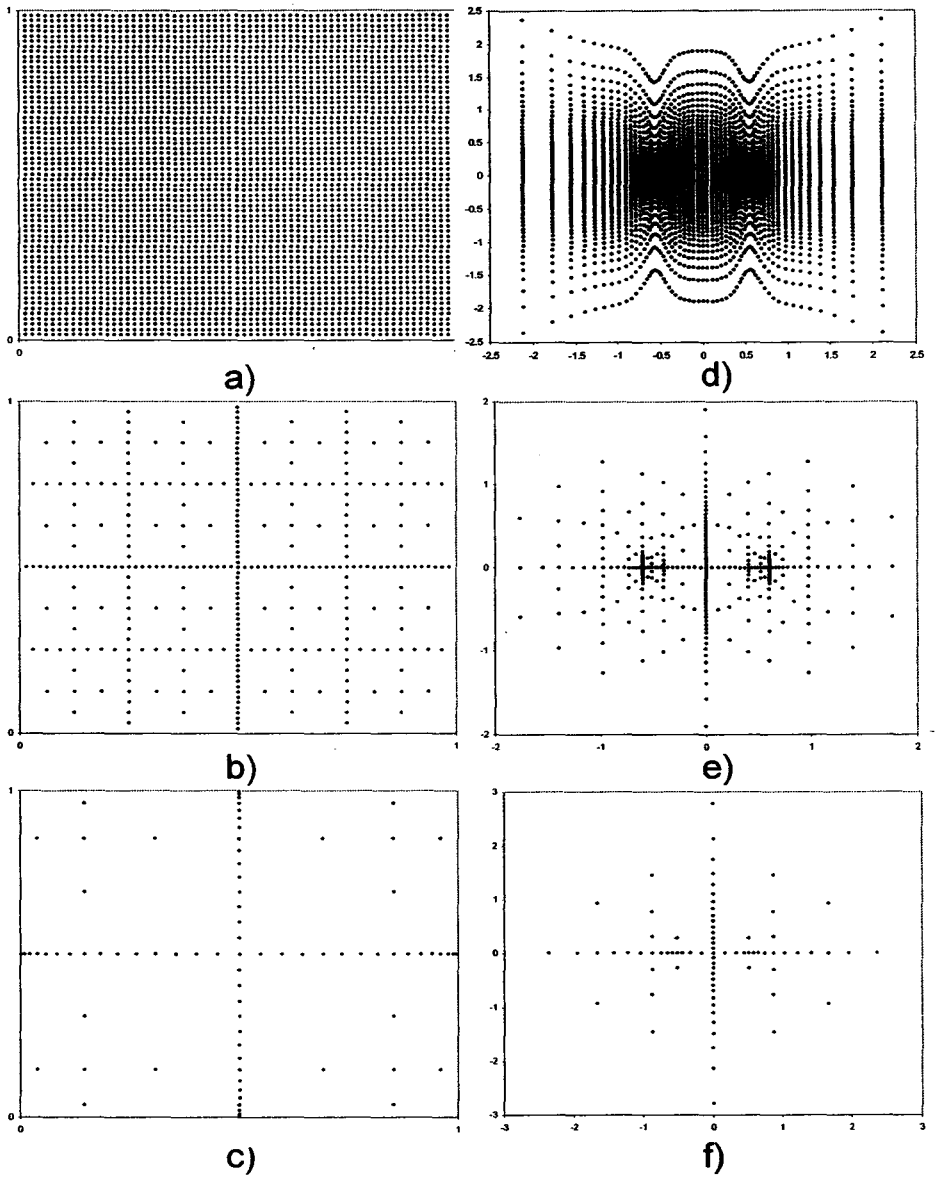

Figure 2.1 Grids on the unit cube $[0,1]^3$ and molecular grids in real space for N_2 at its equilibrium bond length. Only the grid points that lie in the *xy*-plane are shown. (a) Tensor-product rectangle rule with $L = 6$. This grid has 250,047 points. (b) Smolyak sparse-tensor product rectangle rule with $L = 6$. This grid has 1,023 points. (c) Smolyak sparse-tensor product Clenshaw-Curtis rule with $L = 6$. This grid has 151 points. (d) Transformed full-tensor product grid, in units of Angstroms, for the N_2 molecule. (e) Transformed Smolyak rectangle rule grid. (f) Transformed Smolyak Clenshaw-Curtis grid.

2.3.3 Transformation of coordinates

A. The Conditional Distribution Transformation Method

Using the methods from the previous section, we can obtain a grid on the unit cube, $[0,1]^3$. The integration region of interest in the theory of molecular electronic structure is real space. We can transform our integration formula on the unit cube,

$$\int_0^1\int_0^1\int_0^1 f(x,y,z)dxdydz \approx \sum_{i=1}^{M_L} w_i f(x_i,y_i,z_i) \tag{2.3.13}$$

into an integration formula in real space,

$$\begin{aligned}&\int_{-\infty}^{\infty}\int_{-\infty}^{\infty}\int_{-\infty}^{\infty} g(X,Y,Z)\mathrm{P}(X,Y,Z)dXdYdZ \\ &\quad\approx\left(\sum_{i=1}^{M_L} w_i g(X_i,Y_i,Z_i)\right)\times\int_{-\infty}^{\infty}\int_{-\infty}^{\infty}\int_{-\infty}^{\infty}\mathrm{P}(X,Y,Z)dXdYdZ\end{aligned} \tag{2.3.14}$$

using a coordinate transformation based on the conditional distribution method.[74] Here $\mathrm{P}(X,Y,Z)$ is any positive integrable function. The distribution of the grid points in real space is obtained by solving the equations,

$$x_i(X_i) = \frac{\int_{-\infty}^{X_i}\int_{-\infty}^{\infty}\int_{-\infty}^{\infty} P(X,Y,Z)\,dXdYdZ}{\int_{-\infty}^{\infty}\int_{-\infty}^{\infty}\int_{-\infty}^{\infty} P(X,Y,Z)\,dXdYdZ}$$

$$y_i(X_i,Y_i) = \frac{\int_{-\infty}^{Y_i}\int_{-\infty}^{\infty} P(X_i,Y,Z)\,dXdYdZ}{\int_{-\infty}^{\infty}\int_{-\infty}^{\infty} P(X_i,Y,Z)\,dXdYdZ} \qquad (2.3.15)$$

$$z_i(X_i,Y_i,Z_i) = \frac{\int_{-\infty}^{Z_i} P(X_i,Y_i,Z)\,dXdYdZ}{\int_{-\infty}^{\infty} P(X_i,Y_i,Z)\,dXdYdZ}$$

Equation (2.3.14) is derived by noting that the Jacobian determinant for this transformation is just

$$|\mathbf{J}| = \frac{P(X,Y,Z)}{\int_{-\infty}^{\infty}\int_{-\infty}^{\infty}\int_{-\infty}^{\infty} P(X,Y,Z)\,dXdYdZ}. \qquad (2.3.16)$$

The grid points in real space are concentrated in regions where $P(X,Y,Z)$ is relatively large and depleted in regions where $P(X,Y,Z)$ is relatively small. If the distribution of grid points on the unit cube were uniform, then the probability distribution function of grid points in real space would be proportional to $P(X,Y,Z)$. The transformation used by Pérez-Jordá is a special case of this general formalism.[63] We have also used this transformation in some of our previous work.[104]

Notice that points on the surface of the unit cube are mapped to infinity by this transformation. We will neglect all the points that are mapped to infinity in our grids. This means that our grids are only appropriate for integrals with the form of Eq. (2.3.14) if $g(X,Y,Z)$ decays to zero at the boundary of the interval. This constrains the choice of $\mathrm{P}(X,Y,Z)$ somewhat.

It is ideal, in fact, for both $g(X,Y,Z)$ and all of the derivatives of $g(X,Y,Z)$ to be zero asymptotically, e.g., $g(X,Y,Z)$ could decay exponentially. In that case, the correction terms in the Euler-McLaurin expression that depend on derivatives of the function at the boundary of the interval will always vanish. In such cases, the rectangle rule integration method is expected to be highly accurate.

B. The Promolecular Density

What is the best choice of $\mathrm{P}(X,Y,Z)$? In general, one should choose $\mathrm{P}(X,Y,Z)$ to resemble the integrand of interest. In that case, the function $g(X,Y,Z)$ in Eq. (2.3.14) will be nearly constant or, failing that, at least readily approximated by a low-order polynomial. In such cases, accurately approximating the integral in Eq. (2.3.14) does not require a large integration grid.

The integrands that are considered in DFT calculations are "density-like," and are often naturally decomposed as the product of the electron density and another function. For this reason, it seems reasonable to guess that the best choice for $\mathrm{P}(X,Y,Z)$ is the molecular electron density. Of course, the molecular electron density is not known until after the computation is performed. However, the promolecular density,

$$\mathrm{P}(\mathbf{R}) = \rho^{\mathrm{pro}}(\mathbf{R}) = \sum_{\alpha=1}^{N_{\mathrm{atoms}}} \rho_{\alpha}^{(\mathrm{isolated})}(\mathbf{R}-\mathbf{R}_{\alpha}) \approx \rho_{\mathrm{molecule}}(\mathbf{R}), \qquad (2.3.17)$$

is a reasonably accurate approximation to the true molecular density for most molecules. The promolecular density is defined as the sum of the densities of the *isolated* atoms, with each atomic density centered at the location of the corresponding atomic nucleus, $\mathbf{R}_{\alpha}$.[105] In our work, the atomic densities are approximated using the *s*-type Gaussian fits of Constans and Carbó,

$$\rho_{\alpha}^{(\mathrm{isolated})}(\mathbf{R}) = \sum_{i=1}^{N_{\alpha}} C_{i\alpha} e^{-\beta_{i\alpha} R^2} . \qquad (2.3.18)$$

The coefficients and exponents in the Constans-Carbó fits are obtained by fitting atomic densities obtained at the HF/6-311G level.[106] These fits are very convenient for our purposes because it is easy to perform the indefinite integrals that arise in Eq. (2.3.15) when $\mathrm{P}(X,Y,Z)$ is expressed as a sum of *s*-type Gaussian functions.

Figure 2.1d shows the transformed full-tensor grid (from Figure 2.1a) for the N_2 molecule at its equilibrium geometry. Figures 2.1e and 2.1f show the corresponding Smolyak grids (from Figures 2.1b and 2.1c). The points are concentrated near the atomic nuclei because this is where the promolecular density is the highest.

When a geometry optimization is performed, the promolecular density changes at each iteration (because the atomic nuclei move) and thus the grid changes. (The same is true in atom-centered grids, because the fuzzy Voronoi polyhedra are altered by changes in molecular geometry.) As is common in DFT implementations, the Pulay-type forces associated with the change in the grids induced by changes in molecular geometry are neglected; this omission is always acceptable if the grid is accurate enough. One can have convergence difficulties if the grid is not accurate enough, however, so geometry optimization provides a good test for the accuracy of an integration grid.

2.3.4 Interpretation

There are two equivalent ways to interpret the integration method here proposed. One way—perhaps the simplest—is to think of this approach as a "coordinate transformation" approach, in which a real-space integral is transformed to $[0,1]^3$, and integrated over that region. The other approach is to interpret this as a real-space integration method. This is the way that the authors usually think of matters, since it is easier for us to imagine electrons moving in real space. In fact, we initially attempted to

construct the Gaussian cubature grid associated with the orthogonal polynomials built with respect to the inner product,

$$\left\langle \mathcal{P}_k \middle| \mathcal{P}_l \right\rangle \equiv \int_{-\infty}^{\infty}\int_{-\infty}^{\infty}\int_{-\infty}^{\infty}\left[\mathcal{P}_k(X,Y,Z)\mathcal{P}_l(X,Y,Z)\right]\cdot\rho^{\text{pro}}(X,Y,Z)dXdYdZ. \qquad (2.3.19)$$

The advantage of this approach is that it would yield well-defined expressions for the error in the integration grids in terms of the "implicit" basis set underlying the grids, as described in section II.B.1.. While such a grid would be ideal for our purposes, it seems very hard to construct. The approach presented here is a pragmatic alternative. The basis functions that are "implicit" in the current construction of the grids are not polynomials, but instead the coordinate-transformed polynomials from the unit cube, $P_k(x(X))P_l(y(X,Y))P_m(z(X,Y,Z))\sqrt{\rho^{\text{pro}}(X,Y,Z)}$, where the coordinate transformation is defined as in Eq. (2.3.15). While we find this interpretation conceptually useful (perhaps because we tend to favor basis-set-based reasoning), it does not seem mathematically useful for understanding the accuracy of these integration formulae. For that, it seems, one needs to consider this method as "transforming the problem to the unit cube, where efficient grids are known" rather than "transforming efficient grids from the unit cube to real space."

2.4 Results and discussion

The grids generated by the preceding procedure were incorporated into an in-house version of the *deMon2k* program[76] and used to evaluate the exchange-correlation energy (Eq. (2.2.1)) and exchange-correlation potential (Eq. (2.2.2)) integrals. We compared the results to the *deMon2k* reference grid, which is a highly accurate atom-centered grid using 200 radial shells, each of which carries the Lebedev angular grid with 1202 angular points.[24]

To establish the superiority of the Smolyak procedure over conventional tensor products, we performed a thorough comparison of the two techniques. Figure 2.2 shows the results for the H_2 molecule. Notice that the Smolyak grids are orders of magnitude more efficient than the full-tensor grids: the Smolyak grids achieve much higher accuracy in both the exchange-correlation energy and the total SCF energy for a given number of grid points. Both grids achieve better relative error for the exchange-correlation energy than the SCF energy; this probably indicates that the grids are better suited to integrating the exchange-correlation energy than they are to integrating the exchange-correlation potential. This is not that surprising, since the exchange-correlation potential is often more strongly peaked near the nucleus than the local exchange- correlation energy. (As an extreme example of this phenomenon, consider that the exchange-correlation potential diverges at the nucleus for GGA-type functionals.)

To determine whether it was better to choose the Clenshaw-Curtis or the rectangle rule to construct the Smolyak grid, we considered a set of five representative molecules: H_2, N_2, H_2O, CH_4, and CO_2. Figure 2.3 presents the dependence of the average absolute error in the computed exchange-correlation energies for these molecules on the number of grid points per atom. The full tensor grid is significantly less efficient than either of the Smolyak-type grids, and the rectangle rule grids converge significantly faster than the Clenshaw-Curtis grids. As discussed above, the rectangle (a.k.a. Euler-MacLaurin) rule

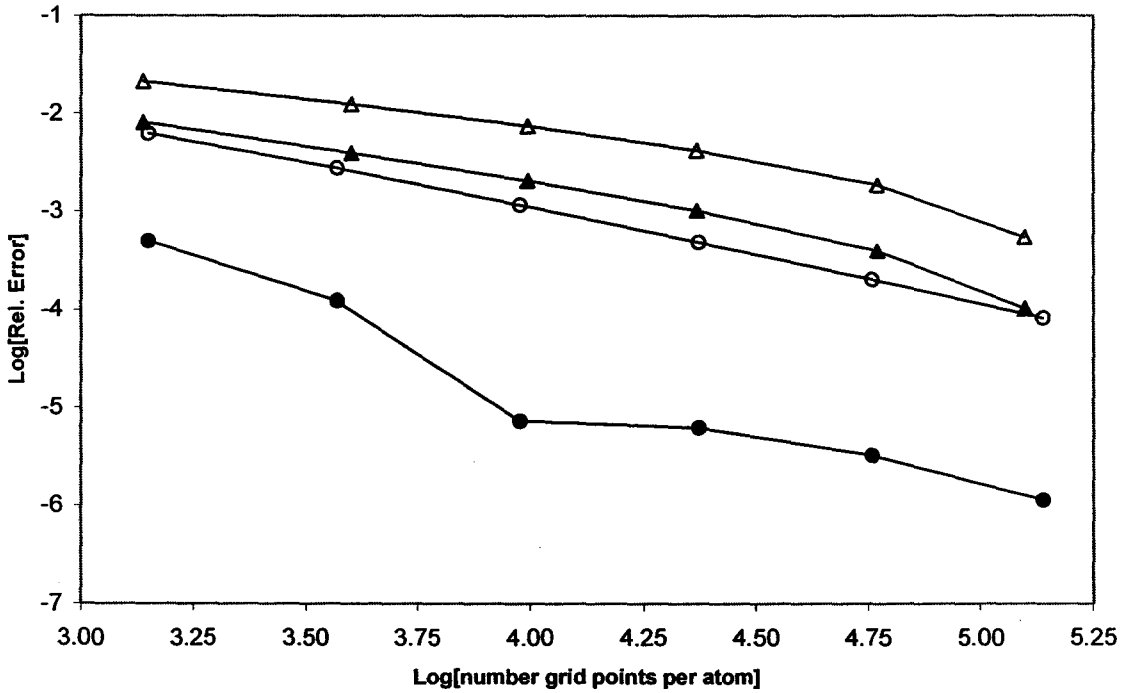

Figure 2.2 Logarithm (base-10) of the relative error in the exchange-correlation energy (closed symbols) and the total electronic energy (open symbols) versus $\log_{10}$(number of grid points per atom) for the Hydrogen molecule at its equilibrium geometry. Notice that the full-tensor grid (triangles) is much less accurate than the Smolyak grid (circles) for a given number of points.

will be very accurate when the derivatives of the function, $g(\mathbf{R})$, in Eq. (2.3.14) are asymptotically uniform. In the case of the exchange-correlation energy, $g(\mathbf{R}) = \varepsilon_{xc}(\mathbf{R}) / \rho^{\text{pro}}(\mathbf{R})$ decays exponentially as $\mathbf{R} \to \infty$, and so *all* of the derivatives of $g(\mathbf{R})$ are zero (and thus match) at the endpoints of the integration interval. This is the best possible case for the rectangle rule. Note, however, that there could be problems when the specific Gaussians used in the promolecular fits decay more quickly than those used in the basis set expansion of the Kohn-Sham orbitals. Although this is not a problem for any of the molecules considered in the present study, we observed that our results are less accurate for molecules in which the asymptotic decay of $g(\mathbf{R})$ is slower.

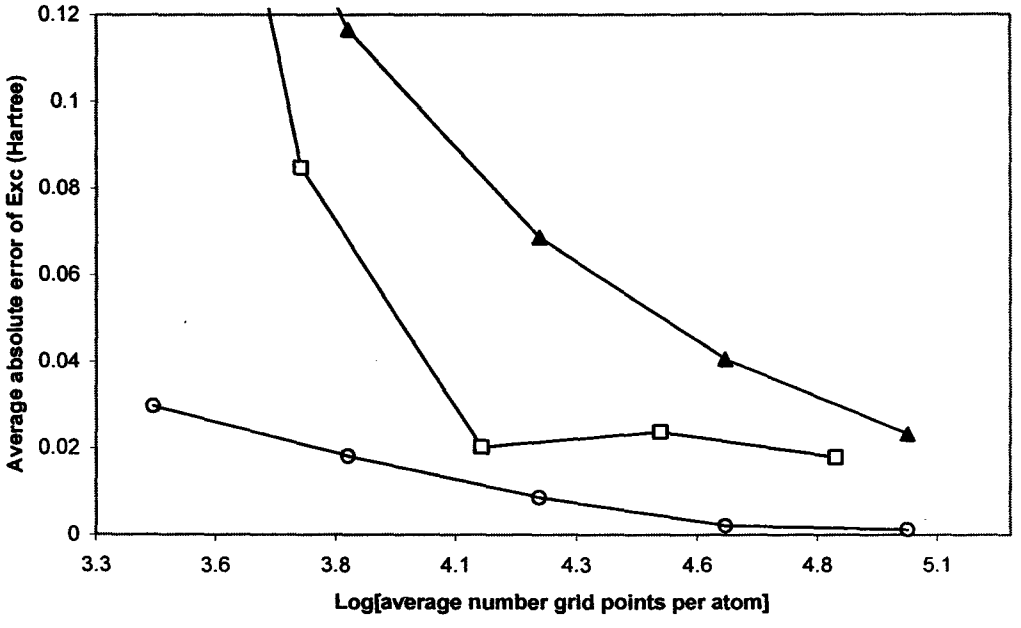

Figure 2.3 The average absolute error in the exchange-correlation energy for a set of five representative molecules (H_2, N_2, H_2O, CO_2, CH_4) versus $\log_{10}$(average number of grid points per atom). Data is presented for the tensor product grid (—▲—), the Smolyak grid built from the Clenshaw-Curtis formula (—□—), and the Smolyak grid built from the rectangle-rule formula (—○—). The units of energy are Hartree.

Having identified the sparse rectangle rule as the most promising integration formula for our purposes, we computed the atomization energy and exchange-correlation energies for the larger set of molecules given in Table 1. The convergence of these energies towards the reference value is satisfactory, as is shown in Figure 2.4.

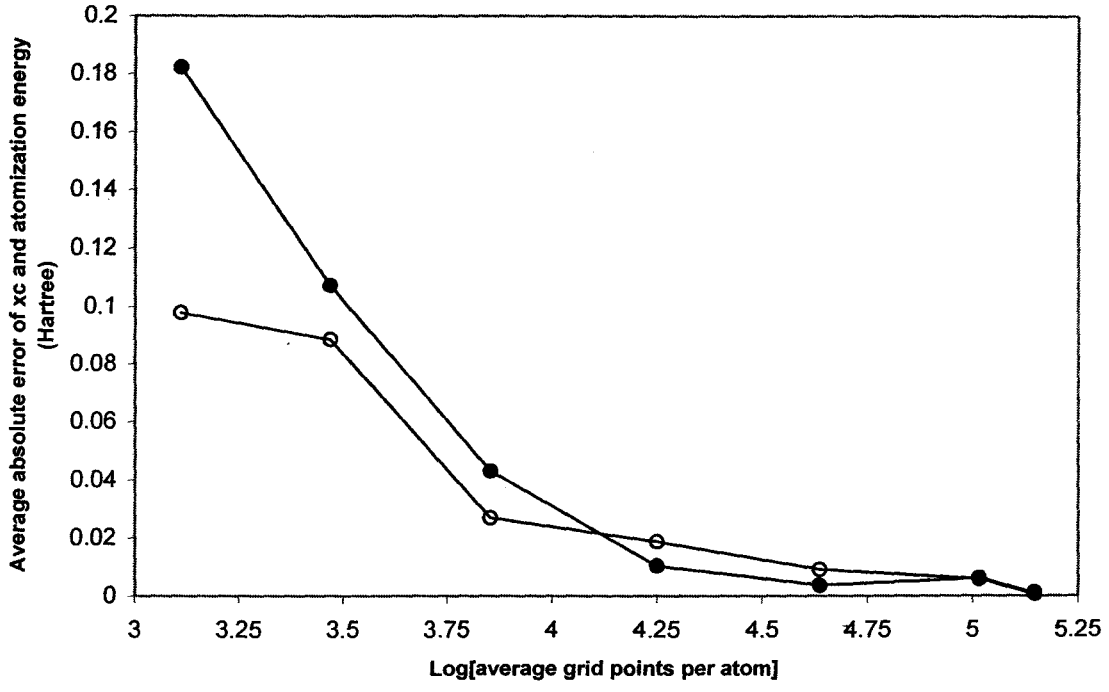

Figure 2.4 The average absolute error in the exchange-correlation energy (—o—) and the atomization energy (—●—) versus $\log_{10}$(average number of grid points per atom) for the molecules in Table 1. The units of energy are Hartree.

Table 2.1 contains the results of our tests of the Smolyak grids for geometry optimizations. Both bond length and angles obtained using sparse grids are in good agreement with the accurate deMon2k reference grid. Except for LiH and Cu_2, equilibrium bond lengths obtained using the Smolyak grid differ from the reference values by at most 0.002 Angstroms. It may be significant that Lithium and Copper are the two atoms for which the asymptotic condition on the integrals are most nearly violated.

More probably, the error in Cu_2 is indicative of a general problem that occurs for molecules containing heavy atoms: in these cases it is probably unwise to choose the promolecular density to distribute the grid points, because this leads to an extreme concentration of grid points in the (chemically unimportant) core regions and substantial depletion of grid points in the chemically relevant valence regions.

The error in LiH may arise from the fact that the hydrogen atom in LiH has a much higher density than predicted by the promolecular approximation; thus there are not enough grid points in the vicinity of the hydrogen atom in our grids for LiH.

The Smolyak grids reproduce bond angles very well. The largest difference from the reference grid is 0.2 degrees (for formaldehyde); the error is an order of magnitude smaller for all other molecules.

Comparing the computed results to the experimental geometries reaffirms the well-known fact that the local density approximation gives remarkably accurate geometries.[107,108] It is interesting to note that the Smolyak grids have significantly fewer points than the *deMon2k* reference grids, but still give excellent results.

Table 2.1 Geometries obtained using the rectangle-rule Smolyak grids and the *deMon2k* reference grids with 200 radial shells with 1202 angular points apiece. Bond lengths are given in Angstroms and Bond angles are given in degrees. The first row for each molecule reports the number of grid points, per atom, in each type of grid.

Molecule Parameter	Sparse grid	Reference	Exp.
H_2	57344	184860	
r(HH)	0.774	0.774	0.741[a]
N_2	57344	186179	
r(NN)	1.113	1.115	1.098[a]
Cu_2	57344	176745	
r(CuCu)	2.181	2.208	2.219[a]
LiH	57344	185916	
r(LiH)	1.599	1.602	1.595[a]
LiF	57344	187305	
r(LiF)	1.556	1.550	1.564[a]
CO	57344	186700	
r(CO)	1.143	1.146	1.128[a]
CO_2	38229	185275	
r(CO)	1.175	1.175	1.160[b]
H_2O	38229	183310	
r(OH)	0.974	0.975	0.957[b]
∡(HOH)	105.327	105.334	104.51[b]
NH_3	28672	180811	
r(NH)	1.025	1.026	1.012[b]
∡(HNH)	107.345	107.375	106.68[b]
CH_2O	28672	182291	
r(CO)	1.212	1.213	1.206[c]
r(CH)	1.123	1.124	1.108[c]
∡(OCH)	121.923	121.726	121.7[c]

Table 2.1 (Continued)

Molecule Parameter	Sparse grid	Reference	Exp.
CH_4	22937	179091	
r(CH)	1.101	1.102	1.086[d]
C_2H_4	19115	179382	
r(CC)	1.334	1.334	1.339[b]
r(CH)	1.098	1.099	1.085[b]
∡(CCH)	121.538	121.506	121.1[b]

[a]Ref.114; [b]Ref. 115; [c]Ref. 116; [d]Ref. 117

2.5 Conclusions

We have introduced a new approach to evaluating integrals in density-functional theory based on sparse-tensor grids and the conditional distribution transformation with respect to a preselected weight function. In this work, we have used the promolecular density as the weight function, which causes grid points to concentrate in regions where the electron density is large (atomic cores, heavy atoms, etc.) and causes the grid points to become depleted where the electron density is small (light atoms (especially hydrogen) and valence regions). While this works satisfactorily it was, in retrospect, rather naïve. It is particularly problematic in the vicinity of hydrogen atoms (where there are not enough grid points) and for heavy atoms (where there are not enough grid points in the valence regions to achieve the desired accuracy).

This paper is one of the first steps towards a much larger long-term goal—to develop a systematic procedure for developing molecular quadrature grids of arbitrary accuracy, with applications to density-functional theory and, eventually, *ab initio* quantum chemistry. Here we have focused on the mathematical framework and some "proof of principle" calculations of exchange-correlation energies, atomization energies, and molecular geometries. The advantages we see in our approach are:

(a) Our construction is completely general. It can be used for any integral of interest, including those of interest to density-functional theorists, but also those of interest to other branches of quantum chemistry and, more generally, mathematical modeling. Given a "good guess" for an integrand ($\mathrm{P}(X,Y,Z)$), we can fit that guess to a sum of Gaussians (or any other function for which the integrals in Eq. (2.3.15) can be performed). The integrals can then be evaluated using any of the many highly efficient formulae on the unit cube. The Smolyak approach is a relatively easy and systematic approach for constructing highly efficient formulae on the unit cube. The entire procedure we have sketched here is easily generalized to arbitrary dimensions by constructing Smolyak grids on appropriately dimensioned hypercubes, and then transforming the grids to real space using the conditional distribution transformation technique.

(b) The grids have a "whole molecule" nature and are not atom-centered. This is essential in systems (e.g., electrons confined in regions of various shapes and electrons bound by non-Coulomb potentials) where atom-centered grids are not applicable. It is also very helpful for basis-set-free calculations, because it facilitates the development of derivatives and other linear operators on the grid. (In fact, the Smolyak "trick" can be used to develop grid-based expressions for any linear operator, not just integration, and this is one reason we have favored Smolyak grids in this work.) Basis-set-free calculations performed using these grids are equivalent to basis-set-based calculations using a basis set of transformed orthogonal polynomials, $P_k\left(x\left(X\right)\right)P_l\left(y\left(X,Y\right)\right)P_m\left(z\left(X,Y,Z\right)\right)\sqrt{\rho^{\text{pro}}\left(X,Y,Z\right)}$. (Cf. section II.D.) These basis functions have the same atomic cusps, asymptotic decay, and general nodal structure as Kohn-Sham orbitals, which bodes well for the accuracy of such an approach. The ability to relate grid-based calculations to basis-set-based calculations is a strength of "whole molecule" grids; it is more difficult (but not impossible) to explicitly construct the implicit basis set for atom-centered integration grids.

Before fully basis-set-free calculations are really possible, however, we need to answer some of the questions raised in this study. These are topics for future work.

1. We saw that the accuracy of the integration formula requires that the weight function—here, the promolecular density—decay much more slowly than the integrand of interest. (See, for example, the discussion at the end of section II.C.1.) Clearly this can be a problem when one uses Gaussian functions, $e^{-\alpha r^2}$, to expand the promolecular density, and it would be an even bigger problem in basis-set-free calculations: the electron density and density matrix both decay exponentially.[109-112] (Thus, they decay exponentially slower than any Gaussian.) The indefinite integrals needed for Eq. (2.3.15) can be evaluated analytically for the Lorentzian power functions ($\left(r^2 + a^2\right)^{-2n}$) using partial fractions, and so we are currently exploring whether fitting the promolecular density to a mixed sum of Gaussians and powers of Lorentzians is a viable alternative to the Gaussian-only approach used in this paper.
2. As stated above, choosing the promolecular density as the weight function was, in retrospect, naïve. One reason why basis-set-based calculations are so efficient is that they exploit the fact that chemistry is dominated by "valence electron" effects because (a) atomic cores are transferable and (b) errors in description of the atomic cores do not contribute very much to the energy differences associated with molecular rearrangements and reactions. We are currently developing some approaches that, we hope, will allow us to exploit the transferability of atomic cores in molecular cubature grids. If successful, this would allow us to drastically

reduce the number of points in the core regions of the molecule, and lead us to weight functions with more points in the "valence regions" of atoms.

3. It is not clear that the Smolyak grids are truly the best grids for this purpose. Recent work in the applied mathematics community has suggested that one might be able to use even fewer points. Some of these approaches are based on the Smolyak grids, but choose the grid points in a different way. For example, the following grids with l=15 are predicted by theory to all have the same order of accuracy.

   (a) A full-tensor grid, with $3.51 \cdot 10^{13}$ points.

   (b) A conventional Smolyak grid, with 3,473,407 points. Notice that this is ten million times fewer points than the conventional full-tensor grid.

   (c) A Bungartz-Griebel grid with 452,607 points. The Bungartz-Griebel grids are related to the Smolyak grids, but are based on minimization of a different norm for the error.[113]

   (d) A Griebel-Knapek grid with 350,719 points. The Griebel-Knapek grids are a family of grids that range from the tensor product grids ($T = -\infty$) through the Smolyak grids ($T = 0$), to a *very* sparse grid $T = .\overline{9}$, depending on a parameter, T, which reflects how smooth the integrand is.[86] The number of points listed above is for $T = .5$.

(e) A Petras-style "delayed" Smolyak grid with 1135 points. The Petras-style grids are similar to the Smolyak grids, but some of the one-dimensional quadrature formulae are "reused" for several different levels of the many-dimensional grid.[97] The number of points in the Petras-style grids begins to approach the accuracy/efficiency of a true Gaussian cubature formula, which would have between 560 and 816 points.

Generating the hypothetically more efficient formulae based on methods (c)-(e), however, requires writing a different computer program, since these formulae cannot be expressed in a form as simple as Eq. (2.3.12). Work along these lines is underway, and based on the results listed above, it is reasonable to suspect that such a method might be one or two orders of magnitude more efficient than the approach used here.

We should reiterate, however, that the method presented here is already useful. It suffices to compute accurate molecular exchange-correlation energies and molecular geometries. The method also performs well for geometry optimizations. The biggest strengths of the current method, however, are its simplicity and flexibility. The "whole molecule" grids constructed here are promising tools for basis-set-free calculations not only in density-functional theory, but also in *ab initio* quantum chemistry (where higher-dimensional grids would be needed). In addition, the accuracy of the grids is systematically improved by simply increasing the order of the integration formula on the

unit cube. Other—less systematic, but still straightforward—modifications (e.g., modifying the weight function and considering alternative sparse grids) should improve the accuracy and efficiency of the grids further still.

2.6 References for Chapter 2

1 W. Kohn, A. D. Becke, and R. G. Parr, J.Phys.Chem. **100**, 12974 (1996).

2 W. Kohn, Reviews of Modern Physics **71**, 1253 (1999).

3 J. A. Pople, Reviews of Modern Physics **71** (5), 1267 (1999).

4 M. Head-Gordon, J. Phys. Chem. **100** (31), 13213 (1996).

5 K. Raghavachari and J. B. Anderson, J. Phys. Chem. **100** (31), 12960 (1996).

6 A. D. Becke, J. Chem. Phys. **88** (4), 2547 (1988).

7 P. M. W. Gill and S. H. Chien, J. Comput. Chem. **24** (6), 732 (2003).

8 V. I. Lebedev, Sibirskii Matematicheskii Zhurnal **18** (1), 99 (1975).

9 V. I. Lebedev, Russian Acad.Sci.Dokl.Math. **45** (3), 587 (1992).

10 V. I. Lebedev, Russian Acad.Sci.Dokl.Math. **50** (2), 283 (1992).

11 V. I. Lebedev, Dokl. Akad. Nauk **338** (4), 454 (1994).

12 V. I. Lebedev and D. N. Laikov, Dokl. Akad. Nauk **366** (6), 741 (1999).

13 S. H. Chien and P. M. W. Gill, J. Comput. Chem. **27** (6), 730 (2006).

14 P. M. W. Gill, B. G. Johnson, and J. A. Pople, Chem. Phys. Lett. **209** (5-6), 506 (1993).

15 M. Krack and A. M. Koster, J. Chem. Phys. **108** (8), 3226 (1998).[16] R. Lindh, P. A. Malmqvist, and L. Gagliardi, Theor. Chem. Acc. **106** (3), 178 (2001).

17 M. E. Mura and P. J. Knowles, J. Chem. Phys. **104** (24), 9848 (1996).

[18] C. W. Murray, N. C. Handy, and G. J. Laming, Mol. Phys. **78** (4), 997 (1993).

[19] O. Treutler and R. Ahlrichs, J. Chem. Phys. **102** (1), 346 (1995).

[20] A. El-Sherbiny and R. A. Poirier, J. Comput. Chem. **25** (11), 1378 (2004).

[21] M. R. Pederson and K. A. Jackson, Phys. Rev. B **41** (11), 7453 (1990).

[22] G. T. Velde and E. J. Baerends, J. Comput. Phys. **99** (1), 84 (1992).

[23] J. M. Perez-Jorda, A. D. Becke, and E. San Fabian, J. Chem. Phys. **100** (9), 6520 (1994).

[24] A. M. Koster, R. Flores-Moreno, and J. U. Reveles, J. Chem. Phys. **121** (2), 681 (2004).

[25] A. D. Becke, Int. J. Quantum Chem. **S23**, 599 (1989).

[26] A. D. Becke and R. M. Dickson, J. Chem. Phys. **89** (5), 2993 (1988).

[27] A. D. Becke and R. M. Dickson, J. Chem. Phys. **92** (6), 3610 (1990).

[28] B. Delley, J. Chem. Phys. **92** (1), 508 (1990).

[29] B. Delley, J. Chem. Phys. **94** (11), 7245 (1991).

[30] B. Delley, J. Chem. Phys. **113** (18), 7756 (2000).

[31] J. Kong, S. T. Brown, and L. Fusti-Molnar, J. Chem. Phys. **124** (9) (2006).

[32] S. T. Brown, L. Fusti-Molnar, and J. Kong, Chem. Phys. Lett. **418** (4-6), 490 (2006).

[33] L. Kronik, A. Makmal, M. L. Tiago, M. M. G. Alemany, M. Jain, X. Y. Huang, Y. Saad, and J. R. Chelikowsky, Physica Status Solidi B-Basic Solid State Physics **243** (5), 1063 (2006).

[34] J. R. Chelikowsky, Y. Saad, S. Ogut, I. Vasiliev, and A. Stathopoulos, Physica Status Solidi B-Basic Research **217** (1), 173 (2000).

[35] J. R. Chelikowsky, N. Troullier, and Y. Saad, Phys. Rev. Lett. **72** (8), 1240 (1994).

[36] J. R. Chelikowsky, N. Troullier, K. Wu, and Y. Saad, Phys. Rev. B **50** (16), 11355 (1994).

[37] T. L. Beck, Reviews of Modern Physics **72** (4), 1041 (2000).

[38] S. R. White, J. W. Wilkins, and M. P. Teter, Phys. Rev. B **39** (9), 5819 (1989).

[39] J. Bernholc, J. Y. Yi, and D. J. Sullivan, Faraday Discuss., 217 (1991).

[40] E. L. Briggs, D. J. Sullivan, and J. Bernholc, Phys. Rev. B **52** (8), R5471 (1995).

[41] E. L. Briggs, D. J. Sullivan, and J. Bernholc, Phys. Rev. B **54** (20), 14362 (1996).

[42] T. L. Beck, K. A. Iyer, and M. P. Merrick, Int. J. Quantum Chem. **61** (2), 341 (1997).

[43] J. Bernholc, E. L. Briggs, D. J. Sullivan, C. J. Brabec, M. B. Nardelli, K. Rapcewicz, C. Roland, and M. Wensell, Int. J. Quantum Chem. **65** (5), 531 (1997).

[44] T. L. Beck, Int. J. Quantum Chem. **65** (5), 477 (1997).

[45] F. Ancilotto, P. Blandin, and F. Toigo, Phys. Rev. B **59** (12), 7868 (1999).

[46] T. L. Beck, J. Comput. Chem. **20** (16), 1731 (1999).

[47] J. Wang and T. L. Beck, J. Chem. Phys. **112** (21), 9223 (2000).

[48] W. Hierse and E. B. Stechel, Phys. Rev. B **50** (24), 17811 (1994).

[49] E. Tsuchida and M. Tsukada, Solid State Commun. **94** (1), 5 (1995).

[50] E. Hernandez and M. J. Gillan, Phys. Rev. B **51** (15), 10157 (1995).

[51] E. Tsuchida and M. Tsukada, Phys. Rev. B **52** (8), 5573 (1995).

[52] E. Hernandez, M. J. Gillan, and C. M. Goringe, Phys. Rev. B **53** (11), 7147 (1996).

[53] E. Tsuchida and M. Tsukada, Phys. Rev. B **54** (11), 7602 (1996).

[54] E. Hernandez, M. J. Gillan, and C. M. Goringe, Phys. Rev. B **55** (20), 13485 (1997).

[55] C. M. Goringe, E. Hernandez, M. J. Gillan, and I. J. Bush, Comput. Phys. Commun. **102** (1-3), 1 (1997).

[56] S. Goedecker and C. Chauvin, Journal of Theoretical & Computational Chemistry **2** (4), 483 (2003).

[57] K. Cho, T. A. Arias, J. D. Joannopoulos, and P. K. Lam, Phys. Rev. Lett. **71** (12), 1808 (1993).

[58] T. A. Arias, Reviews of Modern Physics **71** (1), 267 (1999).

[59] F. Gygi, Europhys. Lett. **19** (7), 617 (1992).

[60] F. Gygi, Phys. Rev. B **48** (16), 11692 (1993).

[61] F. Gygi, Phys. Rev. B **51** (16), 11190 (1995).

[62] F. Gygi and G. Galli, Phys. Rev. B **52** (4), R2229 (1995).

[63] J. M. Perez-Jorda, Phys. Rev. A **52** (4), 2778 (1995).

[64] J. L. Fattebert and F. Gygi, Phys. Rev. B **73** (11) (2006).

[65] R. Cools and P. Rabinowitz, Journal of Computational and Applied Mathematics **48** (3), 309 (1993).

[66] R. Cools, Journal of Computational and Applied Mathematics **112** (1-2), 21 (1999).

[67] R. Cools, Journal of Complexity **19** (3), 445 (2003).

[68] S. A. Smolyak, Dokl. Akad. Nauk **4**, 240 (1963).

[69] G. W. Wasilkowski and H. Wozniakowski, Journal of Complexity **11** (1), 1 (1995).

[70] R. Cools, E. Novak, and K. Ritter, Computing **62** (2), 147 (1999).

[71] E. Novak and K. Ritter, Constructive Approximation **15** (4), 499 (1999).

[72] E. Novak and K. Ritter, Numerische Mathematik **75** (1), 79 (1996).

[73] T. Gerstner and M. Griebel, Numerical Algorithms **18** (3-4), 209 (1998).

[74] L. Devroye, *Non-uniform Random Variate Generation.* (Springer-Verlag, New York, 1986).

[75] J. M. Perez-Jorda, European Journal of Physics **10**, 224 (1989).

[76] deMon2k. A. M. Köster, P. Calaminici, M. E. Casida, R. Flores-Moreno, G. Geudtner, A. Goursot; T. Heine, A. Ipatov, F. Janetzco, J. M. del Campo, S. Patchkovskii, J. U. Reveles, D. R. Salahub, and A. Vela. deMon developers 2006. See http://www.demon-software.com

[77] N. Godbout, D. R. Salahub, J. Andzelm, and E. Wimmer, Canadian Journal of Chemistry-Revue Canadienne De Chimie **70** (2), 560 (1992).

[78] P. A. M. Dirac, Proc.Cambridge Phil.Soc. **26**, 376 (1930).

[79] S. H. Vosko, L. Wilk, and M. Nusair, Can. J. Phys. **58** (8), 1200 (1980).

[80] W. Kohn and L. J. Sham, Phys.Rev. **140**, A1133 (1965).

[81] A. M. Koster, J. Chem. Phys. **118** (22), 9943 (2003).

[82] A. M. Koster, J. U. Reveles, and J. M. del Campo, J. Chem. Phys. **121** (8), 3417 (2004).

[83] J. U. Reveles and A. M. Koster, J. Comput. Chem. **25** (9), 1109 (2004).

[84] N. I. Achieser, *Theory of Approximation.* (Dover, New York, 1992).

[85] A. F. Timan, *Theory of Approximation of Functions of a Real Variable.* (Dover, New York, 1994).

[86] M. Griebel and S. Knapek, Constructive Approximation **16** (4), 525 (2000).

[87] H. Yserentant, Numerische Mathematik **105** (4), 659 (2007).

[88] R. Cools, Journal of Computational and Applied Mathematics **149** (1), 1 (2002).

89 Y. Xu, *Common zeros of polynomials in several variables and higher dimensional quadrature*. (Wiley New York, 1994).

90 G. G. Hall and D. Rees, Int. J. Quantum Chem. **53** (2), 189 (1995).

91 D. Rees and G. G. Hall, Mol. Phys. **88** (4), 1077 (1996).

92 D. Rees and G. G. Hall, Int. J. Quantum Chem. **60** (1), 99 (1996).

93 G. G. Hall and D. Rees, Int. J. Quantum Chem. **63** (1), 197 (1997).

94 D. Rees and G. G. Hall, Int. J. Quantum Chem. **89** (6), 503 (2002).

95 D. Rees and G. G. Hall, Int. J. Quantum Chem. **102** (1), 19 (2005).

96 G. G. Hall and D. Rees, Int. J. Quantum Chem. **107** (4), 845 (2007).

97 K. Petras, Numerische Mathematik **93** (4), 729 (2003).

98 K. Petras, Advances in Computational Mathematics **12** (1), 71 (2000).

99 W. Fraser and M. W. Wilson, SIAM Review **8**, 322 (1966).

100 C. W. Clenshaw and A. R. Curtis, Numerische Mathematik **2**, 197 (1960).

101 J. A. C. Weideman and L. N. Trefethen, Numerische Mathematik **107** (4), 707 (2007).

102 L. N. Trefethen, SIAM Review **50**, 67 (2008).

103 T. N. L. Patterson, Mathematics of Computation **22**, 847 (1968).

104 D. C. Thompson and P. W. Ayers, Int. J. Quantum Chem. **106**, 787 (2006).

105 F. L. Hirshfeld, Theor.Chim.Acc. **44**, 129 (1977).

106 P. Constans and R. Carbó, Journal of Chemical Information and Computer Sciences **35** (6), 1046 (1995).

107 B. G. Johnson, P. M. W. Gill, and J. A. Pople, J. Chem. Phys. **98** (7), 5612 (1993).

108 R. M. Dickson and A. D. Becke, J. Chem. Phys. **99** (5), 3898 (1993).

109 J. Katriel and E. R. Davidson, Proceedings of the National Academy of Sciences **77** (8), 4403 (1980).

110 M. Levy and R. G. Parr, J. Chem. Phys. **64** (6), 2707 (1976).

111 M. M. Morrell, R. G. Parr, and M. Levy, J. Chem. Phys. **62** (2), 549 (1975).

112 C. O. Almbladh and U. Von Barth, Phys. Rev. B **31** (6), 3231 (1985).

113 H. J. Bungartz and M. Griebel, Journal of Complexity **15** (2), 167 (1999).

114 K. P. Huber and G. Herzberg, *Molecular spectra and molecular structure IV: Constants of diatomic molecules.* (Van Nostrand Reinhold, New York, 1979).

115 J. H. Callomon, E. Hirota, K. Kuchitsu, W. J. Lafferty, A. G. Maki, and C. S. Pote, *Structure data of free polyatomic molecules.* (Springer, Berlin, 1976).

116 M. D. Harmony, V. W. Laurie, R. L. Kuczkowski, S. R. H., D. A. Ramsay, F. J. Lovas, W. J. Lafferty, and A. G. Maki, J. Phys. Chem. Ref. Data **8**, 619 (1979).

117 D. L. Gray and A. G. Robiette, Mol. Phys. **37**, 1901 (1979).

"... But, in addition to this search for new concepts,
there is a constant effort directed toward the deepening and broadening of
our knowledge of phenomena which , we believe,
can be understood on the basis of existing concept and theories."

E. P. Wigner, *Scientific Monthly, Jan. 1936.*

Chapter 3

A PHYSICALLY MOTIVATED PSEUDO-GAUSSIAN CUBATURE SCHEME WITH APPLICATIONS TO MOLECULAR DENSITY-FUNCTIONAL THEORY*

* The content of this chapter was submitted (on 03/27/08) as an article to the *Journal of Physics A.* (Authors: Juan I. Rodríguez, David C. Thompson, James S. M. Anderson, Jordan Thomson, and Paul W. Ayers)

3.1 Statement of the problem

In this Chapter, the n-dimensional transformed Smolyak formula is tested. The transformed Smolyak grid is tested on integrals in one, two, three, and six dimensions. The three-dimensional integration formulae are used to evaluate atomic interaction energies via the Gordon-Kim model. The six-dimensional integration formulae are tested in conjunction with the nonlocal exchange-correlation energy functional proposed by Lee and Parr. We contemplate applications of these grids to diverse fields: frozen-density embedding, next-generation molecular mechanics force fields, "kernel type" exchange-correlation energy functionals, and pair-density functional theory.

3.2 Introduction

One of the most pervasive tasks in modern computational simulation is numerical integration. This is especially true in many-body quantum mechanics, where the integrals that need to be performed often have high dimensionality and where the integrands are often strongly inhomogeneous. Consider, for example, that in order to attain so-called "chemical accuracy" for a molecular system (i.e., enough accuracy in an energy calculation to predict the rate of a chemical reaction to within an order of magnitude), one often has to integrate strongly peaked functions very accurately, with relative errors of less than .001%. (For moderate-sized molecules, the "chemically relevant" portion of the electron density spans five to seven orders of magnitude.) Such daunting integration tasks

would be manifestly impossible were it not for the ability of physicists and chemists to "guess" the structure of the integrand based on mathematical conditions and physicochemical insight. The goal of this paper is to introduce a general approach that leverages prior knowledge about the integrands to design an efficient numerical integration method.

In particular, we will introduce a universally applicable method for performing *d*-dimensional integrals,

$$\int_{\mathbb{R}^d} f(\mathbf{r})P(\mathbf{r})d\mathbf{r} \approx \sum_{i=1}^{M_L} w_i f(\mathbf{r}_i), \tag{3.2.1}$$

where $P(\mathbf{r})>0$ is any nonnegative integrable "weight function." This form of integration allows one to leverage most of one's knowledge about the integrand of interest. In particular, one can ensure that $f(\mathbf{r})$ is smooth by ensuring that the analytically-defined $P(\mathbf{r})$ correctly models all of the singularities and nondifferentiability of the integrand. (In molecular-electronic structure calculations, for example, $P(\mathbf{r})$ should model the electron-nuclear cusps in the electron density/wavefunction.[1-7]) Ideally $P(\mathbf{r})$ should be chosen so that $f(\mathbf{r})$ is slowly varying. To the extent that this cannot be achieved, then $P(\mathbf{r})$ should be largest in the regions

where $f(\mathbf{r})$ varies most strongly. In this way, knowledge of the structure of the integrand allows us to construct more efficient quadrature methods.

But what numerical methods should we use to perform these integrals? In one dimension, the answer is clear: Gaussian quadrature formulae with respect to the weight function, $P(x)$, will be the optimal integration method.[8-11] Similarly, Gaussian cubature would be optimal in higher dimensions. However, constructing even low-order Gaussian cubature formulae is very difficult and time-consuming; such methods are clearly inappropriate given the large (usually hundreds; sometimes millions) of integrals required in molecular electronic structure theory calculations, which is the application of greatest interest to us. (Hall and Rees have done work on Gaussian cubature formulae for atoms[12] and homonuclear diatomic molecules[13], but their approach seems daunting even for these systems, and it is not clear how it can be extended to large molecules. Moreover, it does not seem easy to apply their method to arbitrary choices for $P(\mathbf{r})$.)

While Gaussian cubature formulae are not known for arbitrary choices of $P(\mathbf{r})$, Gaussian cubature formulae are known for certain special integration regions and certain special weight functions, e.g., the uniformly weighted unit cube. Even when Gaussian cubature formulae are not known for a region, other efficient formulae are.[14-16] The approach we will take uses one of these "almost as good" cubature formulae for the unit cube, due to Smolyak.[17] After that cubature formula has been defined on the unit cube,

we will transform it to real space using a transformation whose Jacobian determinant is $P(\mathbf{r})$, thereby obtaining an efficient cubature formula for integrals with the form of Eq. (3.2.1). The mathematical details of the procedure are presented in the next section, followed by the results of our numerical tests. We conclude with a short summary of our findings and a brief prospectus for future work.

3.3 Method

3.3.1 One-Dimensional Quadrature Grids on [0,1]

It is commonly asserted that, for smooth functions in one dimension, the best numerical integration formulae are the Gaussian quadrature formulae. There are many different ways to explain why the Gaussian quadrature formulae are "best," but one of the most useful is through a discussion of their computational complexity. The computational complexity, $C(\varepsilon)$, is the computational cost required to achieve accuracy ε.[18,19] The integration error when an n-point Gaussian quadrature formula is applied to an r-times differentiable function is

$$\varepsilon : n^{-r} \tag{3.3.1}$$

The computational cost is proportional to the number of times the function has to be evaluated, n. So

$$C_{\mathrm{Ga}}(\varepsilon): \varepsilon^{-1/r}. \tag{3.3.2}$$

These formulae may be derived from the asymptotic decay of the coefficients of the orthogonal polynomials that underlie the Gaussian quadrature formulae. *It is important to remember that these results are asymptotic: they only hold in the high accuracy (large n, small ε) limit. When lower accuracy suffices, alternative numerical integration techniques may be preferable.*

Gaussian quadrature is "optimal" because the results in Eqs. (3.3.1) and (3.3.2) are optimal. Other common formulae are less efficient. For comparison, the computational complexity of Monte-Carlo integration, the trapezoidal rule, and Simpson's rule are $C_{\mathrm{MC}}(\varepsilon): \varepsilon^{-2}$, $C_{\mathrm{Tr}}(\varepsilon): \varepsilon^{-1/2}$, and $C_{\mathrm{Si}}(\varepsilon): \varepsilon^{-1/4}$, respectively. There are other one-dimensional quadrature formulae that approach the utility of the Gauss formulae; the Clenshaw-Curtis formula is competitive with Gaussian quadrature.[20,21] For periodic integrands, the trapezoidal rule is a "trigonometric" Gaussian quadrature formula; in that context the trapezoidal rule is usually referred to as the rectangle rule. In the quantum chemistry community, the rectangle rule is usually referred to as the Euler-MacLaurin formula.[22]

In this paper we are primarily interested in quadrature formulae on the unit interval,

$$\int_0^1 f(x)dx \approx Q_l[f] \equiv \sum_{i=1}^{m_l} w_i f(x_i). \tag{3.3.3}$$

Here, l denotes the order of the quadrature formula, m_l denotes the number of points in the formula, x_i are the grid points in the formula, and w_i are the weights.

3.3.2 Multi-dimensional Grids on $[0,1]^d$

Numerical integration in many dimensions is intrinsically more difficult than one-dimensional integration. The error and computational complexity for integrating an r-times differentiable d-dimensional function is

$$\begin{aligned} \varepsilon &: n^{-r/d} \\ C(\varepsilon) &: \varepsilon^{-d/r}. \end{aligned} \tag{3.3.4}$$

The complexity of numerical integration grows exponentially with increasing dimension; this is often referred to as the "curse of dimension."

It is possible to break the curse of dimension when the function is more than "just" differentiable. For example, suppose the integrand has mixed derivatives of order r,

$$\left| \frac{\partial^{n_1}\partial^{n_2}\cdots\partial^{n_d} f(x_1, x_2, ..., x_d)}{\partial x_1^{n_1}\partial x_2^{n_2}\cdots\partial x_d^{n_d}} \right| < \infty \qquad n_1, n_2, ..., n_d \le r. \tag{3.3.5}$$

This function is more than "just r-times differentiable" because certain special higher-order derivatives exist, so long as none of the variables is differentiated with respect to

more than r times. The integration error and computational complexity for functions with bounded mixed derivatives of order r no longer depends on the dimension. In fact, the computational complexity is now the same as one-dimensional Gaussian quadrature,

$$C_{\text{Mixed}}(\varepsilon): \varepsilon^{-1/r} \tag{3.3.6}$$

This optimal computational complexity is achieved by Gaussian cubature formulae.

Unfortunately, Gaussian cubature formulae are very difficult to construct. Indeed, one has replaced one very difficult problem (integration in higher dimensions) with another one (determining optimal integration formulae).[23] Instead, one usually constructs higher-dimensional formulae as the tensor product of the one-dimensional Gaussian quadrature formulae,

$$\begin{aligned} Q^{(d)}_{l_1 l_2 \ldots l_d}[f] &= Q_{l_1} \otimes Q_{l_2} \otimes \ldots \otimes Q_{l_d}[f] \\ &= \sum_{i_1=1}^{m_{l_1}} \sum_{i_2=1}^{m_{l_2}} \cdots \sum_{i_d=1}^{m_{l_d}} w_{i_1} w_{i_2} \ldots w_{i_d} f\left(x_{i_1}, x_{i_2}, \ldots, x_{i_d}\right) \end{aligned} \tag{3.3.7}$$

The very commonly used simple product cubature formula, $Q^{(L,d)}_{\text{SP}}[f] = Q^{(d)}_{l_1=l_2=\ldots=l_d=L}[f]$, occurs when one integrates in each dimension using the same one-dimensional formula. The complexity of the simple-product formula is

$$C_{\text{SP}}(\varepsilon): \varepsilon^{-d/r}. \tag{3.3.8}$$

The simple product rule is optimal for functions that are merely differentiable, but is exponentially suboptimal for functions with bounded mixed derivatives.

One can do much better than the simple product rule by considering a linear combination of simple-product formulae with different orders. In this paper we will focus on the Smolyak rule,[17]

$$Q_{\mathrm{Sm}}^{(L,d)}[f] = \sum_{L-d+1 \le |\mathbf{l}|_1 \le L} (-1)^{L-|\mathbf{l}|_1} \binom{d-1}{q-|\mathbf{l}|_1} Q_{l_1 l_2 \ldots l_d}^{(d)}[f] \qquad (3.3.9)$$
$$|\mathbf{l}|_1 = l_1 + l_2 + \ldots + l_d.$$

The Smolyak rule is within a logarithmic factor of the optimal computational complexity for both differentiable functions (Eq. (3.3.4)) and for mixed-differentiable functions (Eq. (3.3.6)).[24,25] The Smolyak rule is not optimal, but more efficient formulae are significantly more difficult to understand and implement.[26,27] There has been some formal mathematical work[28-30] and proof-of-principle applications of the Smolyak method to the quantum theory of electronic structure.[31,32,33]

Most of the previous work on Smolyak rule has focused on integration over hypercubes,

$$\int_0^1 \cdots \int_0^1 \int_0^1 f(x_1, x_2, \ldots, x_d)\, dx_1 dx_2 \ldots dx_d \approx Q_{\mathrm{Sm}}^{(L,d)}[f] = \sum_{i=1}^{M_L} w_i f(\mathbf{x}_i). \qquad (3.3.10)$$

The Smolyak rule for hypercubes can be constructed from any one-dimensional quadrature formula on [0,1]. Our work was guided by that of Novak and Ritter, who have implemented and tested the Smolyak rule built from the one-dimensional Clenshaw-Curtis formula[34] and the one-dimensional rectangle rule[35]. Figure 3.1 shows the distribution of points in the 2-dimensional Smolyak-rectangle rule (Fig. 3.1a) and

Smolyak-Clenshaw-Curtis rule (Fig. 3.1b). Notice that the Smolyak grids are just simple product grids in which most of the points have been pruned away, with the points that remain reweighted accordingly. This can be done because for functions with bounded mixed derivatives, knowing the detailed behavior of the function in certain regions (e.g., along the central lines in the grid) is sufficient to determine the behavior nearby.

Table 3.1 lists the number of grid points in the Smolyak-rectangle rule and Smolyak-Clenshaw-Curtis rule for different dimensions. The number of grid points in the simple-product rectangle rule is listed for comparison. Even though the Smolyak cubatures have many fewer points than the simple product cubatures, the accuracy of the two approaches is similar.

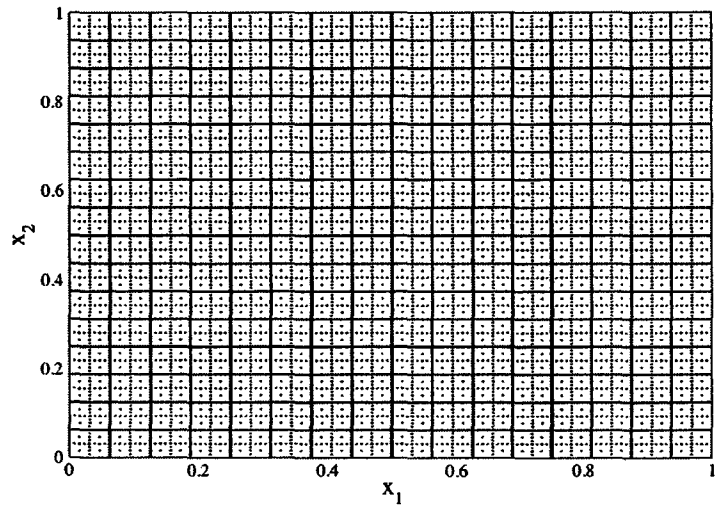

a)

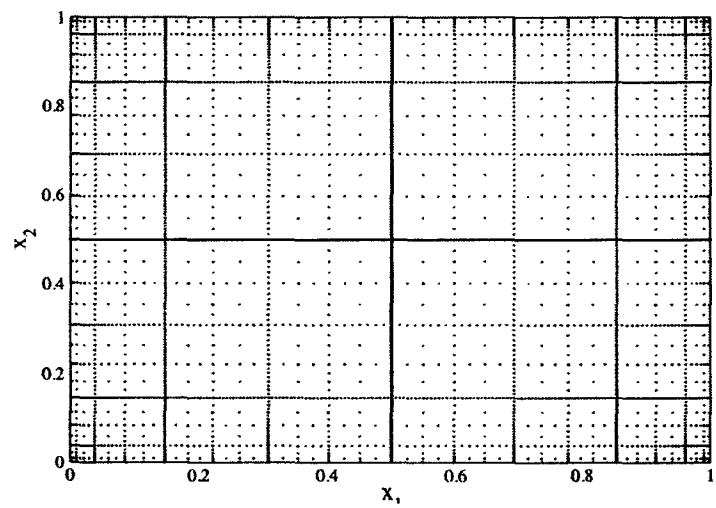

b)

Figure 3.1 The location of the points in the 11^{th} order two-dimensional Smolyak grids for (a) the rectangle rule and (b) the Clenshaw-Curtis rule.

Table 3.1 The number of points, M_L, in the Smolyak integration grid of order L built from the one-dimensional rectangle rule (RR) and Clenshaw-Curtis rule (CC). For comparison, the number of points in a simple product grid (SP) based on the rectangle rule is also included. Points on the boundary of the hypercube are not counted in this tabulation because they are mapped to infinity by the conditional distribution transformation, Eq. (3.3.12).

	1 dimension		2 dimensions			3 dimensions			6-dimensions		
L	RR	CC	RR	CC	SP	RR	CC	SP	RR	CC	SP
1	1	1	1	1	1	1	1	1	1	1	1
2	3	1	5	1	9	7	1	27	13	1	729
3	7	3	17	5	49	31	7	343	97	13	117,649
4	15	7	49	13	225	111	19	3375	545	37	1.1×10^{7}
5	31	15	129	33	961	351	55	29,791	2561	145	8.9×10^{8}
6	63	31	321	81	3969	1023	151	2.5×10^{5}	10,625	481	6.3×10^{10}
7	127	63	769	193	16,129	2815	399	2.0×10^{6}	40,193	1553	4.2×10^{12}
8	255	127	1793	449	65,025	7423	1023	1.7×10^{7}	1.4×10^{5}	4817	2.7×10^{14}
9	511	255	4097	1025	2.6×10^{5}	18,943	2559	1.3×10^{8}	4.7×10^{5}	14,465	1.8×10^{16}
10	1023	511	9217	2305	1.0×10^{6}	47,103	6271	1.1×10^{9}	1.5×10^{6}	42,241	1.1×10^{18}

3.3.3 The Conditional Distribution Transformation to $(-\infty,\infty)^d$

The Smolyak rule provides an accurate integration grid for the cube, $[0,1]^d$. However, we are primarily interested in weighted integrals over all space, Eq. (3.2.1). We will use the conditional distribution method[36-39] to define an appropriate transformation of coordinates. Specifically, we define a coordinate transformation

$$\mathbf{x} \in \left[0,1\right]^d \leftrightarrow \mathbf{R} \in \left(-\infty,\infty\right)^d \tag{3.3.11}$$

with

$$
\begin{aligned}
x_1(R_1) &= \frac{\int_{-\infty}^{R_1}\int_{-\infty}^{\infty}\cdots\int_{-\infty}^{\infty} P(r_1,r_2,\ldots,r_d)\,dr_d\ldots dr_2 dr_1}{\int_{-\infty}^{\infty}\int_{-\infty}^{\infty}\cdots\int_{-\infty}^{\infty} P(r_1,r_2,\ldots,r_d)\,dr_d\ldots dr_2 dr_1} \\
x_2(R_1,R_2) &= \frac{\int_{-\infty}^{R_2}\int_{-\infty}^{\infty}\cdots\int_{-\infty}^{\infty} P(R_1,r_2,r_3,\ldots,r_d)\,dr_d\ldots dr_3 dr_2}{\int_{-\infty}^{\infty}\int_{-\infty}^{\infty}\cdots\int_{-\infty}^{\infty} P(R_1,r_2,r_3,\ldots,r_d)\,dr_d\ldots dr_3 dr_2} \\
&\vdots \\
x_d(R_1,R_2,\ldots,R_d) &= \frac{\int_{-\infty}^{R_d} P(R_1,R_2,\ldots,R_{d-1},r_d)\,dr_d}{\int_{-\infty}^{\infty} P(R_1,R_2,\ldots,R_{d-1},r_d)\,dr_d}
\end{aligned}
\tag{3.3.12}
$$

The Jacobian determinant for this transformation is

$$
|\mathbf{J}| = \frac{\mathrm{P}(\mathbf{R})}{\int_{-\infty}^{\infty}\int_{-\infty}^{\infty}\cdots\int_{-\infty}^{\infty}\mathrm{P}(\mathbf{r})\,d\mathbf{r}} \tag{3.3.13}
$$

and so the cubature rule on the unit cube, Eq. (3.3.10), can be rewritten as a rule for weighted integrals in real space

$$
\begin{aligned}
&\int_{-\infty}^{\infty}\int_{-\infty}^{\infty}\cdots\int_{-\infty}^{\infty} g(\mathbf{R})\mathrm{P}(\mathbf{R})\,d\mathbf{r} \\
&\qquad \approx \left(\sum_{i=1}^{M_L} w_i g\left(\mathbf{R}(\mathbf{x}_i)\right)\right) \times \int_{-\infty}^{\infty}\int_{-\infty}^{\infty}\cdots\int_{-\infty}^{\infty}\mathrm{P}(\mathbf{R})\,d\mathbf{R}
\end{aligned}
\tag{3.3.14}
$$

The points in the real-space grid, $\mathbf{R}(\mathbf{x}_i)$, are determined using the inverse of the coordinate transformation in Eq. (3.3.12).

Notice that this transformation can be used for any integration grid on $[0,1]^d$. In this paper, we will use the transformation for the Smolyak rule, but if better choices were available, one could use those grids also. For example, Gaussian cubature formulae for the three-dimensional cube are known when the number of points is small, and would be a good choice when a small number of grid points will suffice.[14-16] Pérez-Jordá previously applied the conditional-distribution transformation to the simple-product grid, $Q_{SP}^{(d)}$.[40]

A few of the noteworthy features of this transformation follow.

1. The transformed grid points are concentrated in regions where $P(\mathbf{R})$ is large and depleted in regions where $P(\mathbf{R})$ is small. In fact, for uniformly distributed points, the probability of observing a point at $\mathbf{R}$ is precisely $P(\mathbf{R})$. This property is exploited in some other applications, where the conditional-distribution transformation is used for random-number generation with respect to the distribution $P(\mathbf{R})$.[36]
2. Points on the boundaries of the cube are transformed to $\pm\infty$. For this reason, it is important to ensure that the integrand in Eq. (3.3.14) decays faster than

$P(\mathbf{R})$ asymptotically. (I.e., $g(\mathbf{R})$ needs to decay to zero asymptotically.) This is inconvenient because it requires careful selection of the weight function, but it is advantageous because neglecting the boundary points reduces the number of grid points. Both the rectangle rule and the Clenshaw-Curtis rule have points on the boundary of the interval. Those points are not counted in the tabulation of points in Table 3.1.

3. The transformation of coordinates can be performed rapidly if the partial indefinite integrals of $P(\mathbf{R})$ in Eq. (3.3.12) can be performed analytically. In our work, we use fits of $P(\mathbf{R})$ to Gaussian-type functions,

$$P(\mathbf{R}) = \sum_{\alpha} \sum_{i} c_{\alpha i} e^{-a_{\alpha i} |\mathbf{R} - \mathbf{R}_{\alpha}|^2} . \tag{3.3.15}$$

This choice is motivated by the prevalence of Gaussian-type functions in computational models of molecular electronic structure.[41-43]

The selection of an appropriate $P(\mathbf{R})$ will differ from application to application. We are primarily interested in applications to molecular electronic structure; in this field the integrands tend to be largest in regions where the probability of observing an electron is the greatest (because these regions contribute the largest amount to molecular properties). This suggests that it will often be fruitful to choose $P(\mathbf{R})$ to be the electron density of the molecule of interest. In general, the electron density is not known until

after the calculation is complete, however, so one needs to approximate it. For this purpose we will choose the promolecular density:[44] the sum of the densities of the atoms the molecule comprises, centered at the positions of the associated atomic nucleus,

$$P(\mathbf{R}) = \rho_{pro}(\mathbf{R}) = \sum_{\alpha=1}^{N_{atoms}} \rho_{\alpha}(\mathbf{R} - \mathbf{R}_{\alpha}) \approx \rho(\mathbf{R}) \tag{3.3.16}$$

Notice that the promolecular electron density will take the convenient form in Eq. (3.3.15) if each atomic density is expressed as a sum of Gaussian-type functions. Constans and Carbó have fit the atomic densities from accurate Hartree-Fock calculations to Gaussians; we will use their fits in this paper.[43]

For the purpose of illustration, consider the two-dimensional H_4 molecule, with four pseudo-Hydrogen atoms with densities $\rho_{H}(x_1, x_2) = \frac{2}{\pi} e^{-2\sqrt{x_1^2 + x_2^2}}$ centered at (±1, ±1, 0). (Distances are measured in atomic units.) The points in the transformed Smolyak grids corresponding to this "molecule" are shown in Figures 3.2a (rectangle rule) and 2b (Clenshaw-Curtis rule). Notice that the points are concentrated in the regions where the atomic density is largest (near the atoms) and depleted in regions where the electron density is small.

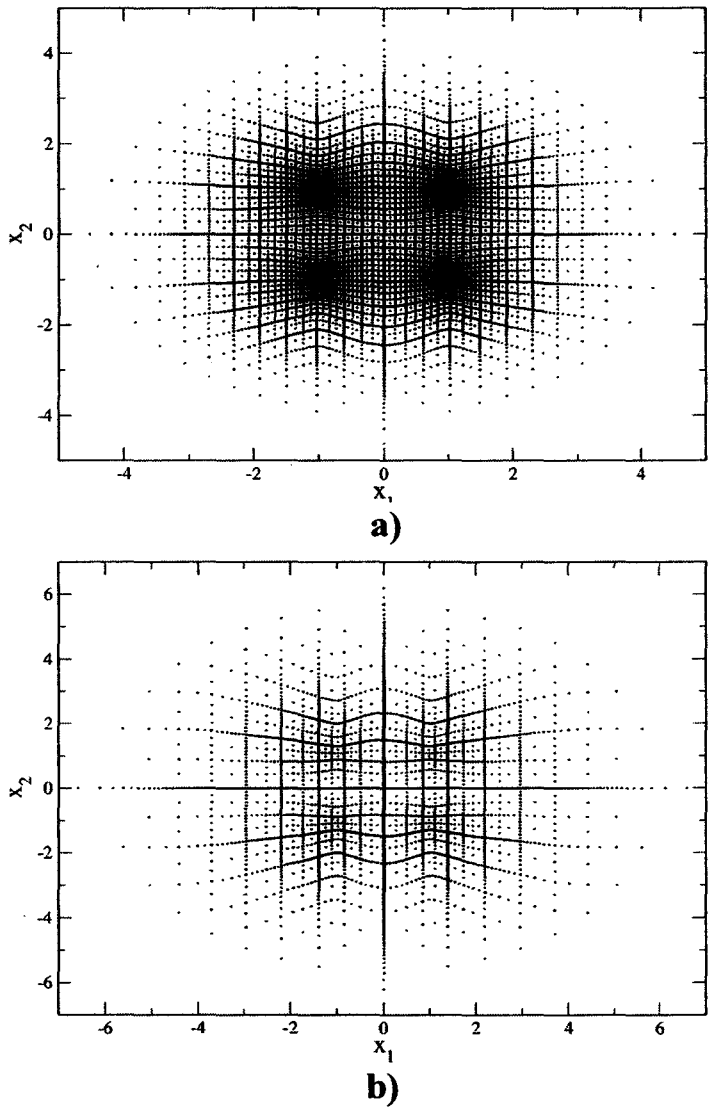

Figure 3.2 The location of the points in the transformed 11^{th} order Smolyak grid for the two-dimensional "pseudo-H_4" molecule with atoms located at (±1, ±1). (a) The transformed Smolyak-rectangle rule from Figure 3.1a. (b) The transformed Smolyak-Clenshaw-Curtis rule from Figure 3.1b.

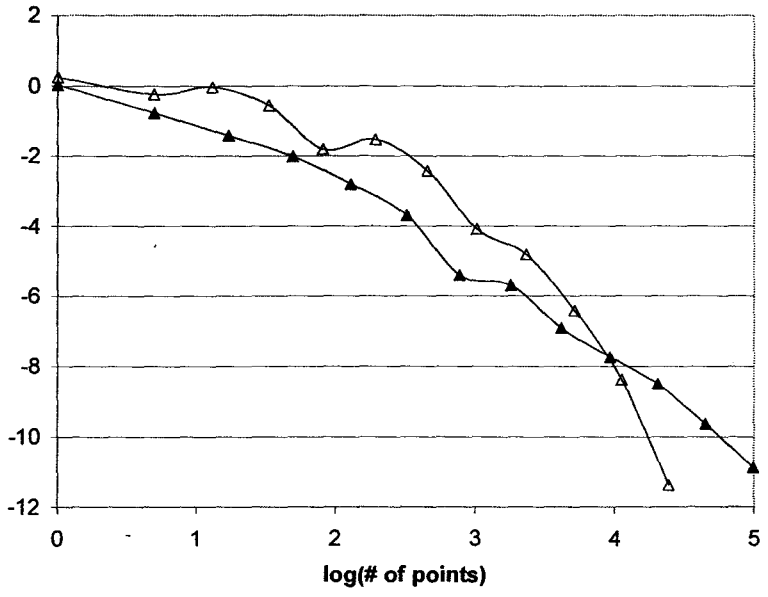

Figure 3.3 The convergence of the Smolyak formulae for the integral of a 2-dimensional Gaussian, Eq. (3.3.17) using the pseudo-H_4 grid shown in Figure 3.2. The $\log_{10}$(relative error) rapidly decreases as $\log_{10}$(number of grid points) increases. Results for the rectangle rule are reported using closed symbols (—▲—) and results for the Clenshaw-Curtis rule are reported using open symbols (—△—).

When the integrand does not resemble $P(\mathbf{r})$, this provides a stringent test for the quality of the grids. Figure 3.3 shows the results obtained by using the pseudo-H_4 grid to integrate a simple Gaussian function,

$$\pi = \int_{-\infty}^{\infty}\int_{-\infty}^{\infty} e^{-x_1^2 - x_2^2} dx_1 dx_2 \,. \tag{3.3.17}$$

As the number of points in the Smolyak grids increases, the results of the integration rapidly converge to the correct value.

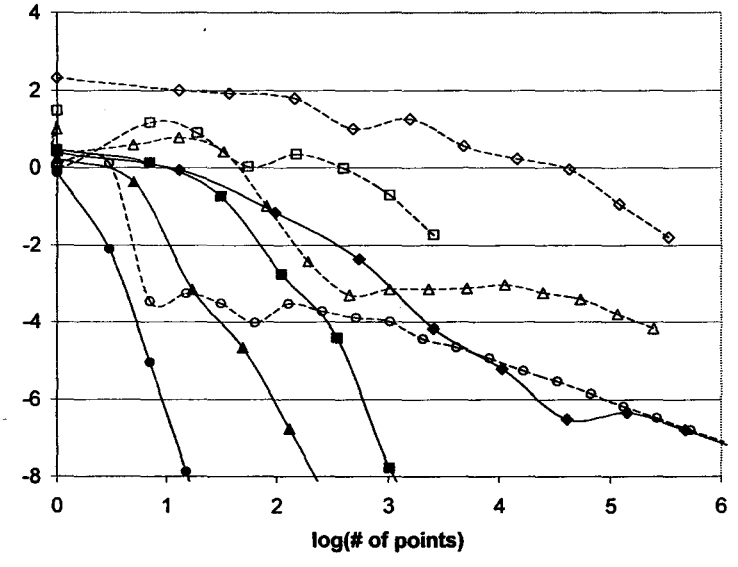

Figure 3.4 The convergence of the Smolyak formulae for integrating the Gaussian in Eq. (3.4.1) using the weight function given in Eq. (3.4.2). The plot shows $\log_{10}$(relative error)) versus $\log_{10}$(number of grid points). The rectangle rule results are denoted by: 1-dimension (—●—); 2-dimensions (—▲—); 3-dimensions (—■—); 6-dimensions (—◆—). The results for the Clenshaw-Curtis rule are denoted with the analogous open symbols.

3.4 Results

3.4.1 Gaussian Function

To provide a more realistic test of the convergence of the Smolyak formulae, Figure 3.4 presents the results for the convergence for an integrand that is a Gaussian,

$$\begin{aligned} f(x_1, x_2, ..., x_d) &= \prod_{i=1}^{d} \exp\left(-(d-i+1)x_i^2\right) \\ &= \exp\left(-x_d^2 - 2x_{d-1}^2 - 3x_{d-2}^2 - ...\right) \end{aligned}, \tag{3.4.1}$$

with respect to a weight that is also a Gaussian,

$$P(x_1, x_2, ..., x_d) = \prod_{i=1}^{d} \exp\left(-\tfrac{1}{2}x_i^2\right). \tag{3.4.2}$$

Notice that the Gaussian weight decays significantly more slowly than the integrand; this is required because we are ignoring boundary points.

Referring to Figure 3.4, the rectangle rule seems to be much better than Clenshaw-Curtis. This may be explained by the tendency for the Clenshaw-Curtis rule to "bunch up points" near the edges of the integration interval (see Figure 3.1b). This is advantageous when the function does not behave well near the boundary of the interval, but the function we are integrating here decays exponentially quickly asymptotically. The rectangle rule, which has a higher concentration of points in the center of the interval, performs much better for this sort of integral. We also observed that the rectangle rule formulae seems less prone to round-off error than the Clenshaw-Curtis formulae.

3.4.2 The Gordon-Kim Model

Heartened by the results obtained from this simple test, we decided to explore the efficiency of the transformed Smolyak integration grids for the types of integrals that appear in density-functional theory. Our first test uses the simple density functional theory model of molecular interactions proposed by Gordon and Kim.[45] In this model, the interaction potential between two atoms, one of which (denoted α) is centered at the origin and the other of which (denoted β) is centered R atomic units away, is approximated as

$$V_{\alpha\beta}(R) = \frac{Z_\alpha Z_\beta}{R} + \iint \frac{\rho_\alpha(\mathbf{r})\rho_\beta(\mathbf{r}')}{|\mathbf{r}-\mathbf{r}'|} d\mathbf{r}d\mathbf{r}' - \int \frac{Z_\alpha \rho_\alpha(\mathbf{r})}{r} d\mathbf{r} - \int \frac{Z_\beta \rho_\beta(\mathbf{r})}{|\mathbf{r}-[0,0,R]|} d\mathbf{r}$$
$$+ T_s^{(\text{non-add})}[\rho_\alpha, \rho_\beta] + E_x^{(\text{non-add})}[\rho_\alpha, \rho_\beta] + E_c^{(\text{non-add})}[\rho_\alpha, \rho_\beta]. \quad (3.4.3)$$

In this equation, the electron density for atom α, $\rho_\alpha(\mathbf{r})$, is centered on the origin; the electron density for atom β is centered on the z-axis, R units away. The first four terms in Eq. (3.4.3) are just the electrostatic interactions between the nuclei, between the electron densities of the isolated atoms, and between the electron densities of each atom with the other nucleus. These terms capture the electrostatic contribution to binding in the "frozen density approximation." The frozen density approximation is accurate when the atoms are so far apart that their electron densities are not significantly polarized.

The last three terms in Eq. (3.4.3) are the non-additive contributions to the kinetic energy, the exchange energy, and the correlation energy, respectively; these are defined by subtracting the value of the function for the molecule from the value of the functional for the atoms,

$$Q^{(\text{non-add})}\left[\rho_\alpha,\rho_\beta\right] \equiv Q\left[\rho_\alpha+\rho_\beta\right]-Q\left[\rho_\alpha\right]-Q\left[\rho_\beta\right]. \tag{3.4.4}$$

The non-additive contributions are usually evaluated using explicit Thomas-Fermi-like functionals. Here we have elected to use the Thomas-Fermi kinetic energy functional[46,47]

$$T_s^{TF}\left[\rho\right]=\frac{3\left(3\pi^2\right)^{2/3}}{10}\int\rho^{5/3}\left(\mathbf{r}\right)d\mathbf{r}, \tag{3.4.5}$$

the McWeeny reparameterization[48] of the Wigner correlation functional[49]

$$E_c^{\text{MW}}\left[\rho\right]=-\int\frac{\rho^{4/3}\left(\mathbf{r}\right)}{2.946+9.652\rho^{1/3}\left(\mathbf{r}\right)}d\mathbf{r}, \tag{3.4.6}$$

and the Dirac exchange functional[50-52] with the Rae[53,54] self-interaction correction[55] factor,

$$E_x^{\text{RD}}\left[\rho\right]=-\kappa\left(N\right)\left(\frac{3}{4}\left(\frac{3}{\pi}\right)^{1/3}\right)\int\rho^{4/3}\left(\mathbf{r}\right)d\mathbf{r}. \tag{3.4.7}$$

N denotes the number of electrons. Rae's correction factor is obtained by solving the equation[53,54]

$$1=N\delta^3\left(\delta^3-4.5\delta+4\right) \tag{3.4.8}$$

and then computing

$$\kappa(N) = 1 - \tfrac{8}{3}\delta + 2\delta^2 - \tfrac{1}{3}\delta^3 . \tag{3.4.9}$$

To evaluate the Gordon-Kim expression for the interaction energy, we need an accurate expression for the ground-state electron densities of the isolated atoms. We have again used the Gaussian atomic density fits of Constans and Carbó,[43]

$$\rho_\alpha(\mathbf{r}) = \sum_i c_{\alpha i} e^{-a_{\alpha i} r^2} . \tag{3.4.10}$$

One advantage of this form is that the electrostatic contributions to the energy can be evaluated analytically, so only the non-additive terms in Eq. (3.4.3) require numerical integration. While the Constans-Carbó fits are not accurate enough for truly quantitative results, they are certainly sufficient for testing our integration techniques.

The last three terms in Eq. (3.4.3) need to be evaluated numerically. To do this, we construct the promolecular density (cf. Eq. (3.3.16)) from the Constans-Carbó densities and, as described in section II.C, use this as the weight function for the conditional distribution transformation. Since the promolecular density depends on the position of the atoms, the transformed-Smolyak grids adapt to changes in the internuclear distance by placing more points in regions where the density is the highest (near the atomic nuclei) and fewer points far from the atomic nuclei.

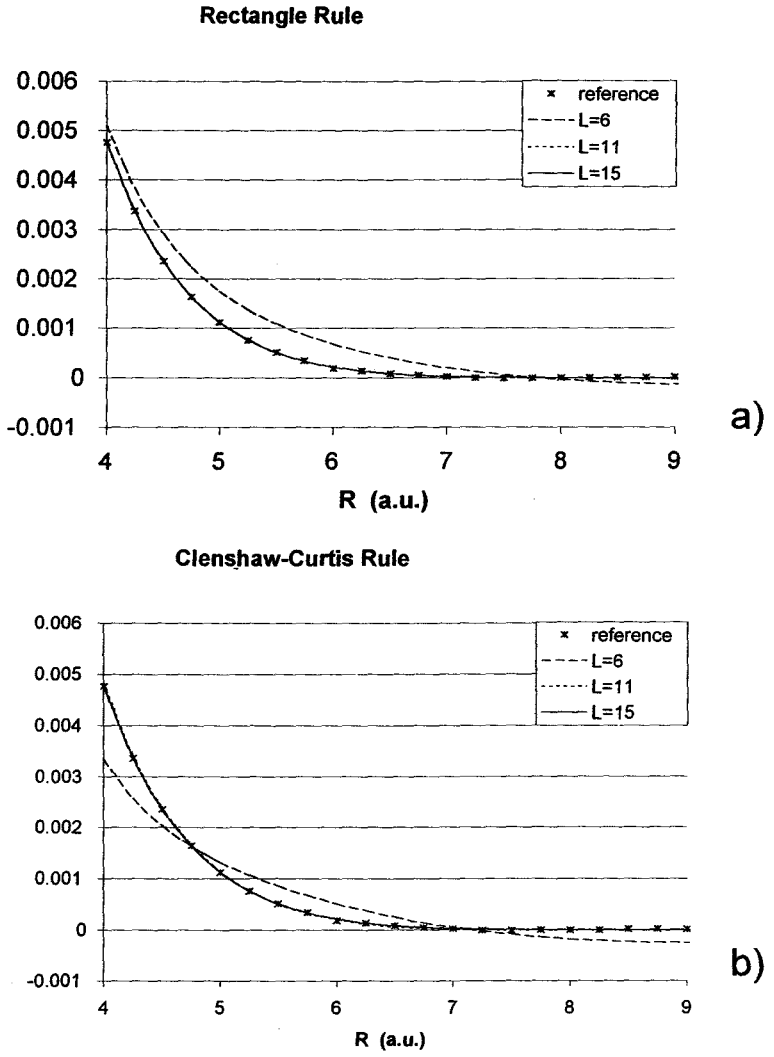

Figure 3.5 Smolyak formulae of various orders, L, are used to construct the potential energy of interaction for the H_2 molecule from applying Thomas-Fermi-Dirac-McWeeny Gordon-Kim model to the Constans-Carbo atomic density fits. (a) Rectangle rules. (b) Clenshaw-Curtis rules. The reference data was obtained using third-party software (*Mathcad*).

In Figure 3.5 we compare our results for the H_2 molecule to the values we obtained using third-party software (*Mathcad*, with integration tolerance TOL=10^{-8} and the default Romberg integration algorithm). As the order of integration increases, our integration method converges rapidly. It should be noted that the Gordon-Kim model fails to describe the substantial electron-density rearrangement that accompanies chemical binding in H_2, and so this interaction energy curve is not qualitatively correct. Our interest in this model is based primarily on its relevance for developing next-generation molecular mechanics force fields, where models similar to Gordon-Kim can be used to model the "repulsive wall" on the potential energy curve that prevents atoms from coming too close together.[56-59]

To evaluate the convergence of our methods in greater detail, we engaged in a detailed study of the interaction energy expression for the Neon dimer, Ne_2. Some of the results from that study are shown in Figure 3.6, where the convergence of the total interaction energy and each of its non-additive components are plotted. In Figure 3.6, we plot the approximate "number of digits of accuracy" in the formula, which we define through

$$\text{digits} = -\log_{10}\left(\frac{Q_L - Q_\infty}{Q_\infty}\right). \qquad (3.4.11)$$

Here Q_L denotes the result from the integration formulae of order L and Q_∞ denotes the infinite-order limit. Since Q_∞ cannot be computed explicitly, we replaced this value with

the result from the highest-order calculation we performed, $Q_{L_{max}}$. Especially at low orders, the resulting plots provide a faithful representation of the rate of convergence with increasing number of points in the integration grid. Examining Figure 3.6 in more detail, one observes that the rectangle rule typically performs better than the Clenshaw-Curtis rule, although the difference in performance is usually not as dramatic as it was for the simple Gaussian test function. The rectangle rule converges more rapidly for the exchange energy than it does for the kinetic energy, which is not surprising since $\rho^{4/3}(\mathbf{r})$ resembles the promolecular density used to construct the grid more closely than $\rho^{5/3}(\mathbf{r})$. The correlation energy component converges most slowly, which indicates that its relatively complicated functional form does not mimic the promolecular density very strongly. All of these results reinforce the expectation that our integration technique will be most accurate when the weight function, $P(\mathbf{R})$, used to transform the grid strongly resembles the integrand of interest.

The largest component of the total interaction energy expression is the kinetic energy component. Thus it is unsurprising that the error in the total interaction energy is dominated by the error in the non-additive kinetic energy.

It should be stressed that the Gordon-Kim model represents a very strenuous test of our grids. For example, the non-additive contribution to the kinetic energy is 400 times smaller than the kinetic energy of the promolecule. In practice, this means that obtaining

four digits of accuracy in the molecular interaction energy requires at least *seven* digits of accuracy in the integrals.

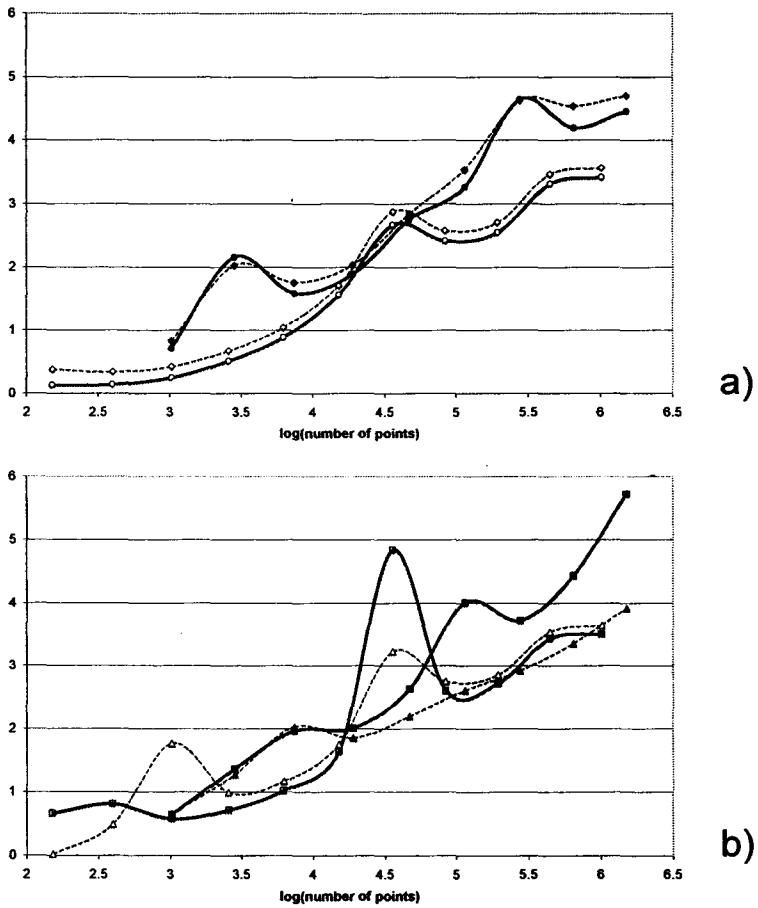

Figure 3.6 The number of digits of accuracy when Smolyak grids of various orders are used to evaluate the Thomas-Fermi-Dirac-McWeeny Gordon-Kim model of the Ne_2 interaction potential using the Constans-Carbo atomic density fits. The number of digits of accuracy (see Eq. (3.4.11) and the surrounding discussion) is plotted versus $\log_{10}$(number of grid points). Results for both the rectangle rule (closed symbols) and the Clenshaw-Curtis formula (open symbols) are reported. (a) Results for total interaction potential (—●—) and the non-additive kinetic energy (---◆---). (b) Results for the non-additive exchange energy (—■—) and the non-additive correlation energy (---▲---).

3.4.3 The Gaussian Model for the Exchange Energy

The favorable results for molecular interaction energies suggests that transformed Smolyak grids are more generally applicable, particularly in the context of density-functional theory. Here we will consider an application to a six-dimensional "kernel-type" approximation to the exchange energy density functional.

Kernel-type density functionals allow us to write the exchange-correlation energy in terms of the exchange-correlation hole, and thus facilitate the direct probabilistic interpretation of exchange and correlation effects. Such functionals have a long and distinguished history, dating back to the weighted density approximation.[60-66] Progress has been impeded by the computational cost of performing six-dimensional integrals but, despite the cost, there has been a recent resurgence of interest in kernel-type functionals. Part of that interest is based on the explicit nonlocality of kernel-type functionals, which make it possible to model systems where the exchange-correlation hole is spatially delocalized.[67,68] This seems to be particularly important for describing dispersion forces.[69-73] There is also interest stemming from the closely-related pair-density functional theory, in which the exchange-correlation hole and the electron density are the fundamental variational parameters.[74-79]

It is difficult to test whether the transformed Smolyak grids can be applied to this problem because of the absence of accurate numerical data to compare to. However, the 6-dimensional Gaussian-kernel model of Lee and Parr is equivalent to a three-

dimensional model.[80] Therefore we can ascertain the accuracy of our numerical integration procedure by comparing the results we obtain from,

$$E_x^{\mathrm{LP}}[\rho]=\frac{-1}{2}\iint\rho^2\left(\tfrac{\mathbf{r}+\mathbf{r}'}{2}\right)\exp\left(-\frac{\pi|\mathbf{r}-\mathbf{r}'|^2}{2^{2/3}\rho^{-2/3}\left(\frac{\mathbf{r}+\mathbf{r}'}{2}\right)}\right)\times\frac{1}{|\mathbf{r}-\mathbf{r}'|}d\mathbf{r}d\mathbf{r}', \quad (3.4.12)$$

to the results of the Dirac-type exchange energy functional,

$$E_x^{\mathrm{LP}}[\rho,0]=-2^{-1/3}\int\rho^{4/3}(\mathbf{r})d\mathbf{r}. \quad (3.4.13)$$

The values of the three dimensional integral, (3.4.13), may be inferred from the results obtained from the Gordon-Kim model. (Compare Eqs. (3.4.7) and (3.4.13).) To evaluate the six-dimensional integral, (3.4.12), we choose the weight to be the product of the promolecular densities, $P(\mathbf{r},\mathbf{r}')=\rho_{\mathrm{pro}}(\mathbf{r})\rho_{\mathrm{pro}}(\mathbf{r}')$. A disadvantage of this symmetric form is that points where $\mathbf{r}=\mathbf{r}'$ occur in our integration grid; this causes problems because the integrand in Eq. (3.4.12) is singular at these points. This can be circumvented by decomposing the functional into short-range and long-range pieces,

$$E_x^{\mathrm{LP}}[\rho]=E_x^{\mathrm{LP\text{-}SR}}[\rho]+E_x^{\mathrm{LP\text{-}LR}}[\rho]. \quad (3.4.14)$$

The short-range and long-range pieces are defined using the complementary error function and the error function, respectively:

$$E_x^{\mathrm{LP\text{-}SR}}[\rho,\mu]=\frac{-1}{2}\iint\rho^2\left(\tfrac{\mathbf{r}+\mathbf{r}'}{2}\right)\exp\left(-\frac{\pi|\mathbf{r}-\mathbf{r}'|^2}{2^{2/3}\rho^{-2/3}\left(\frac{\mathbf{r}+\mathbf{r}'}{2}\right)}\right)\times\frac{\mathrm{erfc}(\mu|\mathbf{r}-\mathbf{r}'|)}{|\mathbf{r}-\mathbf{r}'|}d\mathbf{r}d\mathbf{r}'. \quad (3.4.15)$$

$$E_x^{\text{LP-LR}}[\rho,\mu]=\frac{-1}{2}\iint\rho^2\left(\tfrac{\mathbf{r}+\mathbf{r}'}{2}\right)\exp\left(-\frac{\pi|\mathbf{r}-\mathbf{r}'|^2}{2^{2/3}\rho^{-2/3}\left(\tfrac{\mathbf{r}+\mathbf{r}'}{2}\right)}\right)\times\frac{\operatorname{erf}\left(\mu|\mathbf{r}-\mathbf{r}'|\right)}{|\mathbf{r}-\mathbf{r}'|}d\mathbf{r}d\mathbf{r}'$$

(3.4.16)

A three-dimensional density-functional model for the singular "short-range" functional using the time-honored, but tedious and difficult, approach.[81-83] The integrand of the "long-range" functional is not singular and it can be evaluated numerically. Figure 3.7 shows results for the Neon dimer obtained using the Smolyak-rectangle rule of various orders, L. Notice that as μ increases, the value of the integrand approaches the accurate value computed from Eq. (3.4.13). For the higher values of μ considered here, the integrand is very strongly peaked where $\mathbf{r}\approx\mathbf{r}'$; this is why the order of integration needed to obtained converged results increases rapidly as μ increases. Fortunately, it is possible to develop very good short-range functionals, so the value of μ can remain quite small.

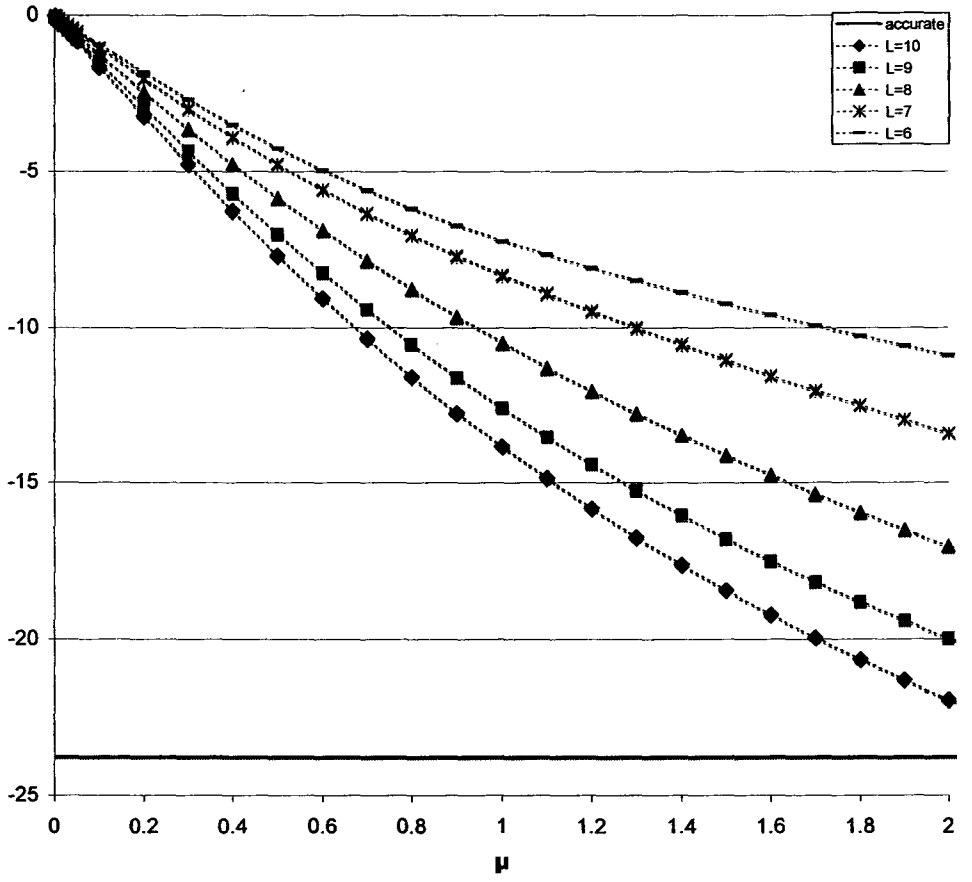

Figure 3.7 The long-range contribution to the exchange energy, Eq. (3.4.16), for the Neon dimer with internuclear separation 2.5 a.u. is computed using the Smolyak-rectangle rule integration of various orders, L, for different values of the range separation parameter, μ. Atomic units are used.

3.5 Summary

We have developed an efficient method for general multi-dimensional integrals with respect to arbitrary weight functions (i.e., integrals with the form of Eq. (3.2.1)). Our approach uses the Smolyak method to first construct cubature grids on the cube, $[0,1]^d$ (cf. Eq. (3.3.9)) and then uses the conditional distribution transformation to generate integration grids in real space with respect to any given weight function (cf. Eq. (3.3.12)). The integration grids converge rapidly to the correct answer. We applied the grids to the Gordon-Kim model for atomic interactions[45] and the Lee-Parr Gaussian model for the exchange energy.[80]

These calculations can be seen as "proof of principle" studies for two areas where we see this method having broad applicability. The Gordon-Kim calculations are directly relevant to the field of frozen-density embedding, where "improved" Gordon-Kim models are used to model non-covalent interactions between solutes and solvents, metals and ligands, etc..[84-88] More generally, the quality of our results for the Gordon-Kim model indicates that this method will be generally useful for the evaluation of density functionals. It would certainly be interesting, for example, to study more sophisticated kinetic-energy functionals. It is of greater direct interest, however, to consider using the transformed Smolyak grids as the default integration method for evaluating the exchange-correlation energies and exchange-correlation potentials in Kohn-Sham density-

functional theory. We performed such studies and obtained excellent results; those findings will be reported separately.[33]

The application to nonlocal, kernel-type, exchange-correlation functionals shows that this integration method may be profitably used for six-dimensional integrals. While nonlocal exchange-correlation functionals are indubitably of great current interest,[60-66] the same methods are relevant to "generalized" density-functional theories,[89,90] most notably the pair-density functional theory[74-79] and the first-order density matrix functional theory.[91-93] We are currently working on applications in both nonlocal exchange-correlation density functionals and pair-density functional theory.

At the mathematical level, we are examining methods for improving the efficiency of our numerical integration grids. For example, would it be helpful use the "promolecular" exchange-correlation energy density (instead of the promolecular electron density) as the weight function for the transformation? How well do other sparse-grid methods work? Are there better one-dimensional formulae than Clenshaw-Curtis and the rectangle rule? Answering these questions will help us advance toward an "optimal" numerical integration method for electronic structure modeling.

3.6 References for chapter 3

1 T. Kato, Commun.Pure Appl.Math. **10**, 151 (1957).

2 E. Steiner, J. Chem. Phys. **39**, 2365 (1963).

3 E. Bene and A. Nagy, Journal of Molecular Structure-Theochem **501**, 107 (2000).

4 A. Nagy and K. D. Sen, Chem. Phys. Lett. **332**, 154 (2000).

5 A. Nagy and K. D. Sen, Journal of Physics B-Atomic Molecular and Optical Physics **33**, 1745 (2000).

6 A. Nagy and K. D. Sen, J. Chem. Phys. **115**, 6300 (2001).

7 P. W. Ayers, Proceedings of the National Academy of Sciences **97**, 1959 (2000).

8 W. Gautschi, ACM Transactions on Mathematical Software **20**, 21 (1994).

9 W. Gautschi, Acta Numerica **5**, 45 (1996).

10 W. Gautschi, ACM Transactions on Mathematical Software **24**, 355 (1998).

11 W. Gautschi, *Orthogonal polynomials: Computation and approximation.* (Oxford UP, New York, 2004).

12 D. Rees and G. G. Hall, Int. J. Quantum Chem. **102**, 19 (2005).

13 G. G. Hall and D. Rees, Int. J. Quantum Chem. **107**, 845 (2007).

14 R. Cools and P. Rabinowitz, Journal of Computational and Applied Mathematics **48**, 309 (1993).

15 R. Cools, Journal of Computational and Applied Mathematics **112**, 21 (1999).

16 R. Cools, Journal of Complexity **19**, 445 (2003).

[17] S. A. Smolyak, Dokl. Akad. Nauk **4**, 240 (1963).

[18] J. F. Traub and H. Wozniakowski, Bull.AMS **26**, 29 (1992).

[19] J. F. Traub and A. G. Werschulz, *Complexity and information.* (Cambridge UP, Cambridge, 1998).

[20] J. A. C. Weideman and L. N. Trefethen, Numerische Mathematik **107**, 707 (2007).

[21] L. N. Trefethen, SIAM Review **50**, 67 (2008).

[22] C. W. Murray, N. C. Handy, and G. J. Laming, Mol. Phys. **78**, 997 (1993).

[23] Y. Xu, *Common zeros of polynomials in several variables and higher dimensional quadrature.* (Wiley New York, 1994).

[24] G. W. Wasilkowski and H. Wozniakowski, Journal of Complexity **11**, 1 (1995).

[25] E. Novak and K. Ritter, Constructive Approximation **15**, 499 (1999).

[26] H. J. Bungartz and M. Griebel, Journal of Complexity **15**, 167 (1999).

[27] M. Griebel and S. Knapek, Constructive Approximation **16**, 525 (2000).

[28] H. Yserentant, Numerische Mathematik **98** (4), 731 (2004).

[29] H. Yserentant, Numerische Mathematik **101** (2), 381 (2005).

[30] H. Yserentant, Numerische Mathematik **105** (4), 659 (2007).

[31] J. Garcke and M. Griebel, J. Comput. Phys. **165** (2), 694 (2000).

[32] M. Griebel and J. Hamaekers, Esaim-Mathematical Modelling and Numerical Analysis-Modelisation Mathematique Et Analyse Numerique **41** (2), 215 (2007).

[33] J. I. Rodriguez, D. C. Thompson, A. Koster, and P. W. Ayers, Phys. Rev. A (submitted).

[34] E. Novak and K. Ritter, Numerische Mathematik **75**, 79 (1996).

[35] R. Cools, E. Novak, and K. Ritter, Computing **62**, 147 (1999).

[36] L. Devroye, *Non-uniform Random Variate Generation.* (Springer-Verlag, New York, 1986).

[37] J. M. Perez-Jorda, European Journal of Physics **10**, 224 (1989).

[38] D. C. Thompson and P. W. Ayers, Int. J. Quantum Chem. **106**, 787 (2006).

[39] J. S. M. Anderson, J. I. Rodriguez, D. C. Thompson, and P. W. Ayers, in *Quantum Chemistry Research Trends* (Nova, Hauppauge, NY, 2007).

[40] J. M. Perez-Jorda, Phys. Rev. A **52**, 2778 (1995).

[41] L. E. McMurchie and E. R. Davidson, J. Comput. Phys. **26**, 218 (1978).

[42] S. F. Boys, Proceedings of the Royal Society of London. Series A **200**, 542 (1950).

[43] P. Constans and R. Carbó, Journal of Chemical Information and Computer Sciences **35**, 1046 (1995).

[44] F. L. Hirshfeld, Theor. Chim. Act. **44**, 129 (1977).

[45] R. G. Gordon and Y. S. Kim, J. Chem. Phys. **56**, 3122 (1972).

[46] L. H. Thomas, Proc.Camb.Phil.Soc. **23**, 542 (1927).

[47] E. Fermi, Z.Phys. **48**, 73 (1928).

[48] R. McWeeny, New World Quantum Chem., Proc.Int.Congress **2**, 3 (1976).

[49] E. Wigner, Phys.Rev. **46**, 1002 (1934).

[50] P. A. M. Dirac, Proc.Cambridge Phil.Soc. **26**, 376 (1930).

[51] J. C. Slater, Physical Review **81** (3), 385 (1951).

[52] W. Kohn and L. J. Sham, Phys.Rev. **140**, A1133 (1965).

[53] A. I. M. Rae, Chem. Phys. Lett. **18**, 574 (1973).

[54] A. I. M. Rae, Mol. Phys. **29**, 467 (1975).

[55] J. P. Perdew and A. Zunger, Phys. Rev. B **23**, 5048 (1981).

[56] G. A. Cisneros, J. P. Piquemal, and T. A. Darden, J. Chem. Phys. **123**, 044109 (2005).

[57] J. P. Piquemal, L. Perera, G. A. Cisneros, P. Y. Ren, L. G. Pedersen, and T. A. Darden, J. Chem. Phys. **125**, 054511 (2006).

[58] J. P. Piquemal, G. A. Cisneros, P. Reinhardt, N. Gresh, and T. A. Darden, J. Chem. Phys. **124**, 104101 (2006).

[59] G. A. Cisneros, J. P. Piquemal, and T. A. Darden, J. Chem. Phys. **125**, 184101 (2006).

[60] O. Gunnarsson, M. Jonson, and B. I. Lundqvist, Phys. Lett. A **59** (3), 177 (1976).

[61] J. A. Alonso and L. A. Girifalco, Solid State Commun. **24** (2), 135 (1977).

[62] O. Gunnarsson, M. Jonson, and B. I. Lundqvist, Solid State Commun. **24** (11), 765 (1977).

[63] J. A. Alonso and L. A. Girifalco, Phys. Rev. B **17** (10), 3735 (1978).

[64] O. Gunnarsson and R. O. Jones, Phys. Scr. **21** (3-4), 394 (1980).

[65] A. C. Pedroza, Phys. Rev. A **33** (2), 804 (1986).

[66] C. Amovilli and N. H. March, Phys. Rev. B **76**, 195104 (2007).

[67] O. V. Gritsenko, B. Ensing, P. R. T. Schipper, and E. J. Baerends, J. Phys. Chem. A **104**, 8558 (2000).

[68] Y. Zhang and W. Yang, J. Chem. Phys. **109** (7), 2604 (1998).

[69] M. Dion, H. Rydberg, E. Schroder, D. C. Langreth, and B. I. Lundqvist, Phys. Rev. Lett. **92**, 246401 (2004).

[70] T. Thonhauser, A. Puzder, and D. C. Langreth, J. Chem. Phys. **124**, 164106 (2006).

[71] A. Puzder, M. Dion, and D. C. Langreth, J. Chem. Phys. **124**, 164105 (2006).

[72] J. Kleis, B. I. Lundqvist, D. C. Langreth, and E. Schoder, Phys. Rev. B **76**, 100201 (2007).

[73] T. Thonhauser, V. R. Cooper, S. Li, A. Puzder, P. Hyldgaard, and D. C. Langreth, Phys. Rev. B **76**, 125112 (2007).

[74] P. Ziesche, Phys. Lett. A **195**, 213 (1994).

[75] P. Ziesche, Int. J. Quantum Chem. **60**, 1361 (1996).

[76] A. Nagy, Phys. Rev. A **66**, 022505 (2002).

[77] A. Nagy and C. Amovilli, J. Chem. Phys. **121** (14), 6640 (2004).

[78] P. W. Ayers, Journal of Mathematical Physics **46**, 062107 (2005).

[79] P. W. Ayers, S. Golden, and M. Levy, J. Chem. Phys. **124**, 054101 (2006).

[80] C. Lee and R. G. Parr, Phys. Rev. A **35** (6), 2377 (1987).

[81] J. Toulouse, P. Gori-Giorgi, and A. Savin, Theor. Chem. Acc. **114** (4-5), 305 (2005).

[82] J. Toulouse, F. Colonna, and A. Savin, J. Chem. Phys. **122** (1) (2005).

[83] J. Toulouse, A. Savin, and H. J. Flad, Int. J. Quantum Chem. **100** (6), 1047 (2004).

[84] P. Cortona, Phys. Rev. B **44** (16), 8454 (1991).

[85] T. A. Wesolowski and A. Warshel, J. Phys. Chem. **97** (30), 8050 (1993).

[86] N. Vaidehi, T. A. Wesolowski, and A. Warshel, J. Chem. Phys. **97** (6), 4264 (1992).

[87] T. A. Wesolowski and J. Leszczynski, in *Computational Chemistry: Reviews of Current Trends* (World Scientific, Singapore, 2006), pp. 1.

[88] N. Govind, Y. A. Wang, and E. A. Carter, J. Chem. Phys. **110** (16), 7677 (1999).

[89] P. W. Ayers, Phys. Rev. A **74**, 042502 (2006).

[90] P. W. Ayers and M. Levy, Journal of Chemical Sciences **117**, 507 (2005).

[91] M. Levy, Proceedings of the National Academy of Sciences **76** (12), 6062 (1979).

[92] T. L. Gilbert, Phys. Rev. B **12**, 2111 (1975).

[93] R. A. Donnelly and R. G. Parr, J. Chem. Phys. **69**, 4431 (1978).

"... neither of us probably know anything that is really good, but he thinks that he has knowledge, when he has not, while I, having no knowledge, do not think that I have. I seem, at any rate, to be a little wiser than he is on this point: I do not think that I know what I do not know"
Socrates.

Socrates' Apology, Plato.

Chapter 4

A NOVEL GRID –BASED APPROACH TO THE ELECTRONIC STRUCTURE PROBLEM: INTERPOLANTS AND DERIVATIVES*

* The content of this chapter was already published: J. S. M. Anderson, J. I. Rodriguez, D. C. Thompson, and P. W. Ayers in *Quantum Chemistry Research Trends.* Mikas P. Kaisas (Editor). New York: Nova Science Publisher, 2007 (see next page).

In: Quantum Chemistry Research Trends
Editor: Mikas P. Kaisas, pp. 103-121
ISBN 978-160021-620-6

Chapter 3

A NOVEL GRID BASED APPROACH TO THE ELECTRONIC STRUCTURE PROBLEM: INTERPOLANTS AND DERIVATIVES

James S.M. Anderson, Juan I. Rodriguez, David C. Thompson and Paul W. Ayers[†]
Department of Chemistry, McMaster University, Hamilton, ON L8S 4M1, Canada

Abstract

The electronic structure problem is introduced and briefly reviewed within the context of density-functional theory. The use of numerical grid based schemes, circumventing the use of a basis set, will be discussed. We will briefly introduce our numerical grid methodology for use in electronic structure theory. This method, which is based upon a combination of the Smolyak cubature construction and a novel nonlinear transformation, has been shown to be efficacious when applied to cubature of physically relevent functions. In this paper we extend these results to interpolation and differentiation; these being the other fundamental operations essential for a numerical solution of the electronic structure problem. We shall investigate the performance of our method as a function of spatial dimension, number of grid points and, across a wide range of relevant functions.

1. Introduction

The fundamental problem of molecular electronic structure determination, or the solution of the underlying equations governing the behaviour of electrons, traditionally involves com-

*Present address: Department of Structural Biology and Computational Chemistry, Chemical & Screening Sciences, Wyeth Research, 200 Cambridge Park Drive, Cambridge, MA 02140
†E-mail address: ayers@mcmaster.ca

4.1 Statement of the problem

The preceding chapters demonstrate that the transformed Smolyak grid is effective for numerical integration of types of functions that arise in molecular electronic structure theory. In this chapter we develop methods for interpolation and differentiation, which are the other fundamental operations required for fully-numerical solutions of the electronic structure problem. We shall investigate the performance of our method across a wide range of relevant functions as a function of spatial dimension and the number of grid points. These results provide the essential methodology for basis-set-free approaches to the electronic structure problem.

4.2 Introduction

The fundamental problem of molecular electronic structure determination, or the solution of the underlying equations governing the behavior of electrons, traditionally involves computing accurate approximations to the ground state electronic wavefuction $\Psi(\mathbf{x}_1,...,\mathbf{x}_N)$. Here, $\mathbf{x}_i$ represents the spin-resolved spatial coordinate, $\mathbf{x}_i = \mathbf{r}_i s_i$. Once determined, all observable quantities are accessible from the wave function via direct integration:

$$Q[\Psi] \equiv \sum_{s_i} \int\int...\int \left[\Psi^*(\mathbf{x}_1,...,\mathbf{x}_N) \hat{Q} \Psi(\mathbf{x}_1,...,\mathbf{x}_N) \right] d\mathbf{r}_1 ... d\mathbf{r}_N, \qquad (4.2.1)$$

with the quantum-classical correspondence principle providing a link between the property Q and its Hermitian operator. The Hamiltonian operator is of great

importance, allowing us to determine the energy spectrum of the system. For a system of N electrons and M nuclei, in atomic units, and within the Born-Oppenheimer approximation, this operator is written as:

$$\hat{H} \equiv \sum_{i=1}^{N}\left(-\frac{1}{2}\nabla_i^2 + \sum_{\alpha=1}^{M} -\frac{Z_\alpha}{|\mathbf{r}_i - \mathbf{R}_\alpha|} + \sum_{i<j}\frac{1}{|\mathbf{r}_i - \mathbf{r}_j|}\right). \tag{4.2.2}$$

One can then obtain the total energy of the system through

$$W[\Psi] \equiv E_{nucl} + E_{elec}[\Psi] \tag{4.2.3}$$

$$= \sum_{\alpha=1}^{M-1}\sum_{\beta=\alpha+1}^{M}\frac{Z_\alpha Z_\beta}{|\mathbf{R}_\alpha - \mathbf{R}_\beta|} + \left\langle \Psi \middle| \hat{H} \middle| \Psi \right\rangle.$$

To determine Ψ a variational construct is employed: we know that no "trial" wave function, Ψ, has a lower energy than the exact ground state, Ψ_{gs}:

$$\left\langle \Psi_{gs} \middle| \hat{H} \middle| \Psi_{gs} \right\rangle \leq \left\langle \Psi \middle| \hat{H} \middle| \Psi \right\rangle. \tag{4.2.4}$$

Thus, minimization of $E_{elec}[\Psi]$, with respect to Ψ, such that Ψ is constrained to be normalized and anti-symmetric with respect to exchange of spatial and spin coordinates, yields the exact ground state energy.

Unfortunately, application of the Hamiltonian operator to the electronic wave function results in a second-order partial differential equation in $3N$ real-valued coordinates and N dichotomic spin coordinates. The ground state is thus inaccessible except for small or model systems.[1-6] Moreover, the scaling of the computational cost is exponential with respect to N. Given this limitation, most chemically relevant

processes of biological activity are outside the scope of this traditional wave function based methodology. Clearly the root of this problem lies in the high dimensionality of the wave function. Should a molecular system, and its properties, be accessible through a function (or functional) with fewer coordinates, then some of these problems encountered when determining the electronic structure of large systems could be circumvented. It is in this light that we now turn to density-functional theory (DFT), wherein the key descriptor of the system is the ground state electronic density.

4.2.1 Density-Functional Theory

In the encompassing theorem of Hohenberg and Kohn it is demonstrated that, like the wave function, the ground state's electron density determines all of the properties of an electronic system in its ground state.[7] This remarkable result is achieved as follows: we recall that the number of electrons is determined directly from the electron density:

$$N[\rho] \equiv \int \rho(\mathbf{r}) d\mathbf{r}. \tag{4.2.5}$$

Next, it is demonstrated that the external potential, $v(\mathbf{r})$, is determined directly from $\rho(\mathbf{r})$. With N and $v(\mathbf{r})$ one can determine the electronic Hamiltonian and solve Schrödinger's equation for the wave function; all observable properties are then easily obtained through Eqn. (4.2.1). Within density-functional theory the independent variable has changed from $\Psi(\mathbf{x}_1,...,\mathbf{x}_N)$ to $\rho(\mathbf{r})$. We have reduced the space of the solution to three spatial variables (from $3N$ spatial and N dichotomic in the wave

function formulation). However, the following problem remains: the Hohenberg-Kohn theorem is one of existence and it gives no clue as to how to determine the unique ground state electronic density. Indeed, the key result of the so-called 'second' theorem of Hohenberg and Kohn, and the foundation of all practical approaches, is suitably vague:

$$E_{gs} = E_v[\rho_{gs}] = \underbrace{\min}_{\text{all } N-\text{electron}\rho(\mathbf{r})} E_v[\rho]. \tag{4.2.6}$$

So the problem of dealing with the $3N$ spatial and N dichotomic variables is transferred into the lack of knowledge of the energy functional. The core problem thus becomes finding suitable approximations to the Hohenberg-Kohn functional, $F[\rho]$:

$$F[\rho] = E[\rho] - \int \rho(\mathbf{r}) v[\rho;\mathbf{r}] d\mathbf{r}. \tag{4.2.7}$$

A practical solution was presented by Kohn and Sham in Ref. (8). One constructs the electron density from one-particle orbitals:

$$\rho(\mathbf{r}) = \sum_{i=1}^{N} |\phi_i(\mathbf{r})|^2 . \tag{4.2.8}$$

Applying the variational principle, Eqn. (4.2.6), to the resulting Euler-Lagrange equations yields:

$$\left(-\frac{1}{2}\nabla^2 + v(\mathbf{r}) + \int \frac{\rho(\mathbf{r}')}{|\mathbf{r}-\mathbf{r}'|} d\mathbf{r}' + \mu_{xc}(\rho) \right) \phi_i(\mathbf{r}) = \varepsilon_i \phi_i(\mathbf{r}). \tag{4.2.9}$$

These are the so-called Kohn-Sham equations. Here, μ_{xc} is the exchange-correlation potential, the functional derivative of the exchange-correlation energy functional with

respect to the density: $\mu_{xc} = \frac{\delta E_{xc}[\rho]}{\delta \rho}$. The total energy is then:

$$E^{KS} = \sum_i \varepsilon_i - \frac{1}{2}\int \frac{\rho(\mathbf{r})\rho(\mathbf{r}')}{|\mathbf{r}-\mathbf{r}'|} d\mathbf{r}d\mathbf{r}' - \int \mu_{xc}(\mathbf{r})\rho(\mathbf{r})d\mathbf{r} + E_{xc}[\rho]. \qquad (4.2.10)$$

The Kohn-Sham equations defined through Eqn. (4.2.9), are to be solved self-consistently. The difficulty in determining the exact ground state density from this formulation has been recast into the unknown form of the *exact* exchange-correlation energy functional E_{xc}. Progress has been made, and the functional 'zoo' containing functionals of varying sophistication, continues to grow.[9-13] The Kohn-Sham formalism has been successfully applied to a wide variety of problems in solid state physics, chemistry, biochemistry, and within the field of drug discovery.[14-20] A fuller description of DFT, its theoretical development, and its usage within quantum chemistry can be found in Ref. (21).

A naive implementation of the Kohn-Sham method would result in an $O(N^3)$ scaling tool, and in such cases DFT may only be successfully applied to systems of around a few hundred atoms; clearly this limits its applicability as a method for use in medicinal chemistry, or biophysics, where the number of particles to treat can be orders of magnitude greater. A successful treatment of these systems requires methods which scale linearly in particle size (and with early onset and a small prefactor). To date, research in this area has focused on avoiding explicitly constructing the Kohn-Sham orbitals, ϕ_i, and directly constructing the density instead.[15,22-26] Our own research is related to the field of linear-scaling DFT calculations and this forms the

content of the rest of this chapter. In the following section we discuss the plane wave and basis-set approaches for solving the Kohn-Sham equations of DFT; these are two commonly used methods for representing orbitals within the Kohn-Sham formalism. Basic background on each method will be presented and we shall focus on the relative strengths and weaknesses of each approach whilst not discussing the merits/demerits of any specific implementation. In section 3 we introduce real space methods, specifically adaptive coordinate approaches. In section 4 we present an overview of our own method for incorporating coordinate adaptability into a real space formalism and then in section 5 we show how this efficiently adapted real space grid can be used to perform all of the fundamental numerical operations necessary for performing an electronic structure calculation; we concentrate our discussion on the operations interpolation and differentiation. In section 6 we present results and discussion and in the final section our concluding remarks.

4.3 Plane wave and basis-set methods

In the plane wave approach orbitals are expanded in a non-local plane wave basis. Core states are modeled using pseudopotentials and allow for a reasonable number of plane waves to represent most of the chemical elements found in a materials simulation.[27] The use of Fast Fourier transform (FFT) techniques when dealing with the orbitals and the electrostatic potential is efficacious, and there is no dependence of the basis on atom positions. Also, subsequent algorithmic

improvements have led to a reduction in the number of steps required to attain self consistency.[28-29] Rigorous control of the numerical convergence is attained through a few parameters, principally the wave vector of the highest frequency Fourier mode, k. However, there are a number of drawbacks to the approach. Even with advances in pseudopotential methods, strong variations in the potential occur within the core region; these are difficult to resolve with a plane wave representation. Moreover, such a representation would extend over the whole domain, into areas where such resolution would most certainly not be necessary. This is particularly troublesome for localized, highly inhomogeneous, systems like clusters, molecules, or surfaces. Here a huge amount of effort is expended in modeling the vacuum accurately. The correct description of charged systems is also somewhat involved, as a uniform neutralizing background needs to be correctly added in order to correctly compute total energies. Finally, without a localized orbital representation, the orthogonalization step is seen to scale as N^3.

In contrast to the use of non-local plane wave methods, one can use a localized basis-set representation, typically with either Slater or Gaussian basis functions.[30] Here molecular orbitals are constructed from a linear combination of atomic orbitals (the LCAO approximation) and ~ 30 Gaussians can provide a very accurate representation of a typical first row chemical element. The use of the localized basis is somewhat more chemically intuitive than the plane wave approach, which heralds from condensed matter physics.

Both choices of localized function have their strengths and weaknesses:[31] Slater functions have an improved form both close to, and far from, the nuclei; they are also more sharply peaked than Gaussian functions. The use of Slater orbitals avoids the cumbersome use of contractions of Gaussian functions. Unfortunately, most integrals involving Slater functions have to be done numerically, while most integrals involving a Gaussian basis are analytically tractable. Gaussian functions also have the attractive property that they can be easily differentiated any number of times, whilst Slater functions have the complication that this repeated differentiation leads to the introduction of factors of $1/r$. Irrespective of which function is used, algorithmic advances have led to significant advances in the acceleration of the convergence behavior of basis-set self-consistent methods.[32-34] However, for basis-set methods in general, care must be taken to account for basis-set superposition error (BSSE). This arises through the overlap of non-orthogonal atom centered functions of composite systems. Finally, we note that scaling in basis-set methods can vary but, with recent developments, linear scaling for large systems is accessible.

There also exist hybrid methods, combining the strengths of both the basis-set, and plane wave approaches. In the Gaussian/Plane wave method (GPW) the wave function is described using an atom centered Gaussian basis, but an auxiliary plane wave basis is used to describe the density.[35-36] This description of the density allows for the use of FFT methods to solve the Poisson equation and to obtain the Hartree energy in a linear scaling fashion. Whilst the GPW method requires a pseudopotential

representation of the core region, the subsequent Gaussian and augmented plane wave (GAPW) method allows for all electron calculations.[37]

4.4 Real space methods

There are a number of key advantages to a real space representation of an atomic or molecular problem, as opposed to either the plane wave or basis-set representations described in the preceding section. Firstly, the potential term is diagonal in coordinate space, whilst the kinetic term, the Laplacian, is nearly local. The near-locality is ideal for linear scaling algorithms and facilitates parallelization. Within the real space formalism it is trivial to deal with both finite or charged systems. In strict contrast to the basis-set, or plane wave methods, the real space approach produces structured highly banded matrices which are efficiently solved using multiscale approaches.[38-39] For an excellent introduction to real space methods and electronic structure calculations we refer the interested reader to Ref. (40).

Real space methods are perhaps closest in structure to the plane wave approach: both are fully 'numerical' with a few parameters controlling convergence (the grid spacing, h, and the wave vector, k, described above). Indeed, the problem of resolution within plane wave methods (the difficulty of representing inhomogenous systems, or the vacuum) is also found within the real space method and is referred to as the *adaptability* of the grid. For a highly efficient description of an inhomogenous system it is beneficial to allow the resolution of the grid to match the requirements of

the physical system. This is achieved by an increase in resolution in the grid near the nuclei (moving the points in the grid to where the density, or some other such representative function, is large). Within the literature there are two strategies that have been used thus far: that of 'local refinement' or that of 'grid curving'. The local refinement approach has been performed within the context of wavelets,[41-42] finite elements[43-44] and multigrid methods.[45-46] As our method is conceptually related to the grid curving approach we shall discuss this in somewhat more detail.

In the ACRES method of Modine *et al.*[47] standard Cartesian coordinates $\mathbf{r}$ are related to curvilinear coordinates through a coordinate transformation $\mathbf{r}(\xi)$. The change of coordinates maps the regular grid in curvilinear coordinates to an adaptive mesh in Cartesian coordinates with a finer resolution where it is needed. This transformation of coordinates is different from the more 'classical' coordinate transformations (e.g. logx-spherical) in a number of key ways. Firstly, the grid is adapted to an arbitrary arrangement of atoms through a linear superposition of the grid displacements of each atom. Secondly, the transformation is smooth and continuous everywhere. The method implemented in the ACRES program was extended into the HARES program although the form of the grid curving remains the same.[48] We note that this form of grid curving was initially implemented by Gygi[49] using a plane wave basis and within this context has been extended by a number of groups.[50-53] Gygi and Gallo have also recently studied real space approaches using curvilinear coordinates and pseudopotentials.[54]

4.5 Grid curving and the Smolyak construct

We shall now briefly summarize our recent research on grid curving methods in electronic structure theory. We shall follow the formalism of Ref. (55) and introduce our methodology in terms of multi-dimensional numerical integration, or cubature.

In one dimension, Gaussian quadrature is the *best possible integration method* for integrals of the form:

$$\int f(x)w(x)dx, \tag{4.5.1}$$

where $f(x)$ has any of the following properties: it is analytic; it is smooth (derivatives of all orders exist); it is a polynomial (or is well approximated by polynomials), or it has derivatives up to some order, n, with $n \geq 0$. For the first three cases, or when $n > 0$, *no other method is comparable.* There are numerous closed form Gaussian quadrature formulae in one-dimension, however, whilst special cases are known of formulae in many dimensions, in general the problem is regarded as one of immeasurable complexity.[56] Notable exceptions to this rule are rules for integration on the unit sphere and unit hypercube, with the Smolyak construction being an example of the latter; the recent work of Rees and Hall represents another special case with an 'atom-like' spherical grid.[57]

Before discussing the Smolyak construction in detail, let us recap. The problem of numerical integration is such that we seek good approximations to the

functional Q_d where

$$Q_d(f) = \int_{[0,1]^d} f(x)dx. \tag{4.5.2}$$

A near optimal choice was suggested by Smolyak[58] and we quote without proof the following formulae, henceforth referred to as the Smolyak construction:

$$A(q,d) = \sum_{q-d+1 \le |\mathbf{i}| \le q} (-1)^{q-|\mathbf{i}|} \binom{d-1}{q-|\mathbf{i}|} (U^{i_1} \otimes ... \otimes U^{i_d}). \tag{4.5.3}$$

In the above expression d is the dimension of the problem and q, the effort, can be thought of as a parameter akin to the grid spacing. Here U^i refers to the one dimensional quadrature formulae:

$$U^i(f) = \sum_{j=1}^{m_i} f(x_j^i).a_j^i \tag{4.5.4}$$

such that $m_i \in N$ is known. The a_j^i and x_j^i are the *weights* and *nodes* of our integration scheme. Thus, the Smolyak construction allows us to define an efficacious grid for Gaussian cubature on the unit hypercube. Our underlying quadrature formulae (the U^i's) will determine the distribution of points throughout the cube, and will be a uniform distribution and certainly not adapted for electronic structure calculations where the region of interest is now $(-\infty,\infty)^d$ and most of our nodes should be placed near the nuclei. However, such a transformation can be constructed in the following way. For ease, we begin with the simplest one dimensional example. We define the coordinate transformation:

$$\Theta(x) = \frac{\int_{-\infty}^{x} w(x)dx}{\int_{-\infty}^{\infty} w(x)dx}. \tag{4.5.5}$$

Then,

$$\int_0^1 f(\Theta)d\Theta = \int_{-\infty}^{\infty} f(x)\frac{d\Theta}{dx}dx \tag{4.5.6}$$

$$= \int_{-\infty}^{\infty} f(x)w(x)dx.$$

It is noted that the weight transformation function, $w(x)$, simply takes the points from [0,1] and distributes them on $(-\infty,\infty)$ such that there are many points where $w(x)$ is large and few where it is small. This is readily extended to $d>1$.[59] For instance, for $d=3$, Eqn. (4.5.4) becomes:

$$\Theta_1(x_1) = \frac{\int_{-\infty}^{x_1}\int_{-\infty}^{\infty}\int_{-\infty}^{\infty} w(\mathbf{r})\mathbf{dr}}{\int_{-\infty}^{\infty}\int_{-\infty}^{\infty}\int_{-\infty}^{\infty} w(\mathbf{r})\mathbf{dr}}$$

$$\Theta_2(x_2) = \frac{\int_{-\infty}^{x_2}\int_{-\infty}^{\infty} w(x_1,r_2,r_3)\mathrm{d}r_2\mathrm{d}r_3}{\int_{-\infty}^{\infty}\int_{-\infty}^{\infty} w(x_1,r_2,r_3)\mathrm{d}r_2\mathrm{d}r_3}$$

$$\Theta_3(x_3) = \frac{\int_{-\infty}^{x_3} w(x_1,x_2,r_3)\mathrm{d}r_3}{\int_{-\infty}^{\infty} w(x_1,r_2,r_3)\mathrm{d}r_3}. \tag{4.5.7}$$

For the purposes of a molecular or atomic electronic structure calculation, a suitable weight transformation might be something that looks like a molecular, or atomic, density. Consider such a 'molecular' density,

$$w(\mathbf{x}) = \rho_{\text{mol}}(\mathbf{x}) = \sum_{\alpha=1}^{N} \rho_{\alpha}(\mathbf{x} - \mathbf{R}_{\alpha}), \tag{4.5.8}$$

consisting of N atoms with the α^{th} atom at $\mathbf{R}_{\alpha}$. To simplify this transformation we consider atomic densities that have been fit to s-type Gaussian functions

$$\rho_{\alpha}(\mathbf{x}) = \sum_{i} c_{\alpha i} \exp\left(-\beta_{\alpha i}\left(\mathbf{x} - \mathbf{R}_{\alpha}\right)^2\right). \tag{4.5.9}$$

We use the $c_{\alpha i}$ and $\beta_{\alpha i}$ as generated by Constans and Carbó. (They have generated tables of coefficients and exponents fitted variationally using s-function Gaussians to atomic densities from H to Kr at the HF/6-311G level of theory.[60-61]) This weight function has the additional advantage that the Jacobian elements are easily computed, are lower diagonal, and are trivially related to the weight.

The transformation we have introduced above is actually the reverse of the one we are interested in: it maps points such that $\mathbb{R}^d \rightarrow [0,1]^d$. To achieve the reverse, we couple the transformation with a non-linear equation solver and treat the problem as a system of equations. We solve consecutively from Θ_1 to Θ_d and as the finding of each x_i is a one dimensional problem, the bisection method is effective. To illustrate the adaptive properties of this transformation, in Fig. 4.1 we show the uniform 2 dimensional grid corresponding to the use of the rectangle rule within Eqn. (4.5.4). This grid has an effort (q) of 9 and is composed of 4,097 points. We define a pseudomolecular 2 dimensional CO_2 molecule using Eqn. (4.5.9) and perform the transformation, and subsequently solve for x_1 and x_2. Within our weight function we

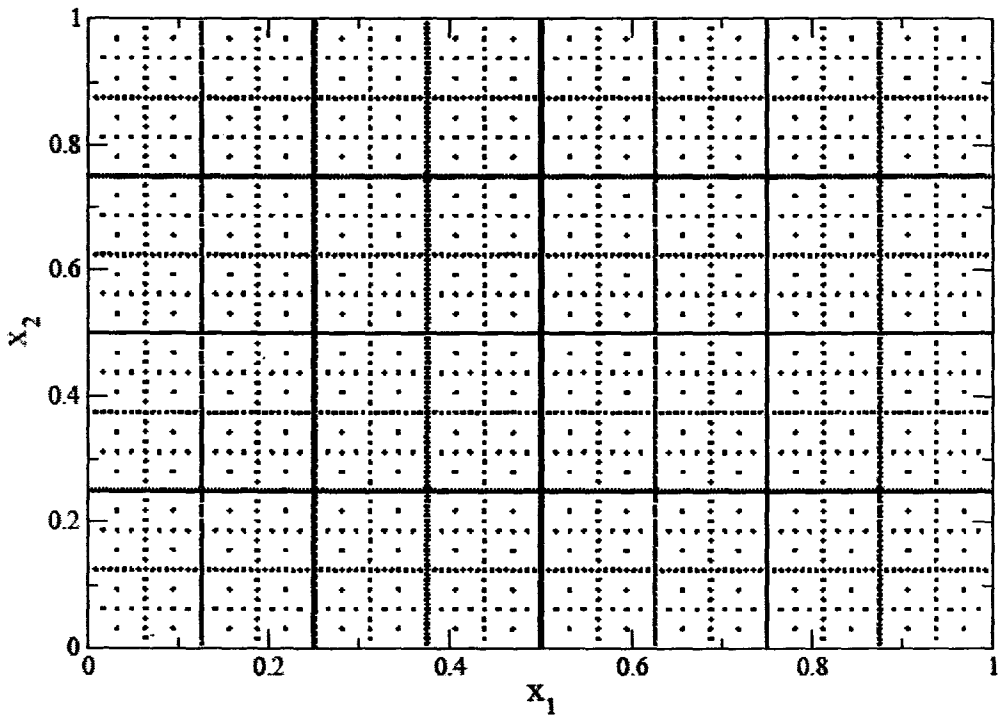

Figure 4.1 A 2 dimensional grid derived from the rectangle rule. The grid corresponds to an effort, q, of 9 and is composed of 4,097 points.

have used a carbon atom at $(0,0)$ and two oxygen atoms at $(\pm 2,0)$ respectively. This results in Fig. 4.2. It is clear that the points on the uniform grid have been moved towards the atomic nuclei, and the grid has been markedly changed. We have shown in an earlier publication that these grids are suitable for the kinds of cubature necessary for electronic structure calculations.[55] In this chapter we extend the usefulness of this result to encompass the other fundamental numerical operations: interpolation, and differentiation.

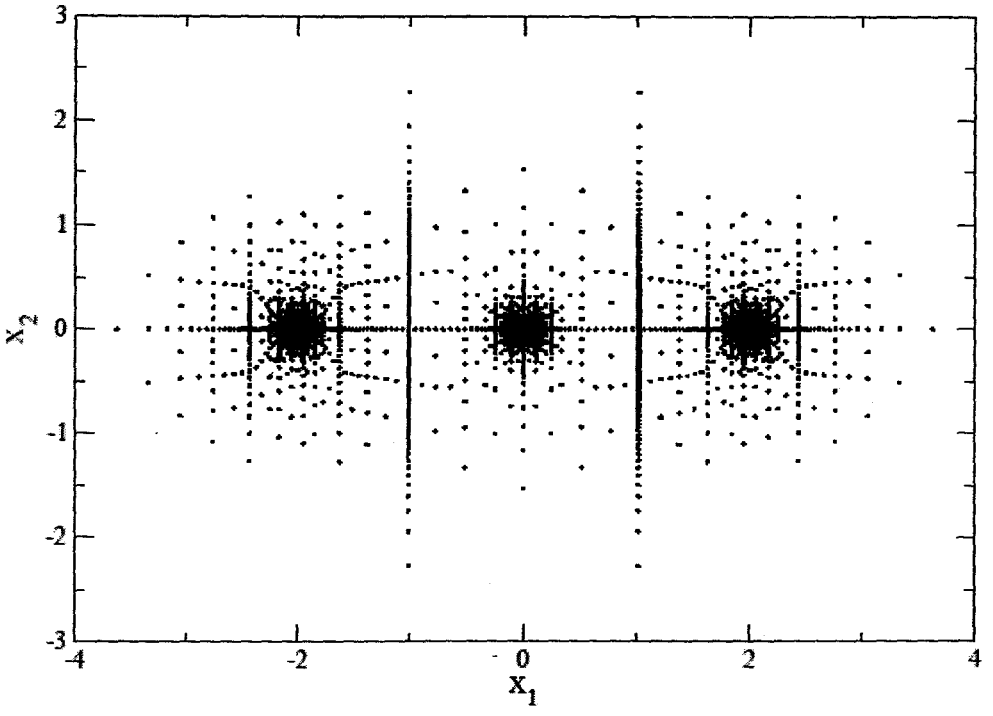

Figure 4.2 The grid in Fig. 4.1 transformed using a 2 dimensional CO_2 pseudo-molecular weight function. The carbon and oxygen atoms are at (0,0) and (± 2,0) respectively. We observe a higher concentration of points where the weight transformation function is large corresponding to the positions of the carbon and oxygen nuclei.

4.6 Grid curving: Interpolation and differentiation

We begin by noting that any linear operator on a function can be written as:

$$\hat{L}[f(x)] \approx \sum_{i=0}^{n(q)-1} w_i f(x_i), \tag{4.6.1}$$

essentially the form shown in Eqn. (4.5.4). Here the effort (q), or grid spacing, is

subsumed into the function $n(q)-1$. Now for periodic functions the Fourier series is a well known function for interpolation:

$$f(x) \approx \frac{a_0}{2} + \sum_{j=1}^{M} a_j \cos(2\pi jx) + b_j \sin(2\pi jx). \tag{4.6.2}$$

We wish to express this in the language of Eqn. (4.5.4) such that we can approximate our function as a sum of weights multiplied by function evaluations at x_i. To achieve this we will use a discrete Fourier transform to find the coefficients in terms of $f(x_i)$. In doing so we require that the number of points, x_i, is a simple power of two. Thus $n(q)-1$ above becomes 2^q-1. We find that our Fourier coefficients are thus:

$$a_0 = \frac{1}{n}\sum_{k=0}^{n-1} f(x_k) \tag{4.6.3}$$

$$a_{0<j<n/2} = \frac{2}{n}\sum_{k=0}^{n-1} f(x_k)\cos\left(\frac{2\pi jk}{n}\right)$$

$$b_j = \frac{2}{n}\sum_{k=0}^{n-1} f(x_k)\sin\left(\frac{2\pi jk}{n}\right)$$

$$a_{n/2} = \frac{1}{n}\sum_{k=0}^{n-1} f(x_k)\cos(k\pi).$$

Note that

$$b_0 = b_{n/2} = 0 \tag{4.6.4}$$

and

$$x_k = \frac{k}{n}. \tag{4.6.5}$$

We now have n points with n coefficients that can be solved for. Hence, M in the above expression becomes $n/2$. Substitution of Eqn. (4.6.4) into Eqn. (4.6.2) and applying the trigonometric identity

$$\cos(A-B) = \cos(A)\cos(B) - \sin(A)\sin(B) \tag{4.6.6}$$

one easily obtains the expression:

$$f(x) \approx \sum_{k=0}^{n-1}\left[\frac{1}{n} + \frac{2}{n}\sum_{j=1}^{n/2-1}\cos(2\pi j(x-x_k)) + \frac{1}{n}\cos(\pi(x-x_k))\right] f(x_k). \tag{4.6.7}$$

The term in the square bracket is the weight for interpolation, w_k, and the portion outside is simply the value of the function at the point x_k. Having this result it is trivial to generate expressions for differentiation. Indeed, the m^{th} derivative of the Fourier series converges pointwise to the m^{th} derivative of the function if that function is at least m times differentiable.

$$f'(x) \approx \sum_{k=0}^{n-1}\left[\frac{-4\pi}{n}\sum_{j=1}^{n/2-1} j\sin(2\pi j(x-x_k)) - \frac{\pi}{n}\sin(\pi(x-x_k))\right] f(x_k) \tag{4.6.8}$$

and

$$f''(x) \approx \sum_{k=0}^{n-1}\left[\frac{-8\pi^2}{n}\sum_{j=1}^{n/2-1} j^2\cos(2\pi j(x-x_k)) - \frac{\pi^2}{n}\cos(\pi(x-x_k))\right] f(x_k) \tag{4.6.9}$$

provide the weights of the first and second derivatives respectively. Integration of Eqn. (4.6.7) results in

$$\int_0^1 f(x)dx \approx \sum_{k=0}^{n-1} \frac{1}{n} f(x_k). \tag{4.6.10}$$

This is just the rectangle rule.

These results correspond to a function on [0,1], and in order to differentiate a function using our coordinate transformation we must apply the chain rule. In three dimensions, a derivative evaluated on our transformed grid becomes:

$$\frac{\partial f}{\partial x_i} = \sum_{j=1}^{3} \frac{\partial f}{\partial \Theta_j} \frac{\partial \Theta_j}{\partial x_i} \tag{4.6.11}$$

with the second derivative being

$$\frac{\partial^2 f}{\partial x_i^2} = \sum_{j=1}^{3} \left[\left[\sum_{k=1}^{3} \frac{\partial^2 f}{\partial \Theta_k \partial \Theta_j} \frac{\partial \Theta_k}{\partial x_i} \right] \frac{\partial \Theta_k}{\partial x_i} + \frac{\partial f}{\partial ta_j} \frac{\partial^2 \Theta_j}{\partial x_i^2} \right]. \tag{4.6.12}$$

The terms $\frac{\partial f}{\partial \Theta_j}$ and $\frac{\partial^2 f}{\partial \Theta_k \partial \Theta_j}$ are computed using the unit cube grid, and the terms $\frac{\partial \Theta_j}{\partial x_i}$ and $\frac{\partial \Theta_j^2}{\partial x_i^2}$ are determined analytically from the form of the transformation.

4.7 Results

To recap, our method takes the regular Smolyak grid of points, as defined through Eqn. (4.5.3), and transforms it using the d dimensional extension of Eqn. (4.5.5). The resulting grid points are now inhomogenously distributed throughout $\mathbb{R}^d$, with localization occurring where the transformation $w(\mathbf{x})$ is large. To illustrate the utility of this approach we have computed interpolants, and both 1st and 2nd derivatives, of a range of functions of varying dimension.

In Fig. 4.3 we see how the effort, q, of Eqn. (4.5.13) affects the log of the number of unique points for different dimensionalities. Fig. 4.4 illustrates the convergence of the 1st and 2nd derivatives as a function of the number of grid points used for the 6 dimensional Gaussian

$$f(\mathbf{x}) = \exp(-3x^2). \tag{4.7.1}$$

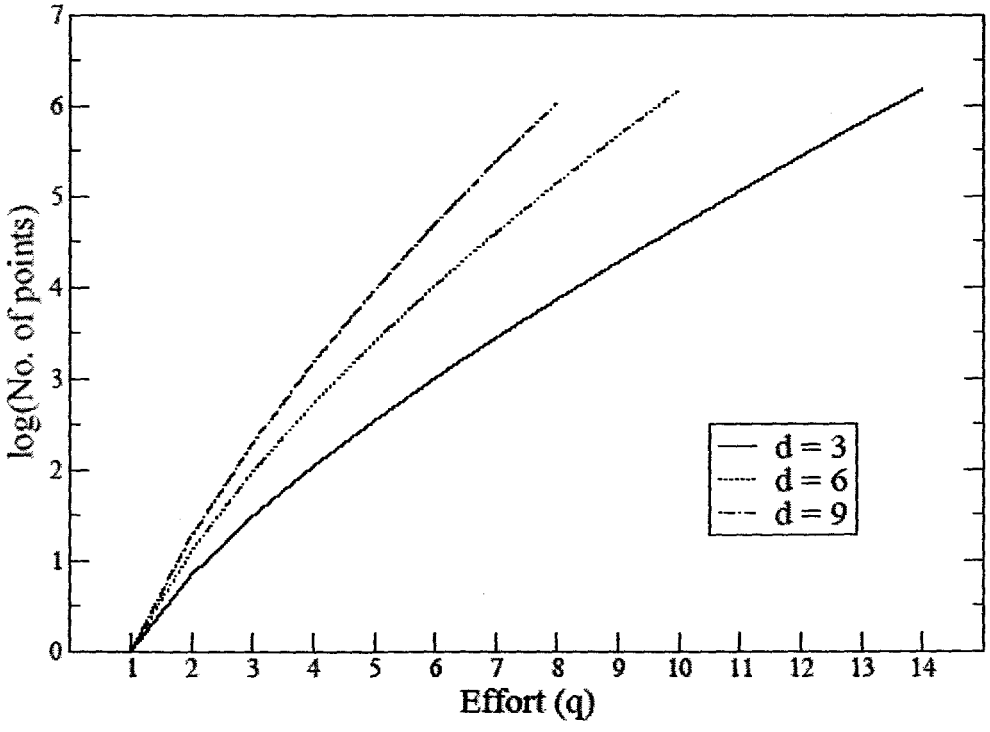

Figure 4.3 An illustration as to the rate of growth of the logarithm of the number of points as a function of effort, for a range of different dimensions.

Here,

$$x^2 = \sum_{i=1}^{d} x_i^2 \tag{4.7.2}$$

represents the radius of a d dimensional hypersphere. In this example, the differentiation is performed on the untransformed Smolyak grid, with respect to x_1, at the point:

$$\mathbf{x}' = (0.4, 0.2, -0.3, 0.5, 0.01, -0.8). \tag{4.7.3}$$

Throughout this article, as a measure of our accuracy, we compute the logarithm of the absolute error:

$$\log(\text{Abs. Error}) = \log(| f^{(n)}_{Exact}(\mathbf{x}') - f^{(n)}_{Computed}(\mathbf{x}') |). \tag{4.7.4}$$

For, $n = 0,1$ or 2 corresponding to interpolation, 1 st, and 2 nd derivatives respectively. We see a systematic improvement in the accuracy of both derivatives with increasing number of grid points. We also see that the 1 st derivative is computed to a higher accuracy than the 2 nd, at all numbers of grid points.

How does our method do for a non-trivial function? Consider the 6 dimensional function:

$$g(\mathbf{x}) = \exp(-3x^2)\left[x_1 + 1 + \sin(x_2) - \cos(x_3) + (x_4 - 3)^2 + x_5^6\right] \tag{4.7.5}$$

and its 1 st and 2 nd derivatives as computed at $\mathbf{x}$ on the untransformed Smolyak grid.

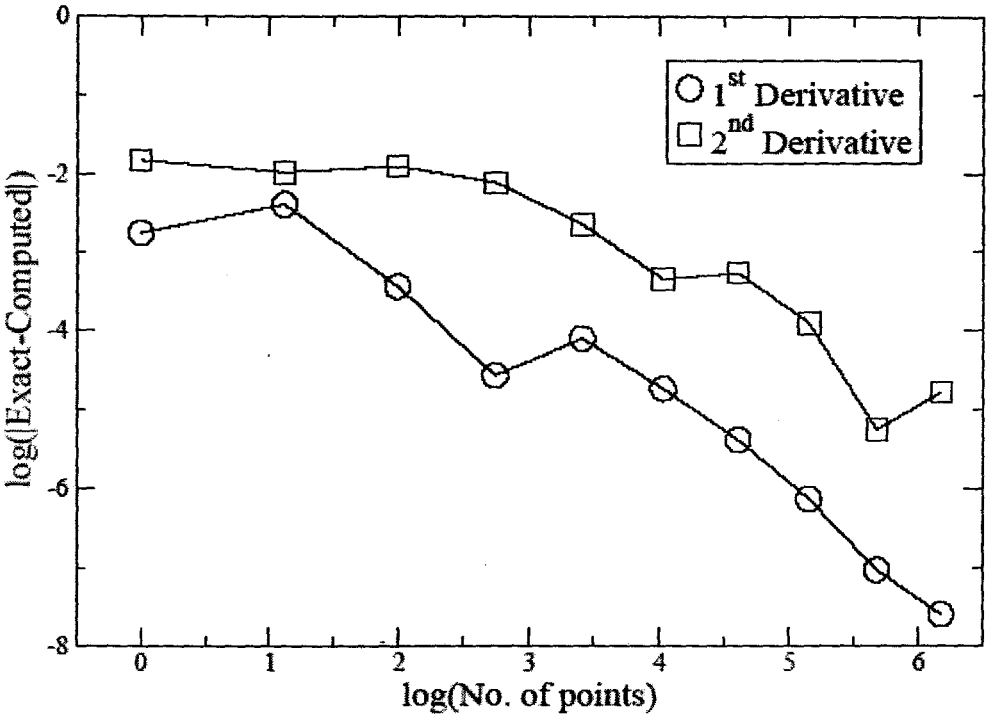

Figure 4.4 Convergence, with respect to the number of grid points, of the 1st and 2nd derivatives of a 6 dimensional function, $f(\mathbf{x})$ (Eqn. 4.7.1), with respect to x_1. The derivatives are evaluated at $\mathbf{x}^r = (0.4, 0.2, -0.3, 0.5, 0.01, -0.8)$ and are performed on an untransformed Smolyak grid.

Pleasingly, Fig. 4.5 shows much the same behavior with respect to accuracy, as Fig. 4.4. Again, we observe a systematic increase in accuracy with respect to the number of grid points.

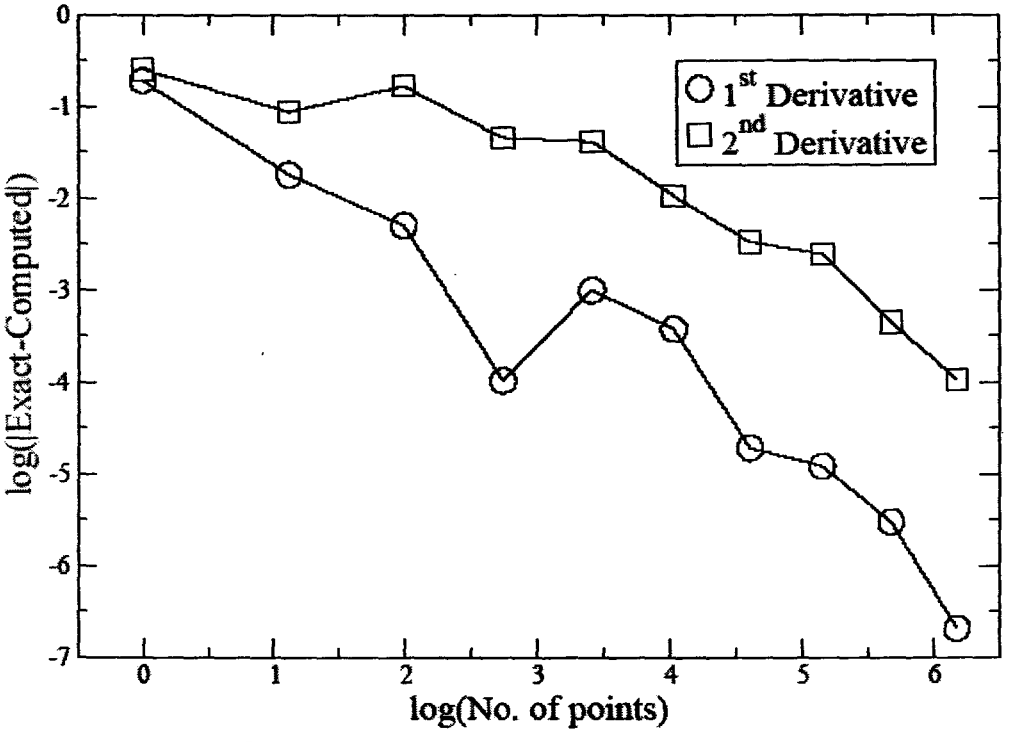

Figure 4.5 Convergence, with respect to the number of grid points, of the 1st and 2nd derivatives of a 6 dimensional function, $g(\mathbf{x})$ (Eqn. 4.7.5), with respect to x_1. The derivatives are evaluated at $\mathbf{x}^r = (0.4, 0.2, -0.3, 0.5, 0.01, -0.8)$ and are performed on an untransformed Smolyak grid.

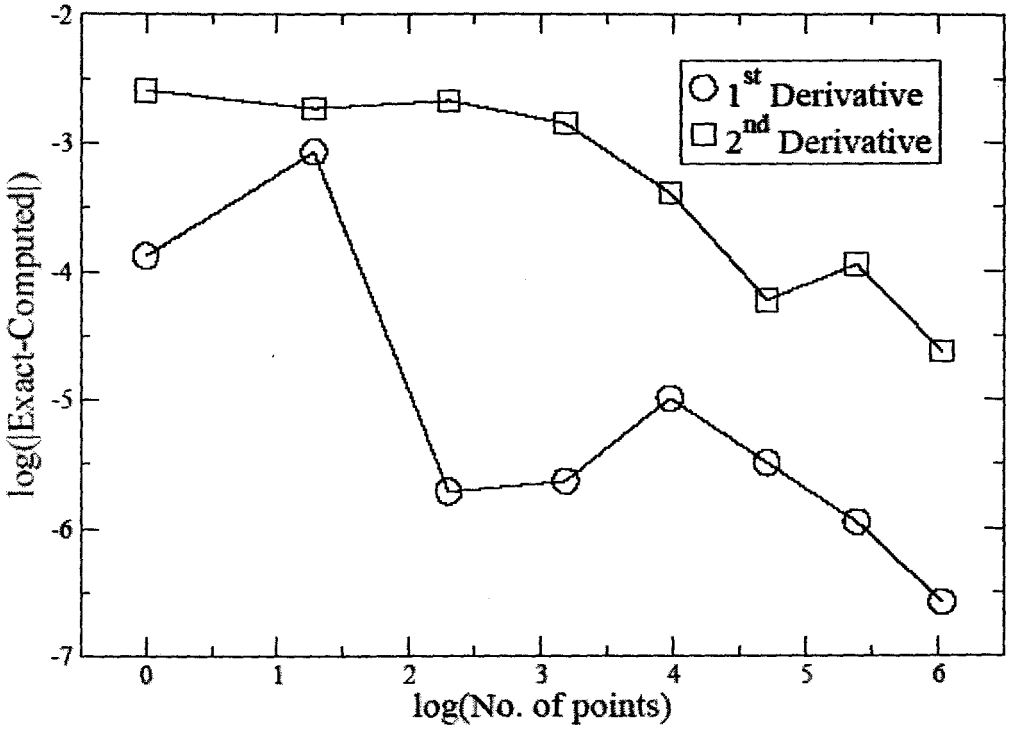

Figure 4.6 Convergence, with respect to the number of grid points, of the 1st and 2nd derivatives of a 9 dimensional function, $h(\mathbf{x})$ (Eqn. 4.7.6), with respect to x_1. The derivatives are evaluated at $\mathbf{x}' = (0.1874, 0.003, 0.425, -0.68636, -0.23496, -0.095905, 0.198655, 0.409012, 0.6114)$ and are performed on an untransformed grid.

In Fig. 4.6 we consider the 1st and 2nd derivatives, with respect of x_1, of a 9 dimensional function

$$h(\mathbf{x}) = \exp(-3x^2) \tag{4.7.6}$$

$$\mathbf{x}' = (0.1874, 0.003, 0.425, -0.68636, -0.23496, -0.095905, 0.198655, 0.40912, 0.6114) \tag{4.7.7}$$

on the untransformed Smolyak grid. In general, as the dimensionality increases, more grid points are required to achieve a given level of accuracy. Thus far we have shown that our underlying Smolyak grids are well suited to compute derivatives (both 1st and 2nd) of a range of functions, and for very large dimensions. In all cases we have examined, the 1st derivative is computed to a greater accuracy than the second however, in both cases systematic improvements are seen upon increasing the effort, q.

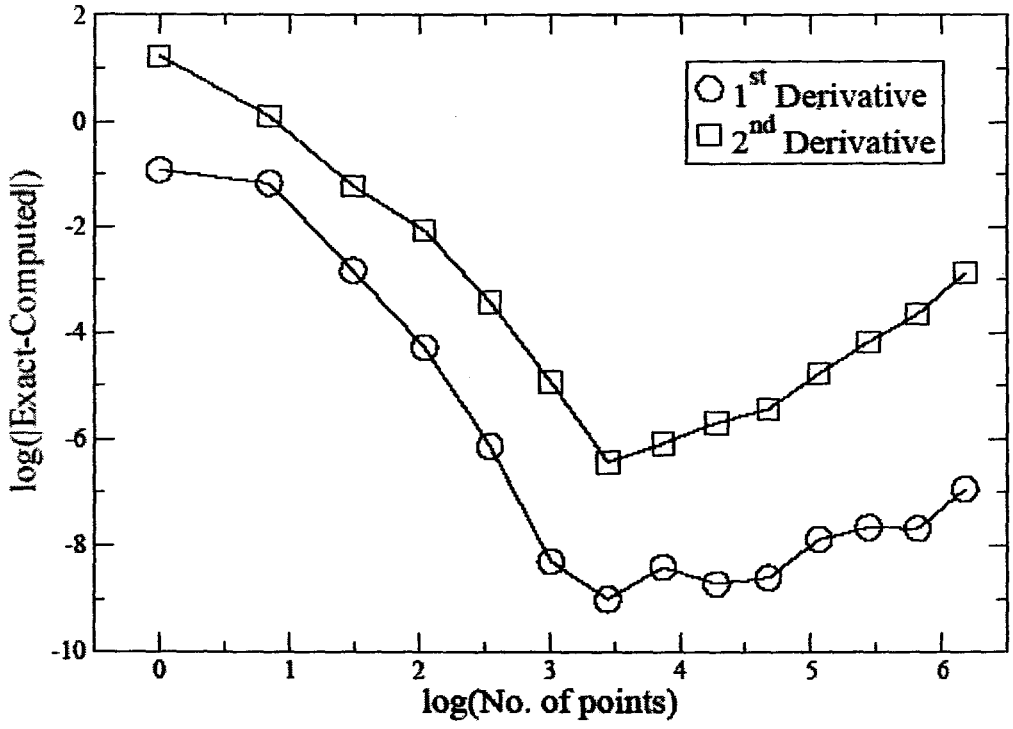

Figure 4.7 Convergence, with respect to the number of grid points, of the 1st and 2nd derivatives of a 3 dimensional function, $F(\mathbf{x})$ (Eqn. 4.7.8), with respect to x_1. The derivatives are evaluated at $\mathbf{x} = 0$ and are performed on a transformed Smolyak grid.

We now investigate our method of computing interpolants and derivatives on a transformed grid in R^d. Plotted in Fig. 4.7 are the logarithm of the absolute errors of the computed 1st and 2nd derivatives of the function

$$F(\mathbf{x}) = \exp(-6[(x_1 - 0.01)^2 + (x_2 - 0.02)^2 + (x_3 - 0.03)^2]) \qquad (4.7.8)$$

$$+2\exp(-6[(x_1 + 0.01)^2 + (x_2 + 0.02)^2 + (x_3 - 0.03)^2])$$

at the point $\mathbf{x} = 0$, and with respect to x_1. This function is a sum of two 3 dimensional Gaussians offset slightly from the origin. The transformation used to map the grid from $[0,1]^3 \to \mathbb{R}^3$ is a single Gaussian, with unit exponent, placed at the origin. The subsequent decrease in accuracy, with increasing effort, is attributed to the resulting expression involving differences between nearly equal numbers; this function presents a particularly challenging numerical example.

Finally, in Fig. 4.8, for the function $F(\mathbf{x})$, we compute the interpolant and both 1st and 2nd derivatives as a function of $\mathbf{x}'$ where $\mathbf{x}' = (x_1, 0.003, -0.523)$ and $x_1 = 0,...,1.5$ in steps of 0.1. As already seen previously, $\text{Error}_{\text{Interpolation}} < \text{Error}_{\text{1st derivative}} < \text{Error}_{\text{2nd derivative}}$ and may be a reflection of the cumulative errors arising from subsequent applications of the Fourier approximation.

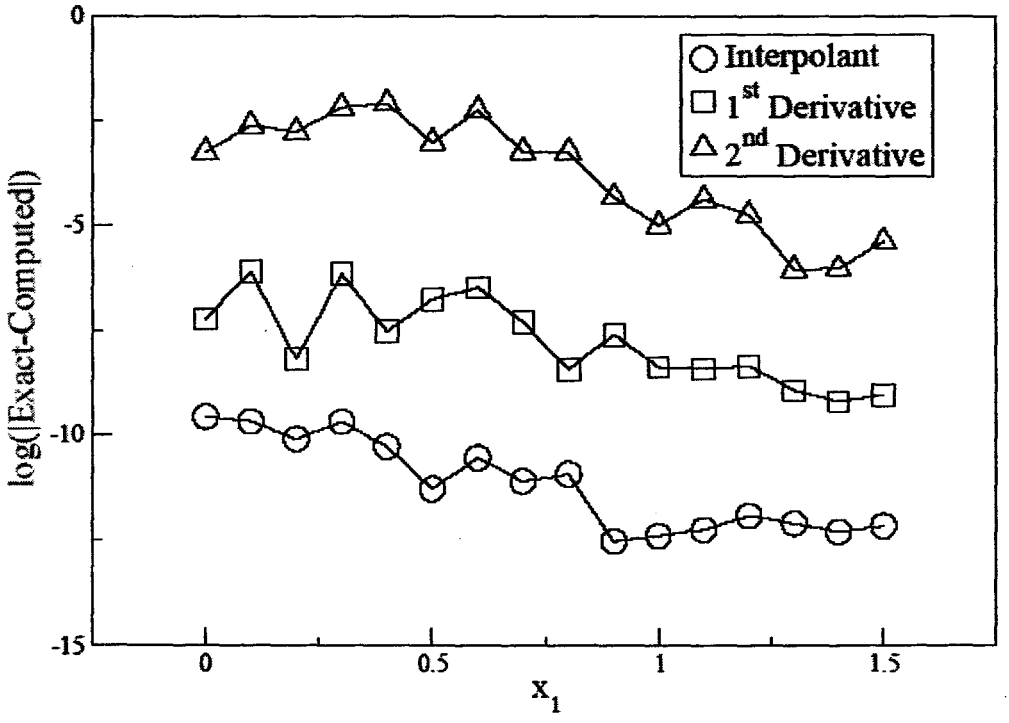

Figure 4.8 The interpolant, 1st, and 2nd derivatives of a 3 dimensional function, $F(\mathbf{x})$ (Eqn. 4.7.8), as a function of x_1. Here $\mathbf{x}' = (x_1, 0.003, -0.523)$ with $x_1 = 0,...,1.5$ in steps of 0.1 on a transformed Smolyak grid.

4.8 Conclusion

By coupling the Smolyak construction with a novel non-linear transformation of coordinates, we have shown that the resulting grid can be efficiently utilized for the purposes of integration, interpolation, and differentiation. The transformation of coordinates has been formulated such that points are moved to where the transforming weight function is largest and, one would hope, most relevant. This method joins the

collection of adaptive coordinate real space methods; we have demonstrated that Smolyak derived grids are thus amply suited to solving problems within molecular electronic structure theory where the electronic density is a spatially heterogeneous function.

The numerical results presented here are encouraging. We observe good convergence in the accuracy of computed interpolants and derivatives at points both on and off of the grid. This convergence is, in general, smooth and concomitant with an increase in "effort;" this parameter is analogous to the wave vector in a plane wave basis, or the grid spacing in other real space methods. We have shown application of this method to a number of functions, of varying difficulty, and of varying dimensionality.

Work continues within our group to improve the utility of these algorithms; non-locality is a bane for numerical differentiation and efforts to improve the near sightedness of this method are ongoing.

4.9 References for chapter 4

1. E. R. Davidson, J. Math. Phys., 725 (1969).

2. M. Taut, Phys. Rev. A , 3561 (1993).

3. A. Alavi, J. Chem. Phys., 7735 (2000).

4. D. C. Thompson, and A. Alavi, Phys. Rev. B , 235118 (2002).

5. J. Jung, and A. Avarellos, J. Chem. Phys., 10825 (2003).

6. D. C. Thompson, and A. Alavi, J. Chem. Phys., 124107 (2005).

7. P. Hohenberg, and W. Kohn, Phys. Rev., B864 (1964).

8. W. Kohn, and L. J. Sham, Phys. Rev., A1133 (1965).

9. Density Functional Repository as developed and distributed by the Quantum Chemistry Group, CCLRC Daresbury Laboratory, Daresbury, Cheshire, WA4 4AD United Kingdom.

10. V. N. Staroverov, G. E. Scuseria, J. Tao, and J. P. Perdew, J. Chem. Phys., 12129 (2003).

11. A. D. Becke, J. Chem. Phys., 064101 (2005).

12. J. P. Perdew, A. Ruzsinszky, J. M. Tao, V. N. Staroverov, and G. E. Scuseria, J. Chem. Phys., 062201 (2005).

13. P. Mori-Sanchez, A. J. Cohen, and W. Yang, J. Chem. Phys., 091102 (2006).

14. R. M. Martin, *Electronic Structure, Basis Theory, and Practical Methods*, Cambridge University Press, Cambridge, (2004).

15. P. W. Ayers, and W. Yang, in *Computational Medicinal Chemistry for Drug*

Discovery, Marcel Dekker, New York, (2004).

16. J. C. Dyson, and M. von Itzstein, Aus. J. Chem. , 663 (2001).

17. H. Hövel, L. S. Johansson, and B. Reihl in *Metal clusters at Surfaces: Structure, Quantum Properties, Physical Chemistry*, Springer Verlag, Berlin, (2000).

18. R. S. Berry, and H. Haberland, in *Clusters of Atoms and Molecules*, Springer Verlag, Berlin, (1994).

19. I. L. Garzón, J. A. Reyes-Nava, J. I. Rodríguez-Hernández, I. Sigal, M. R. Beltrán, and K. Michaelian, Phys. Rev. B , 073403 (2002).

20. I. L. Garzón, M. R. Beltrán, G. González, I. Gutíerrez-González, K. Michaelian, J. A. Reyes-Nava, and J. I. Rodríguez-Hernández, Eur. Phys. J. D , 105 (2003).

21. R. G. Parr, and W. Yang, in *Density-Functional Theory of Atoms and Molecules*, Oxford University Press, Oxford, (1989).

22. W. Yang, Phys. Rev. Lett. , 1438 (1991).

23. A. P. Horsfield, A. M. Bratkovsky, M. Fearn, D. G. Pettifor, and M. Aoki, Phys. Rev. B , 12694 (1996).

24. W. Yang, Phys. Rev. Lett. , 9294 (1997).

25. J. N. Kim, F. Mauri, and G. Galli, Phys. Rev. B , 1640 (1995).

26. L. Xi, W. Nunes, and D. Vanderbilt, Phys. Rev. B , 10891 (1993).

27. D. Vanderbilt, Phys. Rev. B, , 7892 (1990).

28. M. Payne, M. Teter, D. Allan, T. Arias, and J. Joannopoulos, Rev. Mod. Phys. , 1045 (1992).

29. J. Hutter, P. Lüthi, and M. Parrinello, Comput. Matter. Sci., 244 (1994).

30. A. Szabo, and N. S. Ostlund, *Modern Quantum Chemistry*, McGraw-Hill, New York, (1989).

31. A. J. Cohen, and N. C. Handy, J. Chem. Phys., 1470 (2002).

32. P. Pulay, Chem. Phys. Lett., 393 (1980).

33. P. Pulay, J. Comput. Chem., 556 (1982).

34. T. P. Hamilton, and P. Pulay, J. Chem. Phys., 5728 (1986).

35. G. Lippert, J. Hutter, and M. Parrinello, Mol. Phys., 477 (1997).

36. J. VandeVondele, M. Krack, F. Mohamed, M. Parrinello, T. Chassaing, and J. Hutter, Comput. Phys. Commun., 103 (2005).

37. M. Krack, and M. Parrinello, Phys. Chem. Chem. Phys., 2105 (2000).

38. G. Lippert, J. Hutter, and M. Parrinello, Theor. Chem. Acc., 124 (1999).

39. M. Challacombe, Comput. Phys. Commun., 93 (2000).

40. T. L. Beck, Rev. Mod. Phys., 1041 (2000).

41. K. Cho, T. A. Arias, J. D. Joannopoulos, and P. K. Lam, Phys. Rev. B , R5459 (1995).

42. S. Q. Wei, and M. Y. Chou, Phys. Rev. Lett., 2650 (1996).

43. S. R. White, J. Wilkins, and M. P. Teter, Phys. Rev. B , 5819 (1989).

44. E. Tsuchida, and M. Tsukada, Solid State Commun., 5 (1995).

45. J. Bernholc, J.-Y. Yi, and D. J. Sullivan, Faraday Discuss., 217 (1991).

46. E. J. Bylaska *et al.*, in *Proceedings of the 7th SIAM Conference on Parallel*

Processing for Scientific Computing, SIAM, San Francisco, (1995).

47. N. A. Modine, G. Zumbach, and E. Kaxiras, Phys. Rev. B , 10289 (1997).

48. U. V. Waghmare, H. Kim, I. J. Park, N. Modine, P. Maragakis, and E. Kaxiras, Comput. Phys. Commun. , 341 (2001).

49. F. Gygi, Europhys. Lett. , 617 (1992).

50. F. Gygi, Phys. Rev. B , 11692, (1993).

51. F. Gygi, Phys. Rev. B , 11190, (1995).

52. D. R. Hamann, Phys. Rev. B , 7337 (1995).

53. A. Devenyi, K. Cho, T. A. Arias, and J. D. Joannopoulos, Phys. Rev. B , 13373 (1994).

54. F. Gygi, and G. Galli, Phys. Rev. B , R2229 (1995).

55. Juan I. Rodriguez, David C. Thompson, James S. M. Anderson, Jordan Thomson, and Paul W. Ayers submitted (on ?) to *J. Phys. A.*

56. Y. Xu, *Common Zeros of Polynomials in Several Variables and Higher Dimensional Quadrature*, Wiley, New York, (1994).

57. D. Rees, and G. G. Hall, Int. J. Quantum. Chem. , 19 (2005).

58. S. A. Smolyak, Soviet Math. Dokl. , 240 (1963).

59. D. C. Thompson, and P. W. Ayers, Int. J. Quantum Chem. , 787 (2006).

60. P. Constans and R. Carbó, J. Chem. Inf. Sci. , 1046 (1995).

61. http://www.molspaces.com/ .

"Toda incomprensión es fecunda, como os he dicho muchas veces, siempre que vaya acompañada de un deseo de comprender. Por que en el camino de lo incomprendido comprendemos siempre algo importante, aunque sólo sea que *inconprendíamos* profundamente otra cosa que creíamos comprender. Meditando sobre la cuarta dimensión del espacio, llegué yo a dudar de las otras tres, a descubrir que el espacio en que yo pensaba, un gran vacío de toda materia, la nada primigenia anterior a todo cuerpo y a toda forma geométrica imaginable, no podía tener ninguna dimensión.
El día que comprenda (pensaba yo) que ese espacio pueda tener tres dimensiones, ¿por qué no comprender que tenga cuatro?"
Juan De Mairena

A. Machado, *Juan de Mairena, sentencias, donaires, apuntes y recuerdos de un profesor apócrifo.*

Chapter 5

AN EFFICIENT GRID-BASED SCHEME TO COMPUTE QTAIM PROPERTIES WITHOUT EXPLICIT CALCULATION OF ZERO-FLUX SURFACES*

* The content of this chapter was submitted (on 02/19/08) as an article to the *Journal of Computational Chemistry*. (Authors: Juan I. Rodríguez, Andreas M. Köster, Paul W. Ayers, Ana Santos-Valle, Alberto Vela, and Gabriel Merino.)

5.1 Statement of the problem

As discussed previously, the main goal of this dissertation is to construct efficient grid-based methods for DFT electronic structure calculations. These methods are primarily used as the numerical integrators for computing molecular and atomic properties. In the precedent chapters, the application of our grids focused entirely on computing molecular properties (ground state energies, exchange-correlation and atomization energies, etc.) and nothing was said about atomic properties. Computing atomic properties is an important step in interpreting the results from any electronic structure computer program. The chemistry of a molecule (or material) can be understood from the properties of atoms therein, e.g., in terms of atomic charges, electrostatic moments, polarizabilities, etc.. In this chapter, we introduce a novel grid-based method for computing atomic properties within QTAIM. It was implemented in a modified version of deMon2k. For medium accuracy, our method is the fastest one we know of.

5.2 Introduction

The quantum theory of atoms in molecules (QTAIM), proposed and developed by Bader and coworkers,[1-3] is useful because it provides a formal definition for the concept of an atom within a molecule and a method for defining atomic properties based on

quantum mechanical principles. In addition, QTAIM provides precise mathematical definitions for important chemical concepts like the chemical bond, molecular structure and atomic charges. QTAIM is a powerful and beautiful theory because all of these concepts are derived from the empirically observable molecular electron density. This makes QTAIM more broadly applicable than molecular orbital methods, because QTAIM can be used even when electron correlation is very important. Currently QTAIM is being used by both theoreticians and experimentalists in fields ranging from solid state physics and X-ray crystallography[4-5] to drug design[5] and biochemistry.[5-6]

In QTAIM, a property $P(\Omega)$ of an atom in a molecule is defined as the expectation value of an effective single-particle property density $p(\vec{r})$ over its so-called atomic basin Ω,[1-2,8]

$$P(\Omega) = \int_{\Omega} p(\vec{r}) d\vec{r} \ . \tag{5.2.1}$$

The boundaries of the atomic basin are surfaces that satisfy the "zero flux condition" $\nabla\rho(\vec{r}) \bullet \hat{n} = 0$, where $\hat{n}$ is the unit vector normal to the surface and $\rho(\vec{r})$ is the electron density. The atomic basins often have very irregular shapes, which makes the basin integration in Eq. (5.2.1) difficult.

As examples of atomic properties and property densities, we consider two different definitions for the atomic kinetic energy,[1,8]

$$K(\Omega) = -\frac{N}{2}\int_{\Omega}\int\ldots\int \Psi^{*}(\vec{r},\vec{r}_2,\ldots,\vec{r}_N)\nabla^2\Psi(\vec{r},\vec{r}_2,\ldots,\vec{r}_N)d\vec{r}_2\ldots d\vec{r}_N d\vec{r}\ , \tag{5.2.2a}$$

$$G(\Omega) = \frac{N}{2}\int_{\Omega}\int\ldots\int \nabla\Psi^{*}(\vec{r},\vec{r}_2,\ldots,\vec{r}_N)\bullet\nabla\Psi(\vec{r},\vec{r}_2,\ldots,\vec{r}_N)d\vec{r}_2\ldots d\vec{r}_N d\vec{r}\ . \tag{5.2.2b}$$

An important consequence of the zero-flux atomic partitioning is that these two forms of the atomic kinetic energy give the same result. This is because the expectation value of their difference, $L(\Omega)$, is zero in any region bounded by zero-flux surfaces,

$$L(\Omega) = K(\Omega) - G(\Omega) = -\frac{1}{4}\int_{\Omega}\nabla^2\rho(\vec{r})d\vec{r} = 0\ . \tag{5.2.2c}$$

We will test our approach for the basin integration in Eq. (5.2.1) using Eq. (5.2.2c). We will also verify that the sum of the atomic property values recovers the corresponding molecular property.[1,8]

The reader will notice that QTAIM exploits the topology of the electron density. (In fact, QTAIM is sometimes referred to as "Quantum Chemical Topology."[9]) Key concepts for QTAIM include the zero-flux surface that bounds the atomic basins and the critical points in the electron density (where $\nabla\rho(\vec{r}) = 0$). The critical points associated with maxima in the density are called attractors. Attractors can be categorized as either atomic nuclei or non-nuclear attractors (which only occur in special molecules at special geometries[10-12]). Every atomic basin is filled by a web of gradient ascent paths that terminate at a density maximum or attractor.[1-3]

The standard approaches to evaluate Eq. (5.2.1) use a 3-step procedure.[8,13-16] (I) All of the electron density's critical points are determined. (II) The atomic zero-flux surfaces are constructed. (III) Integration over the atomic basin is carried out. Determining the zero-flux surfaces is the most time consuming step in these algorithms. One of the original methods to determine the zero-flux surface (implemented in the program PROAIM[8]) finds points on the zero-flux surface by tracing back trajectories from a so-called bond critical point.[1,8] Other points on the zero-flux surface are obtained by interpolation so that the zero-flux surface is obtained as a function of two angular polar coordinates centered at the nucleus in question.[8] Cioslowski and Stefanov introduced a variational method in which, for every pair of bonded atoms, a function of prolate spheroidal coordinates that represents a zero-flux sheet between the pair of atoms is determined by minimizing a functional of the zero-flux sheet and the gradient electronic density itself. The boundary of the atomic basins is then obtained by joining the zero-flux sheets that surround each atom.[13-14] In an approach introduced by Popelier,[15] the zero-flux surface is obtained by fitting an analytical function to a set of points on the surface.

All these methods produce a representation of the zero flux surface as a function of two curvilinear coordinates, $f(\eta,\xi)$. The actual integration over the atomic basin is then carried out using spherical coordinates centered at the nucleus into consideration. For a given grid for the angular coordinates, the radial integration interval, $r(\theta,\varphi)$, starts

at the attractor and ends where the ray in the direction (θ,φ) intersects the zero-flux surface.[8,13-15] Although these methods achieve outstanding accuracy,[8,13-15] it is not always feasible to apply them to molecules with dozens of atoms. In particular, generating the zero-flux surface is prone to error when either: a) the grid points are too few, or too poorly distributed, for accurate interpolation/fitting[8,15] or b) the function guess in Cioslowski-Stefanov method[13-14] is not good enough. Thus the important question is "How can the inherent problems in computing the zero-flux surfaces be avoided?" The answer we give in this article is: "not compute them at all!"

Recently Henkelman *et al.*[17] and Sanville *et al.*[18] introduced a method to compute atomic charges based on a entirely new philosophy. They partitioned the space into little cubes centered at every point in a regular grid. Then, they ascend along the gradient path that passes through each grid point until the path terminates at a maximum in the electron density. Based on the terminus of the path, they associate each little cube to an atomic basin.[17-18] This approach is faster and simpler than the standard methods described above. However, it still has some problems: For example, there are memory and accuracy problems associated with the use of huge regular grids. Also, the Euler method that is used to construct the steepest ascent path is quite sensitive to small variations in the step size.[19]

In this article we present a grid-based scheme that follows the basic philosophy of the works of Henkelman *et al.*[17] and Sanville *et al.*.[18] Like them we do not explicitly

construct the zero-flux surfaces. Like them, the only input to our program is the system's density and geometry. Unlike them, we do not use regular grids. Instead, we apply efficient cellular grids as they are used in SCF-Kohn-Sham methods;[20-21] this avoids any extra grid construction and the use of large regular grids. We have implemented our approach using both the adaptive[21] and fixed grids implemented in the deMon2k density functional theory package.[22] All grids are based on Becke's atom centered construction,[23] which uses the product of a Lebedev grid for the angular part and a one-dimensional quadrature for the radial part. We tested our algorithm with different sizes of fixed and adaptive grids. The smallest fixed grid was a grid with 50 radial shells each carrying a Lebedev grid with 194 points; this grid is denoted (50,194). We also used (75,302) and (99,590) grids. For the adaptive grids, we used grids with error tolerances of 10^{-5} and 10^{-6} in the numerical integration of the exchange and correlation energies and potentials.[21]

In addition to the use of cellular grids that are especially efficient for integrating the density and density-like properties, our method has two other innovations. First of all, we define "atomic trust spheres" inside each atomic basin. Points inside these spheres can be reliably assigned to the appropriate atomic attractor without further calculation. Second, we prune away grid points that are so far from the molecule that they make no significant contribution to the atomic properties. These developments, and their

application for computing properties of atoms and non-nuclear attractors, are described in the subsequent sections.

5.3 A Grid-Based Algorithm

5.3.1 Algorithm

Let $\vec{r}_0$ be a grid point that is not on the zero-flux surface. We will determine which atomic basin this point belongs to by tracing the steepest-density-ascent path from $\vec{r}_0$ to an attractor. We considered 3 algorithms for constructing the path: the Euler (EU) method, 2nd order Runge-Kutta (RK2), and 4th order Runge-Kutta (RK4).[24-25] The Euler method requires evaluating the gradient of the density once per step. RK2 and RK4 require two and four gradient evaluations, respectively.[24-25] Although the steepest ascent path starts from a grid point, it moves freely in space after the first step. (I.e., the path is not restricted to move through the grid.) It is worth mentioning that an early version of this algorithm to calculate atomic charges was presented in reference (26).

To control the accuracy of the gradient path, in any step where the density decreased, the step size was reduced by 25%. The step was then repeated until an increase in the density was achieved. The steepest ascent path is terminated once it enters an "atomic trust sphere" that allows us to unambiguously assign $\vec{r}_0$ to a particular attractor.

5.3.2 Atomic Trust Sphere

Notice that the algorithm will be faster if the atomic trust sphere is larger. We determine the atomic trust sphere radius using the spherical Lebedev grids. For each point, $\vec{r}_0$, of the Lebedev grid at a given radial shell, we evaluate the gradient of the density $\nabla\rho(\vec{r}_0)$. If the gradient points towards the central atom of the Lebedev grid, it can be assigned to this atom. If this is true for every point of the Lebedev grid at a given radial shell, then obviously all points inside that radial shell will be also assigned to that atom. Thus the biggest radial shell that satisfies this condition will be the trust sphere for an atom. The specific algorithm we used to determine the radius of the trust sphere is as follows.

1) For the attractor at $\vec{X}_A$, we start by considering a Lebedev grid on a radial shell very close (1 a.u.) to the attractor. Let $\vec{r}_k$ be a point of the Lebedev grid and θ_k be the angle between the vector $\vec{X}_A - \vec{r}_k$ and $\nabla\rho(\vec{r}_k)$.
2) If $\theta_k < \theta_0$ (θ_0 is a threshold angle) for every $\vec{r}_k$ of the Lebedev grid, then go to 3. If not, then go to 4.
3) Consider the next Lebedev grid on the next radial shell further outside. Go to 2.
4) Assign the trust radius of the attractor to the radial shell of the previous step. Stop.

We established that an angle of $\theta_0 = 45^o$ suffices by ensuring that atomic properties obtained with and without the trust sphere method were the same for a family of molecules. This choice of the atomic trust sphere reduces the CPU time by more than 25% (see Table 5.2 and Figure 5.3). Note also that the atomic trust sphere has an interesting chemical meaning: it defines the "almost spherical" (and thus "almost transferable") region around each atom in the molecule.

5.3.3 Screening

The electron density and density gradient is very small at grid points that are far away from any nucleus. This makes it difficult to assign these points to an atomic basin, which slows down the algorithm. Because the product of the density at these points and the corresponding integration weight is of the order 10^{-10}, these points do not contribute significantly to the atomic quadrature sum. This motivates our screening procedure: if $w_i\rho(\vec{r}_i) < 10^{-8}$ and $\nabla\rho(\vec{r}_i) < 10^{-8}$ (w_i is the integration weight corresponding to $\vec{r}_i$) are satisfied for a given grid point, then this point is neglected in the integration of the atomic properties. Our tests indicate that omitting these points causes only very small differences ($< 10^{-7}$ a.u.) in the computed values of the atomic properties.

5.3.4 Non nuclear attractors

As already mentioned, our algorithm does not require any input except for the density and the locations of the atomic nuclei. To identify non-nuclear attractors (NNA) in the electron density we find all the points in space that satisfy:

1) $\rho(\vec{r}_0) > 0.001$ a.u.

2) $\nabla\rho(\vec{r}_0)$ is almost zero ($< 10^{-8}$ a.u.)

3) The density's Hessian at $\vec{r}_0$ has three negative eigenvalues

$\vec{r}_0$ must satisfy all three conditions in order to be considered as a non-nuclear attractor. These conditions are applied in sequence. Points that are far from the atomic nuclei will violate the first condition; this reduces the number of points where the (expensive!) third condition must be tested. We successfully applied this algorithm to some molecules with non-nuclear attractors. An example (Li_2) is presented in Table 5.6.

5.3.5 The overall algorithm

The overall algorithm is summarized by the flow chart in Figure 5.1. In more detail,

1. Generate the atomic trust sphere for every atom in the system.
2. Pick up a new grid point $\vec{r}_i^{(0)}$.

3. Is $\vec{r}_i^{(0)}$ far enough from the nuclei to satisfy the screening conditions? If so go to 2; if not, set $\vec{r}_i^{(k)} = \vec{r}_i^{(0)}$ and go to 4.
4. Is $\vec{r}_i^{(k)}$ inside of an atomic trust sphere? If so go to 8; if not, go to 5.
5. Is $\vec{r}_i^{(k)}$ a new NNA? If so go to 6; if not, go to 7.
6. Add $\vec{r}_i^{(0)}$ to the attractor list and assign a trust sphere with an appropriate radius to it. Go to 2.
7. Construct the next step in the steepest ascent path: $\vec{r}_i^{(k+1)} = \vec{r}_i^{(k)} + \Delta\vec{r}_i^{(k)}$. Go to 4.
8. Add the grid point $\vec{r}_i^{(0)}$, i.e., the initial point in the steepest ascent path, to the corresponding atomic basin property quadrature. Go to 2.

This algorithm stops after all non-screened points in the grid are assigned to an atomic basin.

5.4 Computational Methods

All calculations were performed with a modified version of deMon2k[22] at the local spin density approximation level using a DZVP basis.[27] The exchange-correlation functional employed was the Dirac exchange[28] and the Vosko-Wilk-Nusair correlation functional.[29] Unless not otherwise stated, the deMon2k default settings for the SCF and

optimization procedures were used. Molecular symmetry was exploited in the structure optimization and in the building of the integration grids. Molecular symmetry, however, was not exploited while applying the present algorithm to compute atomic properties.

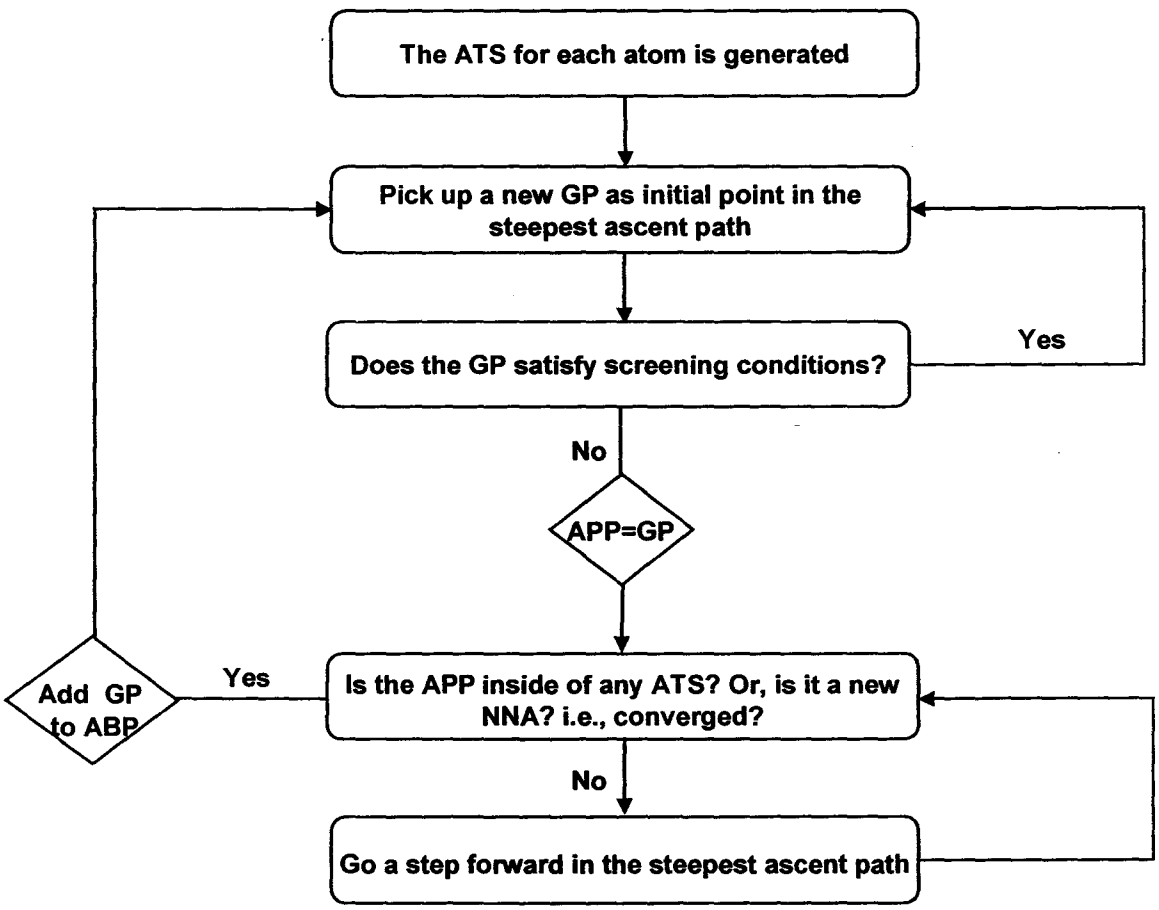

Figure 5.1. Flow chart of the overall algorithm. Abbreviations: ATS=atomic trust sphere; GP=grid point; APP=actual point in the path; NNA=non-nuclear attractor; ABP=atomic basin property.

5.5 Results and Discussion

To compute atomic properties we first optimized the molecular geometry. A single-point SCF calculation at the optimized geometry was used to generate the electron density for our atomic property calculations. We computed the electrostatic multipole moments of each atom using the spherical tensor formulation. Our notation for the multipole moments follows Popelier,[15] except that we chose to define Q_{00} as the total atomic charge, including the contribution from the nucleus, Z_Ω,

$$Q_{00}(\Omega) = Z_\Omega - \int_\Omega \rho(\vec{r})d\vec{r} \tag{5.5.1}$$

$$Q_{10}(\Omega) = -\int_\Omega z\rho(\vec{r})d\vec{r} \tag{5.5.2}$$

$$Q_{11c}(\Omega) = -\int_\Omega x\rho(\vec{r})d\vec{r} \tag{5.5.3}$$

$$Q_{11s}(\Omega) = -\int_\Omega y\rho(\vec{r})d\vec{r} \tag{5.5.4}$$

$$Q_{20}(\Omega) = -\int_\Omega \frac{1}{2}(3z^2 - r^2)\rho(\vec{r})d\vec{r} \tag{5.5.5}$$

$$Q_{21c}(\Omega) = -\int_\Omega \sqrt{3}xz\rho(\vec{r})d\vec{r} \tag{5.5.6}$$

$$Q_{21s}(\Omega) = -\int_\Omega \sqrt{3}yz\rho(\vec{r})d\vec{r} \tag{5.5.7}$$

$$Q_{22c}(\Omega) = -\int_\Omega \frac{1}{2}\sqrt{3}(x^2 - y^2)\rho(\vec{r})d\vec{r} \tag{5.5.8}$$

$$Q_{22s}(\Omega) = -\int_{\Omega} \sqrt{3} xy \rho(\vec{r}) d\vec{r} \,. \tag{5.5.9}$$

Table 5.1 compares the values of atomic properties of formaldehyde obtained using the three different methods for constructing the steepest ascent path. All our results are reported in atomic units unless otherwise stated. Notice that the number of function calls is directly related to the number of steps during the path. Notice also that $L(\Omega)$ is close to the correct value of zero; this confirms the accuracy of our integration method. While the values of the atomic properties are reasonable, it seems that the Euler method for propagating the gradient path is quite sensitive to the step size. We believe this is because the approximate gradient paths cross when the step size is too large. By contrast, RK2 and RK4 are very stable in this respect, and basically give the same numbers. This can be also inferred from Table 5.2.

Table 5.1 Atomic properties for formaldehyde[a] for different integration methods. An adaptive grid with tolerance 10^{-5} was used. The first row shows the step size (Δ_s), the CPU time[b], the number of steps in the longest path during the partition, N_{max}, and the average number of steps for all paths in the whole partition algorithm, N_{ave}.

Atom	Property	EU	RK2	RK4
	Δ_s	0.025	0.15	0.3
	Time[b]	285.5	101.0	109.5
	N_{max}	378	63	32
	N_{ave}	85	15	7
O	Q_{00}	-1.038	-1.038	-1.038
	Q_{10}	0.476	0.476	0.476
	Q_{20}	-0.325	-0.325	-0.325
	Q_{22c}	-0.122	-0.122	-0.122
	K	74.795	74.795	74.795
	G	74.799	74.799	74.799
	L	-3.7×10^{-3}	-3.7×10^{-3}	-3.7×10^{-3}
C	Q_{00}	0.849	0.850	0.850
	Q_{10}	0.993	0.992	0.992
	Q_{20}	-0.784	-0.778	-0.778
	Q_{22c}	0.328	0.328	0.328
	K	36.809	36.809	36.809
	G	36.802	36.801	36.801
	L	7.0×10^{-3}	8.4×10^{-3}	8.4×10^{-3}
H	Q_{00}	0.095	0.094	0.094
	Q_{10}	0.097	0.097	0.097
	$Q_{11s}(-)$	-0.129	-0.129	-0.129
	Q_{20}	0.002	0.001	0.001
	$Q_{21s}(-)$	0.132	0.133	0.133
	Q_{22c}	0.142	0.144	0.144
	K	0.555	0.554	0.554
	G	0.557	0.557	0.557
	L	-2.3×10^{-3}	-3.0×10^{-3}	-3.0×10^{-3}

Table 5.1 (Continued)

	Property	EU	RK2	RK4
Total	Q_{00}	0.000	0.000	0.000
	Q_{10}	1.664	1.662	1.662
	Q_{11s}	0.000	0.000	0.000
	Q_{20}	-1.106	-1.102	-1.102
	Q_{21s}	0.000	0.000	0.000
	Q_{22c}	0.489	0.494	0.494
	K	112.713	112.713	112.713
	G	112.714	112.714	112.714
	L	-1.3×10^{-3}	-1.3×10^{-3}	-1.3×10^{-3}

[a] Only non vanishing moments are shown. The properties of the H atoms are the same except for certain entries [denoted (-)] where symmetry introduces a factor of -1.
[b] On one processor Intel(R)-Xeon(TM) 2.4GHz.

Table 5.2 Parameters in the calculations of the atomic properties for formaldehyde. An adaptive grid with tolerance 10^{-5} was used. Values of the CPU time[a], N_{max} and N_{ave} (see Table 5.1 for definitions of these numbers) using atomic trust spheres (ATS) and without using them (NO-ATS) for different values of the step size Δ_s (in a.u.) are shown.

	Δ_s	Time[a]		N_{max}		N_{ave}	
		NO-ATS	ATS	NO-ATS	ATS	NO-ATS	ATS
EU	0.015	631.4	474.0	666	630	188	141
	0.020	479.1	362.4	500	472	141	106
	0.025	377.0	285.1	400	378	113	85
RK2	0.10	195.7	148.4	100	95	29	22
	0.15	131.1	101.1	67	63	19	15
	0.20	100.8	76.0	50	48	15	11
RK4	0.10	383.4	288.4	100	95	29	22
	0.20	194.8	147.6	50	48	15	11
	0.30	132.9	102.1	34	32	10	8

[a] On one processor Intel(R)-Xeon(TM) 2.4GHz.

For a given method, varying Δ_s in the range shown in Table 5.2 does not change the atomic property values. Obviously, the CPU time decreases as the step size increases. Thus, the biggest step size that ensures no path crossings gives the best performance. From Table 5.2 we can also see that the use of the atomic trust spheres makes the algorithm 25% faster (see also Figure 5.3).

Table 5.3 compares the values of atomic properties for formaldehyde using adaptive and fixed grids. We can see that there is a small variation in the atomic properties with respect to the number of grid points. If we compare the results of the largest adaptive and fixed grids with each other we find only small differences. In particular, the total —i.e. molecular— quantities are almost identical for these two grids. Therefore, the total quantities can be used as an indicator for the grid accuracy. The differences in the individual atomic quantities are usually larger than in the summed total quantities. This indicates that the grid accuracy is not the only factor that determines the quality of the basin integration. For this reason, a medium sized grid is sufficient for the basin integration if errors of around 10^{-3} a.u. are acceptable.

Table 5.3 Atomic properties for formaldehyde[a] for different integration grids using RK4 as integration method with $\Delta_s = 0.3$ a.u.. The first row shows the total number of grid points (NGP), the CPU time[b], and the values of N_{max} and N_{ave} (see Table 5.1 for definitions of these numbers).

		Adaptive		Fixed		
Atom	Property	10^{-5} [c]	10^{-6} [c]	(50,194)	(75,302)	(99,590)
	NGP	21611	39413	10093	26257	73934
	Time[b]	101.2	198.6	30.8	77.2	203.8
	N_{max}	63	62	60	60	61
	N_{ave}	15	16	9	8	7
O	Q_{00}	-1.038	-1.033	-1.033	-1.043	-1.032
	Q_{10}	0.476	0.468	0.467	0.483	0.466
	Q_{20}	-0.325	-0.340	-0.342	-0.319	-0.332
	Q_{22c}	-0.122	-0.116	-0.143	-0.102	-0.113
	K	74.795	74.789	74.785	74.802	74.793
	G	74.799	74.793	74.795	74.805	74.793
	L	-3.7×10^{-3}	-4.6×10^{-3}	-1.0×10^{-3}	-2.9×10^{-3}	-2.1×10^{-4}
C	Q_{22}	0.850	0.846	0.851	0.855	0.842
	Q_{10}	0.992	0.988	0.994	0.996	0.989
	Q_{20}	-0.778	-0.775	-0.741	-0.768	-0.783
	Q_{22c}	0.328	0.326	0.363	0.304	0.315
	K	36.809	36.811	36.815	36.801	36.810
	G	36.801	36.809	36.803	36.796	36.809
	L	8.4×10^{-3}	2.4×10^{-3}	1.1×10^{-2}	5.2×10^{-3}	5.8×10^{-4}
H	Q_{00}	0.094	0.093	0.091	0.094	0.095
	Q_{10}	0.097	0.096	0.091	0.096	0.097
	$Q_{11s}(-)$	-0.129	-0.128	-0.130	-0.129	-0.129
	Q_{20}	0.001	0.000	0.000	-0.001	0.000
	$Q_{21s}(-)$	0.133	0.129	0.125	0.129	0.128
	Q_{22c}	0.144	0.140	0.147	0.146	0.142
	K	0.554	0.557	0.558	0.556	0.556
	G	0.557	0.556	0.558	0.557	0.556
	L	-3.0×10^{-3}	1.1×10^{-3}	-4.7×10^{-4}	-1.2×10^{-3}	-1.8×10^{-4}

Table 5.3 (Continued)

		Adaptive		Fixed		
		10^{-5} [c]	10^{-6} [c]	(50,194)	(75,302)	(99,590)
Total	Q_{00}	0.000	0.000	0.000	0.000	0.000
	Q_{10}	1.662	1.649	1.642	1.671	1.649
	Q_{11s}	0.000	0.000	0.000	0.000	0.000
	Q_{20}	-1.102	-1.116	-1.083	-1.089	-1.115
	Q_{21s}	0.000	0.000	0.000	0.000	0.000
	Q_{22c}	0.494	0.489	0.514	0.494	0.486
	K	112.713	112.714	112.714	112.715	112.715
	G	112.714	112.714	112.714	112.715	112.715
	L	-1.3×10^{-3}	1.8×10^{-5}	-7.2×10^{-5}	-1.2×10^{-5}	3.4×10^{-6}

[a] Only non vanishing moments are shown. [b] On one processor Intel(R)-Xeon(TM) 2.4GHz.
[c] Tolerance in integrating the exchange-correlation potential and energy in the SCF calculation.

Table 5.4 Total CPU time (in sec.) for atomic property calculations.

Molecule	Popelier[15,a]	Sanville *et al.*[18,b]	Stefanov *et al.*[14,c]	This work[d]
H_2O	2400.0	354.2		25.7
N_2	1320			21.6
CH_4	4020.0		707.9	81.4
NH_3			449.2	43.0
CH_2O			652.8	75.8
C_2H_4			913.1	252.5
Li_2			147.3	60.9
CO				20.3
CO_2				80.0
CS_2				130.0
H_2O_2				65.8
CH_3OH				226.7
C_2H_5OH				518.5
C_4H_8				1097.5
C_6H_6				1471.0
$Fe(C_5H_5)_2$				7155.3

[a] On a DEC-α AXP 300LX workstation. Popelier reports timings only for the heavy atoms. The timings reported here are estimated from his data.
[b] On a 2.5GHz PowerPC G5 processor.
[c] On one processor of a Cray-YMP4/32 supercomputer.
[d] On one processor Intel(R)-Xeon(TM) 2.4GHz.

Table 5.4 compares the CPU time for atomic property calculations with previous calculations reported in the literature. Our method is about one order of magnitude faster than the methods of Sanville *et al.*[18] and Stefanov *et al.*.[14] Our method is as much as 2 orders of magnitude faster than Popelier's method.[15] Based on Table 5.4, we believe that our method is one of the most efficient implementations for QTAIM atomic property calculations.

In Figure 5.2 the partition of the integration grid into the atomic basins for formaldehyde is depicted. In part (a) we can see how the grid points nicely outline the interatomic surfaces. The more points in the grid, the smoother and more precise these "imaginary" surfaces will be. In (b) the atomic basin for carbon in formaldehyde is shown. The shape and size of the atomic basins are in good agreement with previous calculations.[1]

In Table 5.5 we list atomic properties for a set of representative molecules. Due to local differences in the molecular density and geometry from one system to another, the atomic trust sphere radius is system dependent. The last row in Table 5.5 shows the total value of each property. Notice that there is a difference between the SCF energy and the molecular energy as sum of atomic energies. Although there is a (small) numerical integration error, this difference is caused by the fact that we did not introduce the local virial correction for the atomic energies reported in this work.[1,30] The "error" in the virial theorem is, in turn, primarily due to the fact $E \neq T_s$ in density functional theory.[31] We

are currently exploring how our method responds to different basis sets and exchange-correlation functionals.

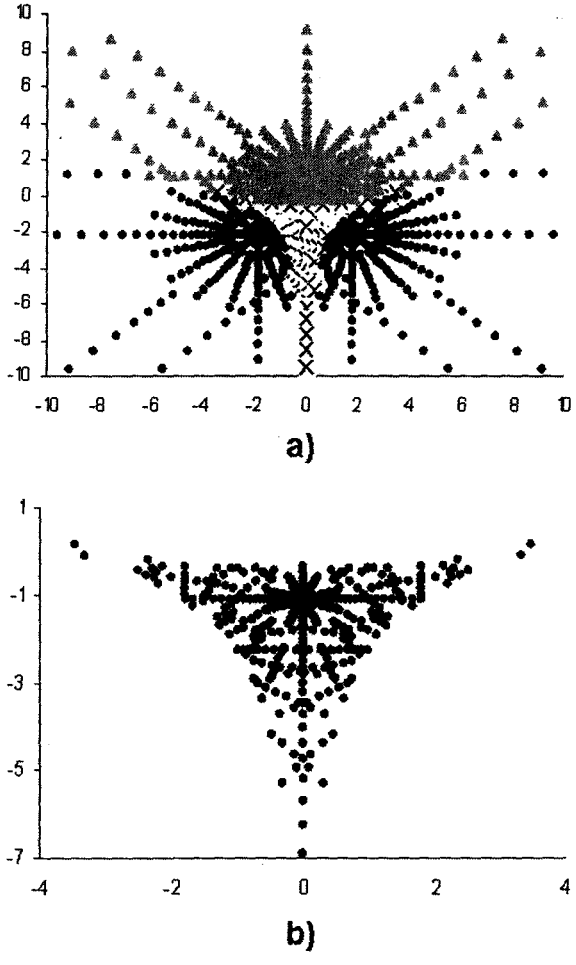

Figure 5.2. (a) Atomic basins for formaldehyde. Grid points are dots in the two hydrogen basins, triangles in oxygen's basin, and crosses in the carbon's basin. (b) Expanded view of the carbon atomic basin in formaldehyde. Only grid points in the plane of the molecule are shown. Lengths are in a.u. (Bohr).

Table 5.5 Atomic properties. Atomic trust sphere radius (ATSR) are also shown. The SCF energy is shown in the last column. Calculations were performed with RK4 and a step size $\Delta_s = 0.3$ a.u..

Molecule	Charge	Energy	L	ATSR	SCF Energy
CO					
C	1.131	-36.512	9.9×10^{-4}	0.650	
O	-1.131	-75.047	-1.0×10^{-3}	1.355	
Total	0.000	-111.558	-1.5×10^{-5}		-112.444
N_2					
N	0.000	-53.883	-8.0×10^{-6}	0.744	
N	0.000	-53.883	-8.0×10^{-6}	0.744	
Total	0.000	-107.766	-1.6×10^{-5}		-108.662
CO_2					
O	-1.037	-74.824	2.3×10^{-3}	1.355	
C	2.074	-36.148	-4.7×10^{-3}	0.723	
O	-1.037	-74.824	2.3×10^{-3}	1.355	
Total	0.000	-185.795	-7.5×10^{-3}		-187.232
H_2O					
O	-1.122	-74.610	8.0×10^{-4}	1.219	
H	0.561	-0.381	-3.9×10^{-4}	0.240	
H	0.561	-0.381	-3.9×10^{-4}	0.240	
Total	0.000	-75.372	2.1×10^{-5}		-75.898
CS_2					
S	0.536	-395.402	-9.8×10^{-4}	1.077	
C	-1.072	-37.937	1.2×10^{-3}	1.228	
S	0.536	-395.402	-9.7×10^{-4}	1.077	
Total	0.000	-828.741	-7.6×10^{-4}		-831.367

Table 5.5 (Continued)

Molecule	Charge	Energy	L	ATSR	SCF Energy
NH_3					
N	-1.115	-54.238	4.3×10^{-3}	1.260	
H	0.372	-0.461	-1.4×10^{-3}	0.381	
H	0.372	-0.461	-1.4×10^{-3}	0.381	
H	0.372	-0.461	-1.4×10^{-3}	0.381	
Total	0.000	-55.620	4.5×10^{-5}		-56.103
C	0.856	-36.801	6.5×10^{-3}	0.723	
O	-1.044	-74.802	-4.2×10^{-3}	1.355	
H	0.094	-0.556	-1.7×10^{-3}	0.529	
H	0.094	-0.556	-1.2×10^{-3}	0.529	
Total	0.000	-112.715	-1.2×10^{-3}		-113.626
H_2O_2					
O	-0.565	-74.401	8.8×10^{-4}	1.219	
O	-0.565	-74.401	8.8×10^{-4}	1.219	
H	0.565	-0.386	-8.8×10^{-4}	0.270	
H	0.565	-0.386	-8.8×10^{-4}	0.270	
Total	0.000	-149.574	4.4×10^{-6}		-150.525
CH_4					
C	-0.289	-37.440	-2.6×10^{-3}	0.9949	
H	0.072	-0.560	5.7×10^{-4}	0.5289	
H	0.072	-0.560	5.7×10^{-4}	0.5289	
H	0.072	-0.560	5.7×10^{-4}	0.5289	
H	0.072	-0.560	5.7×10^{-4}	0.5289	
Total	0.000	-39.678	-2.7×10^{-4}		-40.123

Table 5.5 (Continued)

Molecule	Charge	Energy	L	ATSR	SCF Energy
CH_3OH					
C	0.326	-37.123	-2.8×10^{-3}	0.805	
O	-1.070	-74.687	1.8×10^{-3}	1.219	
H	0.088	-0.564	-1.6×10^{-3}	0.529	
H	0.053	-0.576	1.3×10^{-3}	0.529	
H	0.053	-0.576	1.3×10^{-3}	0.529	
H (alcohol)	0.550	-0.393	2.3×10^{-4}	0.270	
Total	0.000	-113.920	1.3×10^{-4}		-114.835
C_2H_4					
C	-0.178	-37.409	1.8×10^{-4}	0.805	
C	-0.178	-37.409	1.8×10^{-4}	0.805	
H	0.089	-0.559	-1.1×10^{-4}	0.529	
H	0.089	-0.559	-1.1×10^{-4}	0.529	
H	0.089	-0.559	-1.1×10^{-4}	0.529	
H	0.089	-0.559	-1.1×10^{-4}	0.529	
Total	0.000	-77.052	$-9.\times10^{-5}$		-77.855
C_2H_5OH					
C	-0.163	-37.441	1.9×10^{-3}	0.995	
C (alcohol)	0.404	-37.101	5.1×10^{-3}	0.895	
H	0.055	-0.568	-1.7×10^{-3}	0.529	
H	0.069	-0.566	$6.\times10^{-4}$	0.529	
H	0.069	-0.566	$6.\times10^{-3}$	0.529	
O	-1.070	-74.689	$-5.\times10^{-3}$	1.219	
H (alcohol)	0.548	-0.393	-1.0×10^{-4}	0.270	
H (C-alcohol)	0.044	-0.584	-2.9×10^{-4}	0.529	
H (C-alcohol)	0.044	-0.584	-2.9×10^{-3}	0.529	
Total	0.000	-152.491	-8.3×10^{-5}		-153.797

Table 5.5 (Continued)

Molecule	Charge	Energy	L	ATSR	SCF Energy
C_4H_8					
C	-0.097	-37.403	1.4×10^{-3}	0.995	
C	-0.097	-37.403	1.4×10^{-3}	0.995	
C	-0.097	-37.403	1.4×10^{-3}	0.995	
C	-0.097	-37.403	1.4×10^{-3}	0.995	
H	0.050	-0.576	-1.9×10^{-3}	0.529	
H	0.050	-0.576	-1.9×10^{-3}	0.529	
H	0.050	-0.576	-1.9×10^{-3}	0.529	
H	0.050	-0.576	-1.9×10^{-3}	0.529	
H	0.047	-0.577	5.6×10^{-3}	0.529	
H	0.047	-0.577	5.6×10^{-3}	0.529	
H	0.047	-0.577	5.6×10^{-3}	0.529	
H	0.047	-0.577	5.6×10^{-3}	0.529	
Total	0.000	-154.223	1.6×10^{-4}		-155.780
C_6H_6					
C	-0.087	-37.427	2.0×10^{-3}	0.895	
C	-0.087	-37.427	2.0×10^{-3}	0.895	
C	-0.087	-37.427	2.0×10^{-3}	0.895	
C	-0.087	-37.427	2.0×10^{-3}	0.895	
C	-0.087	-37.427	2.0×10^{-3}	0.895	
C	-0.087	-37.427	2.0×10^{-3}	0.895	
H	0.087	-0.562	-2.0×10^{-3}	0.529	
H	0.087	-0.562	-2.0×10^{-3}	0.529	
H	0.087	-0.562	-2.0×10^{-3}	0.529	
H	0.087	-0.562	-2.0×10^{-3}	0.529	
H	0.087	-0.562	-2.0×10^{-3}	0.529	
H	0.087	-0.562	-2.0×10^{-3}	0.529	
Total	0.000	-227.929	1.4×10^{-4}		-230.166

Table 5.5 (Continued)

Molecule	Charge	Energy	L	ATSR	SCF Energy
$Fe(C_5H_5)_2$					
Fe	0.798	-1259.610	5.4×10^{-1}	1.736	
C	-0.175	-37.487	3.3×10^{-3}	0.995	
C	-0.183	-37.489	-2.2×10^{-3}	0.995	
C	-0.178	-37.488	1.1×10^{-3}	0.995	
C	-0.177	-37.488	2.1×10^{-3}	0.995	
C	-0.182	-37.489	-1.4×10^{-3}	0.995	
C	-0.175	-37.487	3.3×10^{-3}	0.995	
C	-0.182	-37.489	-1.2×10^{-3}	0.995	
C	-0.174	-37.487	3.7×10^{-3}	0.995	
C	-0.181	-37.489	-5.3×10^{-4}	0.995	
C	-0.179	-37.486	-1.8×10^{-3}	0.995	
H	0.099	-0.554	-1.8×10^{-3}	0.529	
H	0.099	-0.554	-1.8×10^{-3}	0.529	
H	0.099	-0.554	-1.8×10^{-3}	0.529	
H	0.099	-0.554	-1.8×10^{-3}	0.529	
H	0.099	-0.554	$-1.\times10^{-3}$	0.529	
H	0.099	-0.554	-1.8×10^{-3}	0.529	
H	0.099	-0.554	-1.8×10^{-3}	0.529	
H	0.099	-0.554	-1.8×10^{-3}	0.529	
H	0.099	-0.554	-1.8×10^{-3}	0.529	
H	0.099	-0.557	-1.1×10^{-3}	0.529	
Total	0.000	-1640.040	5.3×10^{-3}		-1644.838

In Table 5.6 the atomic properties for Li_2 are shown. The algorithm located the non-nuclear attractor at the middle of the Li-Li bond as it is predicted.[10-12] The properties of non-nuclear attractors can be easily computed with our method.

Finally Figure 5.3 shows how the computational performance is improved by using atomic trust spheres. Figure 5.3 was obtained from calculations of Table 5.3. When atomic trust spheres were not used, a sphere with a radius of 0.15 Bohr was considered around each atom. Notice that the CPU time saving per atom is proportional to molecule size. This fact is important since one of the goals of the algorithm is to facilitate QTAIM studies of big systems.

Table 5.6 Atomic properties for Li_2[a]. The atomic properties of the non-nuclear attractor (NNA) are also reported.

Property	Li	Li	NNA	Total
Q_{00}	0.392	0.392	-0.784	0.000
Q_{10}	0.255	-0.255	0.000	0.000
Q_{20}	-1.538	-1.538	-4.480	-7.555
K	7.234	7.234	0.056	14.525
G	7.234	7.234	0.057	14.525
L	-1.2×10^{-5}	-1.2×10^{-5}	-1.7×10^{-4}	-2.0×10^{-4}

[a] Only non-vanishing moments are shown.

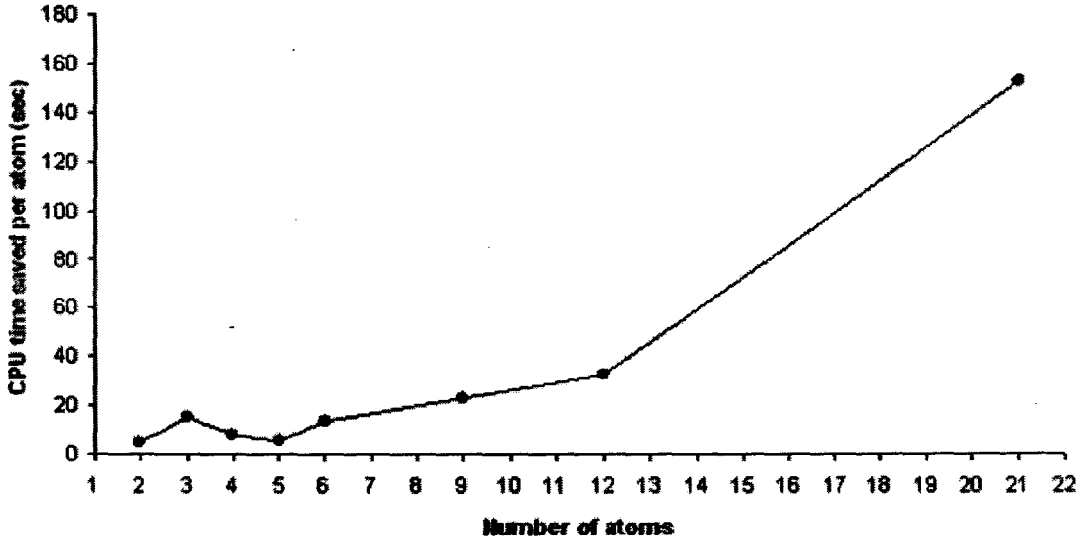

Figure 5.3. CPU time saved per atom when using the atomic trust spheres for the molecules of Table 5.5. An average time was considered when there was more than one molecule with the same number of atoms.

5.6 Conclusion

A new grid-based algorithm to compute QTAIM atomic properties was introduced. It partitions a predefined integration grid into the subsets of points that lie inside each atomic basin. Then, atomic properties are obtained by quadrature over those subsets. Notice that this approach does not require generating the zero-flux surfaces.

Our approach is designed for applications where computational efficiency is critical and moderate accuracy is sufficient. This is because our integration grids make implicit assumptions about the smoothness of the integral that are not strictly valid. This is avoided in methods that construct the zero-flux surfaces directly and could be mitigated in our method by choosing very many radial and angular points in the vicinity of the atomic surfaces. The use of optimal adaptive grids in our algorithm makes it possible to use many fewer grid points, but this compromises the accuracy of the atomic integrations because the zero-flux surfaces are not always precisely located. For moderately accuracy, however, our approach is the fastest method we know of.

To test our program, we computed atomic properties of a set of representative molecules. Our results were consistent with previous calculations.[8,13-18]

5.7 References for chapter 5

1. Bader, R. F. W. Atoms in Molecules: A Quantum Theory; Oxford University Press: New York, 1990.

2. Popelier, P. L. A. Atoms in Molecules: An Introduction; Prentice Hall: Edinburg, 2000.

3. Bader, R. F. W. Monatshefte für Chemie 2005, 136, 819.

4. Farrugia, L. J.; Evans C. J Phys Chem 2005, A 109, 8834.

5. Matta, C. F.; Boyd R. J. (Editors) The Quantum Theory of Atoms in Molecules. From Solid State to DNA and Drug Design; Wiley-VCH: Weinheim, 2007.

6. Matta, C. F. Ph. D. dissertation, McMaster University, 2002.

7. Biegler-Köning, F. W.; Nguyen-Dang, T. T.; Tal, Y.; Bader, R. W.; Duke, A. J. J Phys B 1981, 14, 2739.

8. Biegler-Köning, F. W.; Bader, R. W.; Tang, T. H. J Comput Chem 1982, 3, 117.

9. Malcolm, N. O. J.; Popelier, P. L. A. Faraday Discuss 2003, 124, 353.

10. Edgecombe, K. E.; Esquivel, R. O.; Smith, V. H. Jr. J Chem Phys 1992, 97, 2593.

11. Martín Pendás, A.; Blanco, M. A.; Costales, A.; Mori Sánchez, P.; Luaña, V. Phys Rev Lett 1999, 83, 1930.

12. Luaña, V.; Mori Sánchez, P.; Costales, A.; Blanco, M. A. J Chem Phys 2003, 119, 6341.

13. Cioslowsky, J.; Stefanov, B. B. Mol Phys 1995, 84, 707.

14. Stefanov, B. B.; Cioslowsky, J. J Comput Chem 1995, 16, 1394.

15. Popelier, P. L. A. Mol Phys 1996, 87, 1169.

16. Popelier, P. L. A. Comp Phys Commun 1998, 108, 180.

17. Henkelman, G.; Arnalsson, A.; Jónsson, H. Comput Mater Sci 2006, 36, 354.

18. Sanville, E.; Kenny, S. D.; Smith, R.; Henkelman, G. J Comput Chem 2007, 28, 899.

19. Baldridge, K. K.; Gordon, M. S.; Steckler, R.; Truhlar, D. G. J Phys Chem 1989, 93, 5107.

20. Krack, M.; Köster, A. M. J Chem Phys 1998, 108, 3226.

21. Köster, A. M.; Flores-Moreno, R.; Ulises-Reveles, J. J Chem Phys 2004, 121, 681.

22. *deMon2k,* Köster, A. M.; Calaminici, P.; Casida, M. E.; Flores-Moreno, R.; Geudtner, G.; Goursot, A.; Heine, T.; Ipatov, A.; Janetzco, F.; del Campo, J. M.; Patchkovskii, S.; Reveles, J. U.; Salahub, D. R.; Vela, A. deMon developers 2006. See http://www.demon-software.com

23. Becke, A. D. J Chem Phys 1988, 88, 2547.

24. Press, W. H.; Flannery, B. P.; Teukolsky, S. A.; Vetterling, T. Numerical Recipes in Fortran; Cambridge University Press: Cambridge, 1992.

25. Burden, R. L.; Faires, J. D. Numerical Analysis; Thomson Brooks/Cole: Belmont, 2005.

26. Merino, G. Ph.D. dissertation, Cinvestav: México, 2003.

27. Godbout, N.; Salahub, D. R.; Andzelm, J.; Wimmer, E. Can J Chem 1992, 70, 560.

28. Dirac, P. A. M. Proc. Cambridge Philos Soc 1930, 26, 376.

29. Vosko, S. H.; Wilk, L.; Nusair, M. Can J Phys 1980, 58, 1200.

30. Matta, C. F.; Boyd, R. J. in The Quantum Theory of Atoms in Molecules. From Solid State to DNA and Drug Design. Matta, C. F.; Boyd, R. J. (Editors); Wiley-VCH: Weinheim, 2007.

31. Levy, M; Perdew, J. P. Phys Rev A 1985, 32 (4), 2010.

"... Me preocupa más el metablema o trayecto. El camino y no la meta.
En una obra de arte, y hasta de ciencia o filosofía, me paseo y no voy a la meta.
Y es que no hay sino el camino"

Miguel de Unamuno, *Correspondencias*.

Chapter 6

CONCLUSIONS AND PROSPECTS FOR FUTURE WORK

6.1 Conclusions

This dissertation introduced two new numerical integration methods for computing molecular and atomic properties.[1-4] Both techniques are designed to be used within the standard Kohn-Sham-DFT formalism of electronic structure theory, but the general principles involved are more generally applicable. The techniques were implemented in a modified version of the deMon2k package and showed a remarkable improvement over previous approaches.

The first technique, introduced in Chapters 2-4, is based on a transformed sparse grid designed for integrating, interpolating, and differentiating the electron density and other density-like quantities.[1-3] In Chapter 2, this technique was used as the numerical integration scheme for the exchange-correlation energy and potential in the Kohn-Sham-DFT program deMon2k. The performance and accuracy of the resulting program was tested by computing ground state energies, equilibrium geometries, and atomization energies. The accuracy of the new approach is comparable to existing schemes, but our grids use significantly fewer points than the deMon2k reference grids but still give excellent results.[1]

In Chapter 2, the functions of interest are the electronic density and density-like functions, which are defined in 3-dimensional real space. However, the mathematical formalism developed (see Section 1.3) is valid for any number of dimensions. The extension of the transformed Smolyak integration technique to arbitrary dimensions is

established in Chapter 3. Of particular interest are the 3-dimensional application to the Gordon-Kim model for molecular interactions and the 6-dimensional application to non-local exchange-correlation functionals. The first application has particular relevance for the popular "frozen density embedding" approach for the non-covalent interactions. It is also relevant for next-generation molecular-mechanics force-fields. The second application is important because our approach removes the computational roadblock that has impeded the theoretical development and practical application of non-local "kernel-type" exchange-correlation functionals. The 6-dimensional integration is also relevant to the density-matrix approach to linear-scaling Kohn-Sham DFT and the first-order density matrix functional theory.

In Chapter 4, we develop numerical interpolation and differentiation methods for functions defined on the transformed Smolyak grids. We tested these methods by interpolating and differentiating a wide variety of functions in different dimensions (n = 2, 3, and 6). Our method gives good accuracy for interpolants and derivatives.[3] These results are particularly important because accurate grid-based derivatives and interpolants are an essential component of basis-set-free electronic structure calculations.

The biggest advantages of the transformed Smolyak grids are:

I. Efficiency for integrating functions in n-dimensions. Transformed Smolyak grids achieve acceptable accuracy with fewer points than conventional approaches. This effect is particularly apparent in higher dimensions.

II. "Whole molecule" nature of the grid. In particular, using the conditional distribution transformation we can go back and forth between the unit cube and real space. This facilitates applying important numerical methods, like the fast Fourier transform, that are traditionally formulated for regular grids on the cube. This is an important advantage over the atomic center grids, which do not have any simple connection to a regular grid.

III. Generality. Using the conditional distribution method, grid points can be distributed in space according to any predefined weight function. This weight function is chosen based on the function that is being integrated/differentiated/interpolated. Therefore, the transformed Smolyak grids can be used in many areas outside quantum chemistry.

In Chapter V, we introduce an efficient grid-based method for computing atomic properties within QTAIM.[4] The performance of the method was tested by computing QTAIM atomic energies, charges, dipole moments, and quadrupole moments. Our approach is designed for applications where computational efficiency is critical and moderate accuracy is sufficient. Our method is one to two orders of magnitude faster than previous approaches. This improvement makes it possible to study large systems for which QTAIM calculations were previously impracticable.

6.2 Prospects for future work on transformed sparse grids

The new numerical integration method for computing molecular properties introduced in this dissertation is more efficient than the deMon2k reference grids. However, there is still room for improvement. In the following paragraphs, we will describe some of the problems we discovered while developing and applying the transformed Smolyak grids. Then we will discuss some ideas on how to fix these problems.

6.2.1 Improving the efficiency of our grids

Our detailed investigations have shown that the grids introduced here are not as efficient for integrating the density,

$$N = \int \rho(\vec{r}) d\vec{r}\,, \tag{6.2.1}$$

as they are for integrating exchange-correlation energies. This is because the way we have distributed points in real space is not optimal. Recall that our grids are mapped according to the promolecular density; this concentrates points in the core regions and depletes them in the valence regions. While the promolecule-weighted grids are more efficient than regular cubature grids, the promolecular weighting is not ideal. Unfortunately, there is no practical way to determine the optimal distribution of grid points.

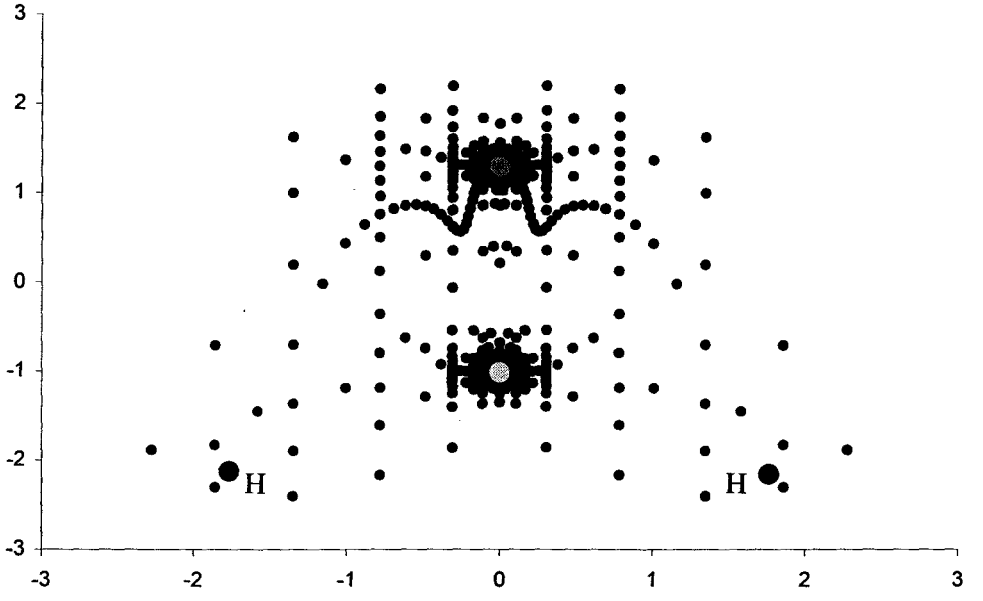

Figure 6.1 Transformed Smolyak grid for formaldehyde. Only points on the plane of the molecule are shown. Atomic units (Bohr) are used.

Some previous approaches to numerical integration in DFT determine the distribution of grid points empirically. For example, some points in the atomic-center grid approach are pruned away so that the number of angular points varies between the radial shells.[5-11] Other approaches solve the problem using automatic integration.[12-14] In automatic integration, the number of points in each direction is optimized before taking the tensor product to construct the *3*-dimensional grid. Usually the optimization is performed by requiring that the integral of a predefined function achieves a desired level of accuracy.[12-14]

In our Smolyak grid method the "pruning process" is carried out in the unit cube.[15-16] Thus, there is no way to selectively prune away points near a specific nucleus. This makes it difficult to fix the problem of having a huge imbalance in the concentration of points around hydrogen and heavy atoms. In Figure 6.1, this imbalance is illustrated for formaldehyde. Note the large difference between the concentration of points around oxygen and carbon compared to the hydrogen atoms. (Compare this distribution to deMon2k's atomic-center grids in the Figure 5.2a). We plan to address this problem in two different ways:

I. New approaches to atomic density fitting. We can fit the atomic densities with functions that decay slower than Gaussians (e.g., Lorentzians). The resulting promolecular densities will decay more slowly and so there will be more grid points far away from the nuclei. This also will help to solve the "boundary problem" for integrands that do not decay rapidly enough.

II. Core-Valence Splitting of the promolecular weighting. We can split the promolecular density into core and valence contributions using an adjustable parameter, λ:

$$\rho_{pro}(\vec{r}) = \rho_{pro}^{core}(\vec{r}) + \lambda \rho_{pro}^{valence}(\vec{r}) . \qquad (6.2.1)$$

In a procedure analogous to automatic integration, the value of λ can be chosen to achieve specified accuracy for integrating a predefined function. Notice that adjusting λ allows one to increase the concentration of points

close to the nuclei ($\lambda < 1$) or in the valence region ($\lambda > 1$). We are currently working to implement these two methods.

6.2.2 Basis-set-free DFT

A more general direction for future work is basis-set free electronic structure theory. The work in this thesis provides the fundamental numerical tools— interpolation, differentiation, and integration—needed for both wave-function-based and DFT-based programs.

I. The simplest approach would be to take an existing program[23-26] and replace its interpolation, differentiation, and integration subroutines with the ones developed in this thesis.

II. A better, but more ambitious, approach would be to create a new algorithm designed to exploit the strengths and mitigate the weaknesses associated with the transformed Smolyak grids. For example, one needs to decide between using finite-difference methods[23-26] (as in Chapter 4) and fast Fourier transform[27] techniques to evaluate derivatives. It is also important to note that the conditional distribution transformation can also be applied to simple-product grids. This may be helpful because techniques for differentiation, interpolation, and Fourier transform are simpler and better- established for this type of grids. The choice between simple-product grids and Smolyak grids

may come down to the accuracy required for integration (where Smolyak approach is much more efficient) versus differentiation (where simple-product grids might be preferable). One consideration is that finite-difference methods on simple product grids give sparse matrices, but the Smolyak-differentiation method in Chapter 4 gives dense matrices. A "sparse" approach to differentiation on Smolyak grids should be pursued.

Whether we use simple-product grids, Smolyak grids, are something else entirely, we still need to pay attention to the asymptotic decay of the weight function, $P(\vec{r})$, in the conditional distribution mapping of the unit cube onto real space. The divergences could be particularly troublesome when solving Poisson equation,

$$\nabla^2 V(\vec{r}) = -\rho(\vec{r}). \tag{6.2.2}$$

Consider the solution of Poisson equation in the integral form,

$$V(\vec{r}) = \int \frac{\rho(\vec{r}\,')d\vec{r}\,'}{|\vec{r} - \vec{r}\,'|}. \tag{6.2.3}$$

If the weight function $P(\vec{r})$ decays faster than $\rho(\vec{r})/r$, then the cubature will be divergent. This can be a problem, then, when a sum of Gaussians is used as a weight function. It is important to note that the suggestions in 6.2.1 for controlling the distribution of points could solve the divergence issue.

6.3 Prospects for future work on the Quantum Theory of Atoms in Molecules (QTAIM)

As already mentioned, our grid-based method for computing atomic properties is the fastest one we know of for medium accuracy calculations.[4] Avoiding the construction of the zero-flux surfaces makes our method faster than traditional methods because constructing the zero-flux surfaces is the most time consuming step in the traditional methods.[17-22]

6.3.1 Increasing the speed and accuracy of our QTAIM method

The most time consuming step in our method is the construction of the gradient path for assigning each grid point to an attractor. In the following paragraphs we introduce some ideas for improving this assigning process.

I. Parallelization. The method is highly suitable for parallelization since the attractor assignation for each grid point is independent of the others.[4] Parallelization will make the code applicable to studies of larger molecules.

II. Faster attractor assignation. As mentioned, the slowest part of the current program is the gradient-trajectory tracing method for assigning each point to the correct attractor. One way to increase the speed of this step is to develop

an "attractor function," f_A, for each atomic attractor. The attractor function would depend on the location of the grid point, $\vec{r}_i^{\,p}$, the location of the attractor, $\vec{R}_A$, the density gradient at the grid point, $\nabla\rho(\vec{r}_i^{\,p})$, the relative distance of the attractor A to the other attractors, and possibly other information. The grid point would then be assigned to the attractor with the largest value of $f_A(\vec{r}_i^{\,p}, \vec{R}_A, \nabla\rho(\vec{r}_i^{\,p}))$. Gradient tracing would be only required if there were a "tie" (or near tie) between two attractor functions.

6.3.2 Study on the dependence on QTAIM properties on other important quantities

Our QTAIM method is based on construction of density gradient trajectories. In an electronic structure calculation, the quality of the molecular density depends on the quality/size of the basis set, and the quality of the exchange-correlation energy functional used in the calculation. Performing a thorough study of these dependences would lead to a set of "best principles" for trustworthy QTAIM calculations. With the speed of our method, a thorough study of this type becomes feasible for the first time.

6.4 References for chapter 6

1. J. I. Rodríguez, P. W. Ayers, D. C. Thompson, and A. M. Köster. Submitted (on 03/25/08) to the *Journal of Chemical Physics*.

2. J. I. Rodríguez, D. C. Thompson, J. S. M. Anderson, J. Thomson, and P. W. Ayers. Submitted (on?) to the *Journal of Physics A*.

3. J. S. M. Anderson, J. I. Rodríguez, D. C. Thompson, and P. W. Ayers in *Quantum Chemistry Research Trends.* Mikas P. Kaisas (Editor). New York: Nova Science Publisher, 2007.

4. J. I. Rodríguez, A. M. Köster, P. W. Ayers, Ana Santos-Valle, Alberto Vela, and Gabriel Merino. Submitted (on 02/19/2008) to the *Journal of Computational Chemistry.*

5. M. R. Pederson and K. A. Jackson, Phys. Rev. B **41** (11), 7453 (1990).

6. G. te Velde and E.J. Baerends, J. Comput. Phys. 99, 84 (1992).

7. S. H. Chien and P. M. W. Gill, J. Comput. Chem. **27** (6), 730 (2006).

8. P. M. W. Gill, B. G. Johnson, and J. A. Pople, Chem. Phys. Lett. **209** (5-6), 50(1993).

9 R. Lindh, P. A. Malmqvist, and L. Gagliardi, Theor. Chem. Acc. **106** (3), 178 (2001).

10. M. E. Mura and P. J. Knowles, J. Chem. Phys. **104** (24), 9848 (1996).

11. C. W. Murray, N. C. Handy, and G. J. Laming, Mol. Phys. **78** (4), 997 (1993).

12. A. M. Köster, R. Flores-Moreno, and J. Ulises-Reveles, J.Chem. Phys. 121, 681 (2004).

13. M. Krack and A. M. Köster, J. Chem. Phys. 108, 3226 (1998).

14. J. M. Pérez-Jordá, A. D. Becke, and E. San-Fabián, J. Chem. Phys. 100, 6520 (1994).

15. E. Novak and M. Griebel, Numerical Algorithms 18, 209 (1998).

16. E. Novak and K. Ritter, Numer. Math. 75, 79 (1996).

17. J. Cioslowsky and B. B. Stefanov, Mol. Phys. 84, 707 (1995).

18. B. B. Stefanov and J. Cioslowsky, J. Comput. Chem. 16, 1394 (1995).

19. P. L. A. Popelier, Mol. Phys. 87, 1169 (1996).

20. P. L. A. Popelier, Comp. Phys. Commun. 108, 180 (1998).

21. G. Henkelman, A. Arnalsson, and H. Jónsson Comput., Mater Sci. 36, 354 (2006).

22. E. Sanville, S. D. Kenny, R. Smith, and G. Henkelman, J. Comput. Chem. 28, 899 (2007).

23. A. D. Becke, Ph. D. dissertation, McMaster University, 1981; J. Chem. Phys. 76, 6037 (1982); 78, 4787 (1983).

24. A. D. Becke, Numol, Intern. J. Quantum Chem. Symp. 23, 1280 (1989).

25. L. Laaksonen, D. Sundholm, and P. Pyykkö, Int. J. Quantum Chem. 27, 601 (1985).

26. J. R. Chelikowsky, N. Troullier, and Y. Saad, Phys. Rev. Lett. 72, 1240 (1994).

27. V. Gradinaru. Computing 80, 1-22 (2007).